ROBUST MEMORY-TYPE CONTROL CHARTS FOR MONITORING LOCATION PARAMETER UNDER NON-NORMAL DATA

NOR FASHIHAH MOHD NOOR

DOCTOR OF PHILOSOPHY
UNIVERSITI UTARA MALAYSIA
2025

Awang Had Salleh
Graduate School
of Arts And Sciences

Universiti Utara Malaysia

PERAKUAN KERJA TESIS / DISERTASI
(Certification of thesis / dissertation)

Kami, yang bertandatangan, memperakukan bahawa
(We, the undersigned, certify that)

NOR FASHIHAH MOHD NOOR

calon untuk Ijazah **PhD**
(candidate for the degree of)

telah mengemukakan tesis / disertasi yang bertajuk:
(has presented his/her thesis / dissertation of the following title):

"ROBUST MEMORY-TYPE CONTROL CHARTS FOR MONITORING LOCATION PARAMETER UNDER NON-NORMAL DATA"

seperti yang tercatat di muka surat tajuk dan kulit tesis / disertasi.
(as it appears on the title page and front cover of the thesis / dissertation).

Bahawa tesis/disertasi tersebut boleh diterima dari segi bentuk serta kandungan dan meliputi bidang ilmu dengan memuaskan, sebagaimana yang ditunjukkan oleh calon dalam ujian lisan yang diadakan pada : **18 Julai 2024.**
That the said thesis/dissertation is acceptable in form and content and displays a satisfactory knowledge of the field of study as demonstrated by the candidate through an oral examination held on: ***18 July 2024.***

Pengerusi Viva: *(Chairman for VIVA)*	**Assoc. Prof. Dr. Nor Aishah Ahad**	Tandatangan *(Signature)*
Pemeriksa Luar: *(External Examiner)*	**Assoc. Prof. Dr. Zainol Mustafa**	Tandatangan *(Signature)*
Pemeriksa Dalam: *(Internal Examiner)*	**Assoc. Prof. Dr. Suhaida Abdullah**	Tandatangan *(Signature)*
Nama Penyelia/Penyelia-penyelia: *(Name of Supervisor/Supervisors)*	**Dr. Ayu Abdul Rahman**	Tandatangan *(Signature)*
Nama Penyelia/Penyelia-penyelia: *(Name of Supervisor/Supervisors)*	**Dr. Abdu Mohammed Ali Atta**	Tandatangan *(Signature)*

Tarikh:
(Date) ***18 July 2024***

Permission to Use

In presenting this thesis in fulfilment of the requirements for a postgraduate degree from Universiti Utara Malaysia, I agree that the Universiti Library may make it freely available for inspection. I further agree that permission for the copying of this thesis in any manner, in whole or in part, for scholarly purpose may be granted by my supervisor(s) or, in their absence, by the Dean of Awang Had Salleh Graduate School of Arts and Sciences. It is understood that any copying or publication or use of this thesis or parts thereof for financial gain shall not be allowed without my written permission. It is also understood that due recognition shall be given to me and to Universiti Utara Malaysia for any scholarly use which may be made of any material from my thesis.

Requests for permission to copy or to make other use of materials in this thesis, in whole or in part, should be addressed to:

Dean of Awang Had Salleh Graduate School of Arts and Sciences
UUM College of Arts and Sciences
Universiti Utara Malaysia
06010 UUM Sintok

Abstrak

Carta kawalan sering digunakan untuk memantau dan meningkatkan kualiti sesuatu proses. Kaedah statistik ini boleh dikategorikan kepada carta kawalan tanpa memori dan jenis-memori. Contoh carta kawalan tanpa memori ialah carta Shewhart yang menggunakan maklumat sampel paling terkini dalam sebarang proses. Sebaliknya, carta kawalan jenis-memori seperti hasil tambah kumulatif (CUSUM) dan purata bergerak berpemberat eksponen (EWMA) yang menggunakan kedua-dua maklumat lampau dan terkini dalam proses. Justeru, menjadikan carta lebih sensitif dalam mengesan anjakan kecil hingga sederhana. Terbaharu, carta CUSUM dan EWMA telah digabungkan untuk membentuk carta campuran EWMA-CUSUM (MEC) dan campuran CUSUM-EWMA (MCE) bagi meningkatkan lagi keupayaan pengesanan anjakan kecil. Walau bagaimanapun, carta MEC dan MCE adalah berasaskan min, maka carta ini bergantung pada andaian kenormalan. Dalam keadaan ketidaknormalan, penganggaran parameter berdasarkan min akan terganggu, membawa kepada peningkatan isyarat palsu dan melengahkan pengesanan anjakan. Untuk menyelesaikan masalah ini dan meningkatkan proses pemantauan, tiga penganggar lokasi berasaskan-median (median, *M*-satu langkah terubahsuai (*MOM*), *MOM* terwinsor (*WMOM*)) yang mempunyai titik kerosakan tertinggi (50%) telah digunakan dalam pembinaan carta MEC dan MCE, menghasilkan enam carta teguh yang baharu, dinamakan sebagai $\text{MEC}_{\tilde{X}}$, MEC_{MOM}, MEC_{WMOM}, $\text{MCE}_{\tilde{X}}$, MCE_{MOM}, dan MCE_{WMOM}. Melalui kajian simulasi yang mendalam menggunakan perisian pengaturcaraan SAS, carta teguh yang dicadangkan telah diuji dalam beberapa keadaan, menumpu kepada taburan *g*-dan-*h*, saiz sampel, anjakan reka bentuk dan saiz anjakan. Parameter optimum untuk carta telah diterbitkan bagi mencapai pra-penentu purata panjang larian (ARL) dalam keadaan normal dan seterusnya, keteguhan carta dinilai berdasarkan ARL apabila tersimpang daripada taburan. Pengesahan prestasi carta telah dijalankan menggunakan data kualiti air dan data jalur penanda. Daripada simulasi, carta MEC berdasarkan penganggar *MOM* dan *WMOM* adalah terbaik memandangkan carta tersebut mempunyai keteguhan dalam keadaan terkawal yang baik dan keupayaan pengesanan yang pantas. Tambahan pula, carta yang dicadangkan telah disahkan menggunakan data sebenar, mempamerkan kebolehgunaan carta secara praktikal. Kedua-dua simulasi dan analisis data sebenar menunjukkan bahawa carta berasaskan-median yang dicadangkan mengatasi carta piawai meliputi pelbagai keadaan yang dinyatakan dalam kajian ini. Hasil kajian menawarkan kepada pengamal carta alternatif berdaya saing untuk proses kawalan apabila data tersasar dari kenormalan.

Kata Kunci: Purata panjang larian, carta kawalan jenis-memori, ketidaknormalan, penganggar teguh, kawalan proses statistik.

Abstract

Control chart is popularly used to monitor and improve the quality of a process. This statistical tool can be categorized into memoryless and memory-type control charts. An example of memoryless control chart is Shewhart chart which uses the most recent information of samples in a process. Conversely, the memory-type control charts such as cumulative sum (CUSUM) and exponentially weighted moving average (EWMA) use both past and recent information in the process. Thus, make the charts more sensitive in detecting small to moderate shifts. Recently, the CUSUM and EWMA charts were combined to form mixed EWMA-CUSUM (MEC) and mixed CUSUM-EWMA (MCE) charts to further improve small shift detection. However, these MEC and MCE charts are based on mean, thus they rely on the normality assumption. Under non-normality, parameters estimation based on the mean will be perturbed, leading to increased false signal and delayed detection of shifts. To solve this problem and improve the monitoring process, three median-based location estimators (median, modified one step *M*-estimator (*MOM*), winsorized *MOM* (*WMOM*)) which possess the highest possible breakdown point (50%) were used in the construction of the MEC and MCE charts, yielding six newly robust charts, namely $\text{MEC}_{\tilde{X}}$, MEC_{MOM}, MEC_{WMOM}, $\text{MCE}_{\tilde{X}}$, MCE_{MOM}, and MCE_{WMOM}. Via extensive simulation studies using SAS programming software, the proposed robust charts were tested under several conditions, focusing on *g*-and-*h* distributions, sample sizes, design shifts and shift sizes. Optimal parameters for the charts were derived to achieve the pre-determined average run length (ARL) under normality and subsequently, the robustness of the charts were assessed based on the ARL upon departure from the distribution. Validation of the charts' performance were conducted using water quality and marker band data. From the simulation, the MEC charts based on the *MOM* and *WMOM* estimators are the best since the charts have good in-control robustness and fast detection capability. Moreover, the proposed charts have been validated using real data, demonstrating their practical applicability. Both simulation and real data analyses show that the proposed median-based charts outperform the standard charts across various conditions specified in this study. The findings offer practitioners feasible alternative charts for monitoring processes when the underlying data deviate from normality.

Keywords: Average run length, memory-type control charts, non-normality, robust estimators, statistical process control.

Acknowledgement

I am deeply grateful to my supervisor, Dr. Ayu Abdul Rahman, Dr. Abdu Mohammed Ali Atta and my ex-supervisor, Prof. Dr. Sharipah Soaad Syed Yahaya for their unwavering support, invaluable guidance, and mentorship throughout the journey of my doctoral study. Their expertise, encouragement, and feedback have been instrumental in creating the direction and quality of this thesis.

I am grateful to Scholarship of Universiti Malaysia Perlis and Skim Latihan Akademik Bumiputera (SLAB) for providing financial support for this research study. Their funding has enabled me to pursue my academic aspirations and conduct in-depth investigations in my field of study.

I extend my sincere thanks to the faculty and staff of the SQS and AHSGS for creating a conducive academic environment and fostering intellectual growth and collaboration among students and scholars.

I am indebted to my colleagues and fellow researchers for their encouragement and intellectual exchange. Their friendship and support have made the research process both enriching and enjoyable.

Furthermore, I would like to acknowledge the valuable contributions of the Selangor Maritime Gateway officers in providing databases of Water Quality Index (WQI) for validation purposes in this study. Their dedication to data archiving greatly facilitated in the analysis phase.

My deepest gratitude goes to my husband (Mohd Hanis Alyas), my kids (Daniyal Zafran & Farrel Aryan) and my parents (Mohd Noor Arshad & Norlilah Ismail) for their unwavering love, motivation, and understanding throughout my academic journey. I am deeply thankful to my family for their unconditional love, encouragement, and understanding throughout the ups and downs of this challenging endeavor. Their support has been a constant source of strength and motivation.

Table of Contents

List of Tables

List of Figures

List of Appendices

List of Abbreviations

ARL	Average Run Length
ARL_0	In-control average run length
ARL_1	Out-of-control average run length
C_i^+	Upper CUSUM statistic
C_i^-	Lower CUSUM statistic
CL	Control limit
CUSUM	Cumulative Sum
δ	Actual shift
δ^*	Design shift
DOC	Dissolve Oxygen Concentrated
EWMA	Exponentially weighted moving average
FIR	Fast Initial Response
G0.5H0	Skewed normal-tailed distribution
G0.5H0.5	Skewed heavy-tailed distribution
G0H0	Normal distribution
G0H0.5	Symmetric heavy-tailed distribution
h	Optimal parameter for MEC
H	MEC control limit
IC	In-control
k	Reference value
K_C	Optimal parameter for MCE
λ	Smoothing parameter of EWMA
LCL	Lower Control Limit
m	Subgroup
$MADn$	Median Absolute Deviation
MCE	Mixed CUSUM-EWMA
$MCE_{\bar{X}}$	Standard MCE $\bar{X}$ chart
$MCE_{\tilde{X}}$	MCE $\tilde{X}$ chart
MCE_i^+	Upper MCE statistic

MCE_i^-	Lower MCE statistic
MCE_{MOM}	MCE *MOM* chart
MCE_{WMOM}	MCE *WMOM* chart
MEC	Mixed EWMA-CUSUM
$MEC_{\bar{X}}$	Standard MEC $\bar{X}$ chart
$MEC_{\tilde{X}}$	MEC $\tilde{X}$ chart
MEC_i^+	Upper MEC statistic
MEC_i^-	Lower MEC statistic
MEC_{MOM}	MEC *MOM* chart
MEC_{WMOM}	MEC *WMOM* chart
MOM	Modified one-step *M*-estimator
n	Sample size
NWQS	Malaysian National Water Quality Standard
RL	Run length
SDRL	Standard deviation run length
SMG	Selangor Maritime Gateway
SPC	Statistical process control
TSS	Total Suspended Solid
UCL	Upper Control Limit
WMOM	Winsorized modified one-step *M*-estimator
WQI	Water Quality Index
Z_i	EWMA Statistic

CHAPTER ONE
INTRODUCTION

1.1 Background of Statistical Process Control

Statistical process control (SPC) is a collection of statistical tools that is used to monitor, control, and enhance the quality of a process through variance reduction (Montgomery, 2009). In utilizing the SPC tools to monitor and reduce variation, samples are taken randomly from the production process, and some quality characteristic is measured and plotted on a graph known as a control chart. Subsequently, the presence of 'harmful' variations in the process shall be detected. Consequently, a corrective action may be undertaken to remove the source of the variations and hence, improve the quality of the process (Parkash et al., 2013).

Control chart was initially pioneered in the manufacturing process by Walter Andrew Shewhart in the 1920s (Montgomery, 2009). It is used to differentiate between two types of variations in the process, namely chance causes and assignable causes. The chance causes of variation, also known as common causes, are inherent to the process and thus, harmless. According to Swamidass (2000), examples of this type of variation include "poor lighting, poor temperature and humidity, vibration of machinery, inadequate maintenance of equipment, and inadequate environmental conditions due to noise and/or dust."

Conversely, the assignable causes of variation, generally known as special causes, are variability larger than the background noise; typically caused by improperly adjusted machines, human errors, or malfunctioning raw material (Montgomery, 2009).

Thus, their presence is considered harmful to the process as they cause the process parameter(s) to shift to an out-of-control value.

Common causes of variation are present when a process is stable or in-control. In this situation, both process parameters, i.e., the mean and standard deviation, are at their in-control values, say μ_0 and σ_0, respectively. Supposedly, at time t_1, a special cause occurs and results in a shift in the process parameter value, either $\mu_1 > \mu_0$ and/or $\sigma_1 > \sigma_0$. Thus, from time t_1 forward, the process is deemed unstable, i.e., out-of-control, until the special cause variability is eliminated. Subsequently, bringing back the process into an in-control state.

Control charts are designed to quickly detect a change in the process caused by special causes. The change in the process, i.e., from an in-control state to an out-of-control state, can easily be ascertained by looking at the graphical display of the measured quality characteristic. Figure 1.1 illustrates a typical set-up of control charts which includes a center line (CL), an upper control limit (UCL), and a lower control limit (LCL). The UCL and LCL are chosen so that if the process is in-control, all the measured quality characteristics are plotted within them. On the other hand, if a point crosses either the UCL or LCL, the process is deemed to be out-of-control. Subsequently, an investigation needs to be done to identify and possibly, remove the special causes responsible for this out-of-control condition.

The graph depicted in Figure 1.1 is known as the Shewhart control chart; a simple but useful statistical tool in SPC (Sinha & Vatsa, 2022). The chart has been used extensively in the manufacturing process (Smajdorova & Noskievicova, 2022). Today, its application has been extended to various fields of study including healthcare (Maravelakis et al., 2022), education (Masnar & Namoco, 2024), engineering (Alduais & Khan, 2023), finance (Yeganeh & Shongwe, 2023), and water quality analysis (Balcerowska-Czerniak & Gorczyca, 2024).

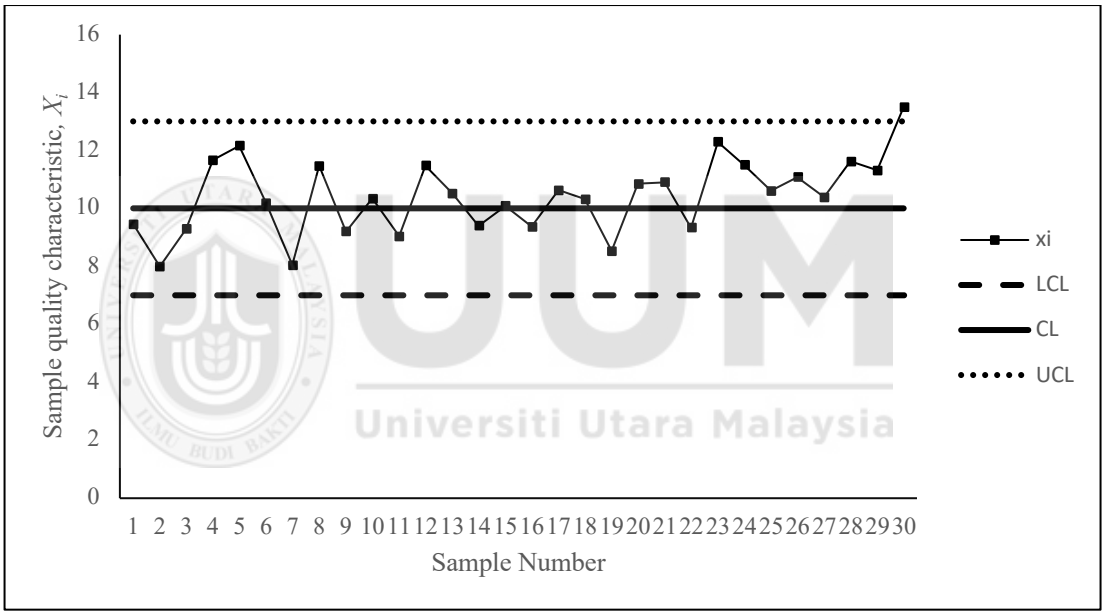

Figure 1.1 Shewhart Control Chart

Generally, control charts can be classified into memoryless and memory-type control charts. The memoryless control charts, such as the Shewhart chart, only utilize information from the most recent samples in the charts' structure. Thus, lacking a wealth of information to quickly detect a small shift in the process parameter values (Ajadi & Riaz, 2017; Naveed et al., 2018; Wu, 2018). Meanwhile, the memory-type charts combine information from both recent and past samples in the process, which makes the charts sensitive to a change in the process even when the shift in the process parameter value is relatively small. The following section focuses on commonly discussed memory-type control charts in SPC literature.

1.2 Memory-type Control Charts

Two main examples of memory-type control charts are cumulative sum (CUSUM) and exponentially weighted moving average (EWMA) charts. Other memory-type control charts are mixed EWMA-CUSUM (MEC) and mixed CUSUM-EWMA (MCE) charts which integrate both the EWMA and CUSUM control structures into one new chart.

The CUSUM control chart was introduced by Page (1954) to overcome the Shewhart's limitation in detecting small shifts. Unlike the Shewhart chart which utilizes only the most recent sample in the process, the CUSUM chart focuses on cumulative observations (based on past and recent samples) in constructing the graph displayed in Figure 1.2. The CUSUM chart signals a change in the process from an in-control state to an out-of-control state when either of its CUSUM statistics, denoted by C_i^+ and C_i^-, crosses the control limit, H.

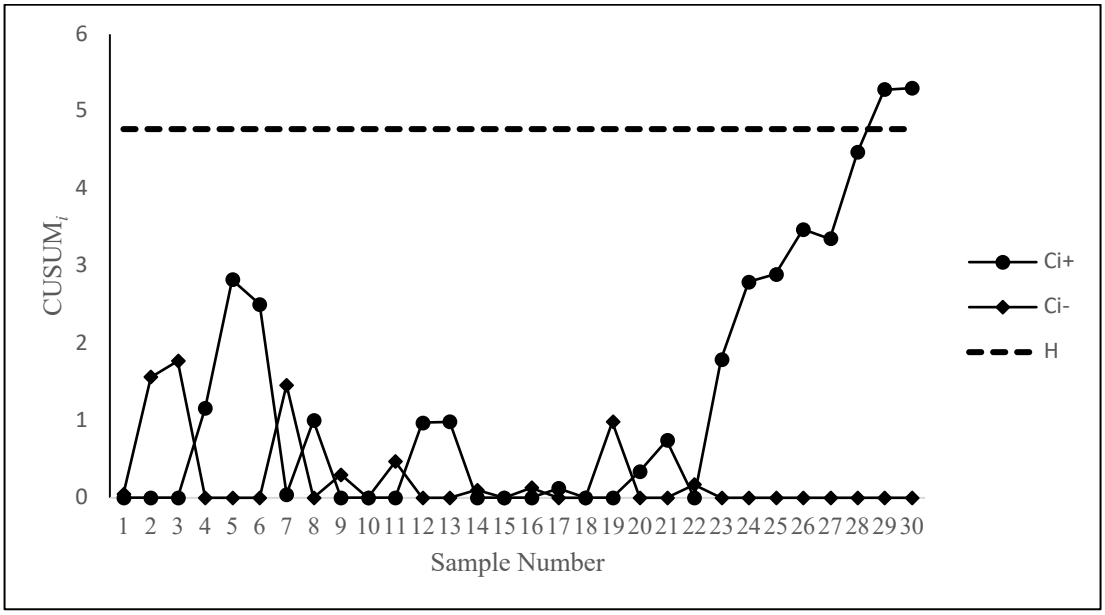

Figure 1.2 CUSUM Control Chart

Like the CUSUM, the EWMA chart also makes use of the past and recent information from the samples. However, unlike the CUSUM chart which accumulates and treats the past and recent samples equally, the EWMA control chart assigns weightage to all samples in the process (Roberts, 1959). The weight decreases exponentially as the sample gets older. In the EWMA structure, the weight is denoted by $\lambda \in (0, 1]$. A small value of λ reflects the high importance of including past samples. Subsequently, more information can be retrieved and used to quickly detect small process shifts (Hamasha et al., 2023). When λ is getting close to 1, the EWMA chart becomes less powerful to quickly detect a small change in the process. This is due to the emphasis on more recent samples while discarding information supposedly obtained from older samples in the process. Notably, when $\lambda = 1$, only information from the most recent sample is used in the chart's structure; essentially reducing the EWMA structure to Shewhart.

A distinction between the EWMA chart and the Shewhart chart is further highlighted in Figure 1.3. The control limits of the EWMA control chart, as illustrated in the figure, are time-varying limits; allowing a quicker detection when shifts occur early in the process, especially when a small λ is used to construct the chart (Letshedi et al., 2021; Taboran & Sukparungsee, 2023). These time-varying limits approach asymptotic limits, i.e., constant limits, as time increases. There is a negligible difference between the time-varying and constant limits in terms of the EWMA performance (Duong-Tran et al., 2022; Li et al., 2024; Thanwane et al., 2021). Using either of the types of control limits, defined by UCL and LCL, the EWMA chart concludes that the process is out-of-control when the chart statistic, Z_i, exceeds the control limit.

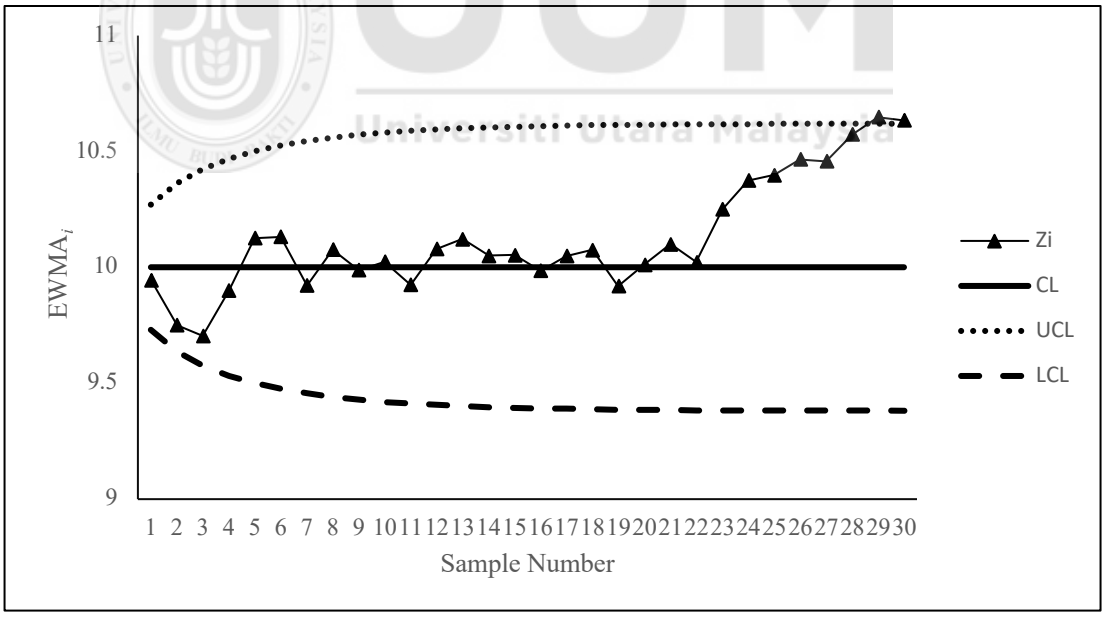

Figure 1.3 EWMA Control Chart

Numerous SPC literature claimed that the EWMA and CUSUM charts are equally good in detecting small process shifts (Kuiper & Goedhart, 2023; Li et al., 2024). However, several researchers claimed that the EWMA chart is more convenient to construct and employ since it resembles the Shewhart's control structure (Alduais & Khan, 2023; Malela-Majika et al., 2024).

The salient feature of both the CUSUM and EWMA charts, i.e., their flexibility to be designed for a quicker small shift detection than the Shewhart chart, is retained in the MEC and MCE charts. Introduced by Abbas et al. (2013a), the MEC chart uses the EWMA chart statistic within the CUSUM structure. Conversely, the MCE chart, which was introduced by Zaman et. al (2015), integrates the CUSUM chart statistic as an input in the EWMA structure. Both the MEC and MCE charts aim to further improve the performance of their predecessors, i.e., the CUSUM and the EWMA, especially when a very small shift occurs in the process (Mohamadkhani & Amiri, 2022). Examples of the MEC and MCE charts are displayed in Figures 1.4 and 1.5, respectively.

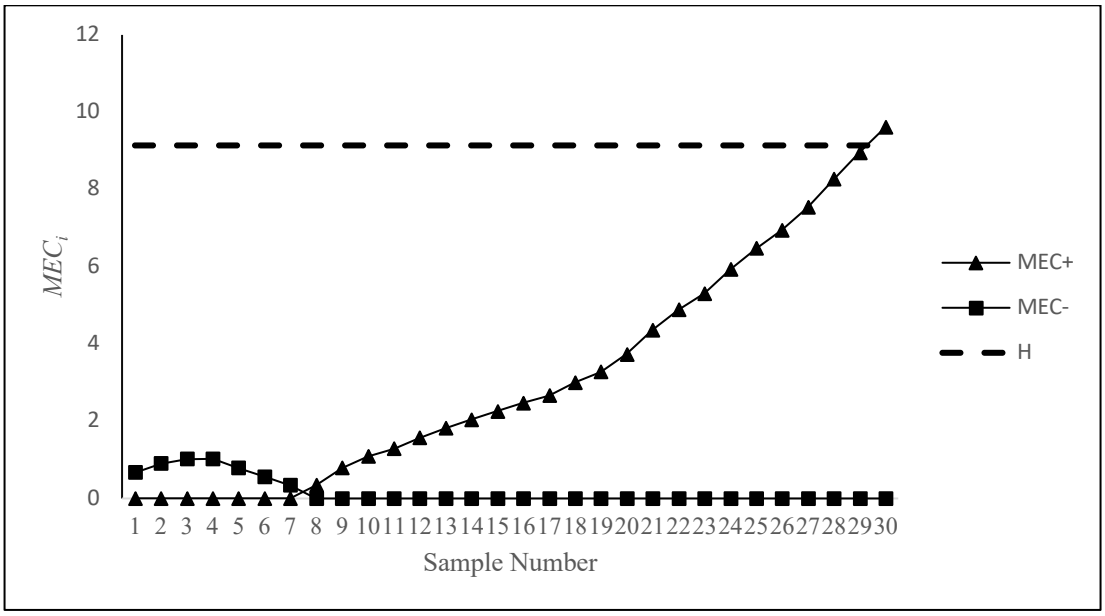

Figure 1.4 MEC Control Chart

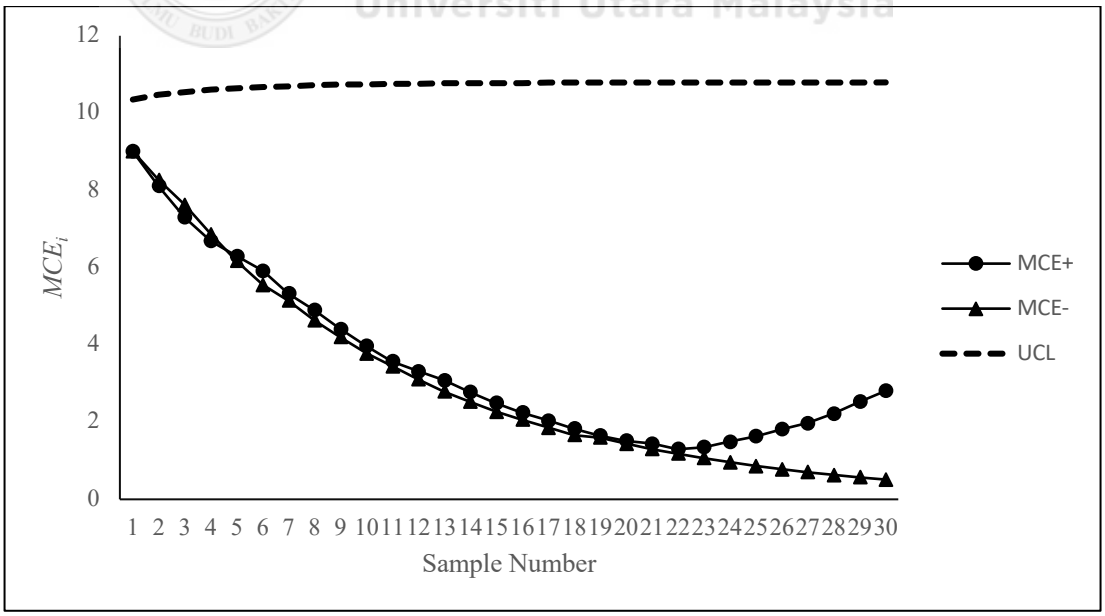

Figure 1.5 MCE Control Chart

Utilizing features in the CUSUM, the MEC and MCE charts also use two chart statistics to identify a change in the process. If either of the chart statistics goes across the control limit, the process is classified as out-of-control. For instance, based on Figure 1.4, the MEC_i^+ indicates a rapid increase in the mean value before the value shifts to an out-of-control at sample 30. A special cause may cause this variation in the mean value and thus, needs to be removed from the process. Subsequently, bringing the process back to an in-control state.

1.3 Problem Statement

Most of the parametric approaches in statistics rely on the normality assumptions which may not be easily practiced (Hernandez, 2021; Kelter, 2021; Osborne & Waters, 2019). Unfortunately, when data contain an outlier(s), which is a common cause of non-normality, classical parameter estimations in the parametric approaches are easily distorted (Knief & Forstmeier, 2021). Consequently, the methods will perform badly, resulting in inaccurate findings (Brobbey, 2021).

The classical estimators, i.e., the sample mean and the sample standard deviation, are very susceptible to outliers, that is, sensitive to even one aberrant value out of the n observations (Aguinis et al. 2013; Domanski, 2020; Rousseeuw, 1991). As such, their breakdown points (BP), i.e., the proportion of aberrant observations that an estimator can handle before being underestimated or overestimated, are 0% (Croux & Rousseeuw, 1992; Geyer, 2006).

The traditional approach control chart utilizes the classical estimators, such as mean and standard deviation to determine the control limits and monitor the process. This approach relies on a normal distribution (Jensen et al., 2006). The robust approach utilizes robust estimators such as median, trimmed mean, winsorized mean and *M*-estimator to make control charts less sensitive to non-normality or outliers (Sanaullah et al., 2024). This approach are less dependent on distributional assumptions and can perform well under various range of conditions.

Unlike the traditional approaches which focus on the classical estimators and thus, are confined to the normality assumption, robust approaches are not influenced by outliers (Cabana et al., 2021). This ensures that the methods work across many different situations regardless of the data distributions. Thus, warrants reliable performance upon its application in the real world.

In SPC, a better control of the Type I error can be achieved when control charts are integrated with robust estimators (Ahsan et al., 2020). Works by Fan et al. (2023), Santhanasamy and Abdul-Rahman (2022), and Wei et al. (2020), indicate the superiority of the robust control charts which is more sensitive in small shift detection upon far deviation from the normality assumption when compared to the standard control charts. Yet, balancing the Type I and Type II errors is not easily achieved in SPC especially when monitoring small process shifts (Lepore et al., 2022; Mohammed, 2024; Zamzmi et al., 2024).

Notably, it is important to quickly detect small process shifts and promptly address them to minimize the occurrence of defective products (Li et al., 2021; Quinino et al., 2021). Moreover, a fast detection of small process shifts can save time and cost in manufacturing and business sectors (Amiri et al., 2022; Naveed et al., 2024; Shamsuzzaman et al., 2022).

Therefore, in this study, an integration of highly robust location estimators was conducted within the structure of the recently introduced memory-type control charts, i.e., MEC and MCE charts. It is important to note that these two charts use classical estimator in their standard structure, thus easily perturb by outliers.

Focusing on the small and moderate shift detection (due to their merits in industries), the MEC and MCE charts were designed for these shift sizes and their performances were later assessed based on the ARL under non-normality. For such purpose, three median-based location estimators which possess the highest *BP* were chosen, namely median, modified one-step *M*-estimator (*MOM*), and the winsorized version of *MOM* (*WMOM*). By incorporating these robust estimators into the MEC and MCE charts, six robust memory-type control charts were formed for monitoring process location.

1.4 Research Questions

Classical estimators used in control charts are highly sensitive to outliers and rely on normality assumptions, making them less effective in real-world scenarios. To address these issues, this study focuses on enhancing memory-type control charts (MEC and MCE) by integrating robust location estimators. The research seeks to answer the following questions:

1. How to develop the robust MEC charts for location using three median-based estimators, i.e., median, *MOM*, and *WMOM*?

2. How to develop the robust MCE charts for location using three median-based estimators, i.e., median, *MOM*, and *WMOM*?

3. How to evaluate the performance of the proposed robust MEC and MCE charts against their standard charts based on the ARL_0 and ARL_1?

4. How to assess the performance of the proposed robust MEC and MCE control charts via water quality and marker band data?

These questions aim to develop more reliable control charts that are better suited for monitoring processes in real-world applications.

1.5 Objectives

The goal is to develop robust control charts which are able to control the Type I error while improving the small shift detection capability of the MEC and MCE control charts for monitoring process location parameter under non-normal data. To accomplish this goal, the following objectives need to be achieved.

1) To develop robust MEC charts for location using three median-based estimators, i.e., median, *MOM*, and *WMOM*.
2) To develop robust MCE charts for location using three median-based estimators, i.e., median, *MOM*, and *WMOM*.
3) To evaluate the performance of the proposed robust MEC and MCE charts against their standard charts based on the ARL_0 and ARL_1.
4) To assess the performance of the proposed robust MEC and MCE control charts via water quality and manufacturing data.

1.6 Scope of the Study

This study concentrates on two specific memory-type control charts, namely the MEC and MCE charts. Both the MEC and MCE charts in this study are targeted to monitor shifts in the process location where only the ARL was used to design and assess the performance of the proposed charts under normal and non-normal distributions. The focus is on small and moderate shift detection due to their merits in industries as explained earlier. Thus, in this thesis, the newly proposed robust control charts were designed to ensure optimal detection of small and moderate shifts. Albeit being designed specifically for the small and moderate magnitude of shifts, the performance of the memory-type charts is claimed to evenly match the one designed for large shifts. This is covered in detail in Chapter 2.

1.7 Significance of the Study

The findings of this research contribute to the industries and practitioners such as engineers, researchers and lecturers who can use the findings to be applied in their fields or works regarding statistical quality control. Specifically, robust tools that can be effectively used to reduce variations in the process. Through this study, robust structures of control charts can be obtained. Subsequently, these robust control charts can be applied to various types of process data without being confined to the normality assumption. Moreover, these robust charts can perform optimally and reliably across all ranges of shifts regardless of the underlying data distributions.

CHAPTER TWO
LITERATURE REVIEW

2.1 Introduction

Normality assumption is crucial in determining the optimal and reliable performance of standard charts, as it ensure the accurate calculation of control limits and effective detection of process variations (Montgomery, 2009). A standard control chart uses classical estimators in its control structure. Thus, under non-normality, its capability to signal a change in the process across various magnitudes of shifts may not be reliable as the control limits can either be underestimated (narrower) or overestimated (wider). A narrow control limits are closer to the center, i.e the center line, there is a higher probability that the plotting statistic will exceed the control limits, thus leading to an increase in false signals (Type I error). However, a wide control limits will further away from the center line, so become less sensitive to smaller change in the process and leads to a decrease in the chart's statistical power to quickly signal shifts (Mao & Spencer, 2021). Therefore, it is imperative for researchers and practitioners to explore alternative approaches that can solve this dilemma.

2.2 Measures of Control Chart's Performance

The construction of a control chart involves two distinct phases, namely Phase I and Phase II. Phase I is known as the retrospective phase as it involves historical data and concentrates on the estimation of process parameters for control limits. Meanwhile, Phase II is referred to as the prospective phase; commonly known as the monitoring phase and concentrates on monitoring the prospective samples to eliminate possible

variations in the process that may cause the process mean to shift to an out-of-control value. In Phase II, the chart is being evaluated on how quickly it can detect the out-of-control situation. This assessment is typically done based on the ARL.

As previously discussed in Section 2.1 earlier, non-normality will cause the width of the control limits to either be narrower or wider in Phase I (Hernandez, 2020), leading to an increase in false alarm rates or detection delay in out-of-control conditions, respectively. These issues have been covered by many researchers in SPC across different types of control charts. See for examples, Jardim et al. (2020), Noor et al. (2023), and Yao et al. (2023).

2.2.1 Average Run Length (ARL)

Numerous SPC literature focuses on ARL as a fundamental tool for designing and comparing the performance of control charts. See for examples, Atalay et al. (2020), Kostyszyn (2021), Ottenstreuer et al. (2023), and Tegegne et al. (2022). Run length (RL) can be defined as the sequence of samples plot on a chart until a signal (i.e., a sample plots outside a control limit) is detected (Arslan et al., 2023; Chong et al., 2022). Thus, the ARL represent the expected number of plotted samples before a signal is detected (Batool & Haq, 2024).

When the process parameters are known, the Shewhart control chart with 3-sigma control limits is expected to produce ARL = 370 under an in-control state when the process underlying distribution follows normal (Murat et al., 2024; Nidsunkid & Chometee, 2022; Zwetsloot et al., 2023). That is, a user can expect to obtain a signal, on average, once in every 370 plotted statistics.

The memory-type control charts, as discussed earlier, can be designed to produce an in-control ARL value like the Shewhart control chart. See for examples, Muhammad et al. (2023), Noor et al. (2024), Osei-Aning et al. (2017), Shafqat et al. (2023). Meanwhile, the out-of-control ARL assesses how quickly an out-of-control situation can be detected.

In this thesis, the in-control and out-of-control ARLs are henceforth denoted as ARL_0 and ARL_1, respectively, and can be computed as $\frac{1}{Probability\ of\ a\ signal}$. Under an in-control state, the probability of obtaining a signal is analogous to the Type I error, i.e., false alarm rate. Meanwhile, under an out-of-control state, the probability of obtaining a signal is equivalent to $1-\beta$, where β is the Type II error. Thus, an ideal control chart shall produce a large ARL_0 but exhibits small ARL_1 values. The former indicates the chart's capability to minimize false signals while the latter indicates the chart's capability to quickly signal out-of-control conditions (Sunthornwat & Areepong, 2020; Sunthornwat et al., 2024).

In designing a memory-type control chart, it is crucial to balance the Type I and Type II errors carefully under normality, especially without the priori value of the process parameters. A typical approach is to set ARL_0 based on the user's specification and derive control limits in Phase I under normality to achieve that value. A lot of studies focused on the nominal value of 370 as it is said to be a good balance between searching for the nonexistent special causes of variation (i.e., false signals) and true detection of process shifts which is a true signal. This is analogous to the Shewhart's selection criteria of the 3-sigma control limits (Montgomery, 2024).

It is noted that the calculation of the ARL is sensitive to the departure of the normality in the case of standard control charts (Chaudhary et al., 2023; Nazir et al. 2021; Prabawani & Mashuri, 2020). The good balance ARL control chart, i.e., ARL_0 is greater than ARL_1, is favored (Chen et al., 2023). Many studies in SPC strive to obtain the balance ARL chart when extending their work to cover non-normality effect on control charts. However, this feat is not easily achieved as portrayed in the work by Morales and Panza (2022) who focused on skewed distributions. A relatively small value of an ARL_0 implies that there are many false alarms, leading to a waste of time and effort in searching for the non-existent special causes of variation in the process (Does et al., 2020; Kumar & Singh, 2020; Tu & Zi, 2020).

While a higher ARL_0 might seem favorable, it may lead to higher ARL_1 and thus, taking longer to detect a change when a shift occurs in the process (Human et al., 2020). This was hinted in the work by Human et al. (2011) when designing and assessing an in-control performance of the EWMA control chart based on individual observations under two contaminated normal distributions. The findings in Abdul-Rahman (2020) concur with the previous study where the researcher extended the work to cover the out-of-control performance of the EWMA, CUSUM, and generalized Shewhart charts based on the rational subgroup data under specific *g*-and-*h* distributions. Indeed, a high ARL_0 leads to detection delay, specifically when the shift size is relatively small. This beats the purpose of using a memory-type chart that is allegedly superior in detecting tiny changes in the process data.

Therefore, the emphasis on the robust in-control performance of the memory-type charts is prominent in many SPC literature. A control chart is robust if its ARL_0 remains close to the nominal value, say 370, under non-normal data which is the key implementation for a reliable control chart.

2.3 Consequences of Applying Standard Control Charts to Non-Normal Data

Orr et al. (1991) defined outliers as the most extreme observations when compared to the rest of the dataset in which their presence can negatively affect the parameter estimation statistical models. In their study, Orr et al. (1991) have identified five origins of outliers: (i) unrepresentative data, (ii) representative data but modeled incorrectly, (iiii) error components, (iv) erroneous data entry, and (v) erroneous data analysis.

In dealing with outliers, Ratcliff (1993) noted that an outlier is a response produced by processes that are not part of the study interest. Therefore, he advised it to be removed from the data to avoid any misinterpretation of the data. However, removing outliers requires them to be properly identified which is not an easy task. While it is acknowledged that outliers negatively impact classical parameter estimations to be overestimated or underestimate such as mean, the idea to include or exclude outliers from data before performing statistical analyses has been debated among many researchers (Andre, 2022; Bondarenko et al., 2024; Fan et al., 2024; Karch, 2023; Rakotosaona et al., 2020). Kruskal et al. (1960), for instance, argued that it would be best to compare findings between two analyses; one that excludes the outliers and vice versa; especially when the origin of those outliers is unknown. A comparable result

between the two analyses implies that the presence of the outliers is not concerning. Conversely, if the result differs significantly, the root causes of the problems need to be examined before conclusions can be drawn from the research. Yet, this approach is not feasible in practice as argued by Knott et al. (2023).

Outliers are typically observed as extreme values in the elongated tail of a skewed distribution or at both ends of a symmetric distribution (Abdiweli, 2023; Domanski, 2020; Wada, 2020). These types of non-normal distributions are commonly encountered across many control charts' applications (John & Subhani, 2020; Riaz et al., 2021; Taboran et al., 2021). Thus, with importance of control charts across many areas in industries (Emad et al., 2023; Tegegne et al., 2022), there have been continuous efforts over the years to mitigate the effect of outliers on the performance of control charts. In the past decade, many of these efforts have concentrated on robustifying control charts' structure via the use of robust estimators (Ahsan et al., 2020).

Typically, control chart utilizes classical parameters hence known as the standard control chart which is constricted to the normality assumption. Nevertheless, in practical situations, many processes such as semiconductor (Zhuang et al., 2023), economic activity (Nariswari & Nugraha, 2020), and finance (Sunaryo, 2021) are not normally distributed. Often, practitioners' persistent use of the standard control charts on these non-normal processes would result in misinterpretation of the signals. Consequently, costing money and time (Galetto, 2020; Riaz et al., 2021; Shper et al., 2023).

According to Yourstone and Zimmer (1992) concluded that the impact of skewness and kurtosis could be substantial on the ARL_0 of the standard Shewhart chart. As a solution, the researchers proposed non-symmetrical control limits for the chart in dealing with non-normal data. Thus, the chart is able to balance the Type I and Type II errors. By using a heuristic approach, Samanta and Bhattacherjee (2004) employed a weighted variance (WV) method to adjust Shewhart control limits when subjected to skewed distributions. Aiming to control the occurrence of false alarms when the underlying process follows skewed distributions, the method is not suitable when dealing with symmetric heavy-tailed distribution.

2.4 Shifts Detection via Control Charts

The popularity of the Shewhart chart among practitioners in SPC is mainly due to its simple structure that can be easily constructed. However, apart from the normality issue, the Shewhart chart frequently fails to capture shifts in the process when the change is not large (Alduais & Khan, 2023; Sabahno &Amiri, 2023). This limitation is due to the exclusion of past information from the samples in the process; a restriction commonly associated with a memoryless control chart (Diko et al., 2020; Ottenstreuer et al., 2023; Peerajit, 2023). This limitation can be overcome through the application of the memory-type control charts.

The CUSUM and EWMA are the two charts initially introduced as memory-type control charts in SPC. These control charts provide better protection against small and moderate process shifts (Aslam et al., 2021; Malela-Majika, 2021). The merits of the CUSUM and EWMA charts have been widely explored by several

researchers such as Aslam et al. (2021), Faisal et al. (2018), and Nazir et al. (2015) who emphasized that these memory-type charts are good in controlling the false alarm rate under non-normal distributions.

Research focus on the memory-type control charts have been seen increasing since they were first introduced (Jensen et al., 2018). According to Sanusi et al. (2017), Lucas (1982) explored the combination of the Shewhart-CUSUM (CSC) chart by adding the Shewhart limits to CUSUM chart. This modification aimed to improve detection of large shifts while maintaining CUSUM's sensitivity to smaller shifts by widening the control limits of the two charts. However, the study found that this approach was less effective in detecting large shifts when compared to the standard Shewhart chart. For further improvement, a combined Shewhart-EWMA (CSE) chart was recommended by adding the Shewhart control limit to the EWMA chart (Lucas & Saccucci, 1990). The chart has a good performance in terms of the ARL values, akin to the CSC chart. Subsequent discussions on the combined Shewhart-EWMA control chart and its application are covered by Malela-Majika et al. (2022), Nawaz and Han (2020), and Shamsuzzaman et al. (2023).

2.4.1 Detection Ability of Various Control Charts

The modification of the standard CUSUM chart to avoid delay in detecting out-of-control situations was covered by Lucas and Crosier (1982). The approach, known as fast initial response (FIR), is useful when a shift allegedly occurs right upon start-up or restart. While the standard procedure requires the CUSUM chart statistics (C_i^+ and C_i^-) to be set at 0, the FIR procedure sets them to some positive (nonzero) constant. This is to allow an out-of-control condition to be detected in fewer runs unlike in the standard CUSUM procedure. The initial value is suggested at half of the CUSUM limit, *H* (Lucas & Crosier, 1982). The same initial feature was incorporated in the EWMA structure which is fast to detect than the standard EWMA chart (Steiner, 1999).

Unlike the EWMA chart, the CUSUM chart treats past and recent samples indifferently (Kuiper & Goedhart; 2023). While this feature still makes the two charts perform comparably (Haq et al., 2021; Rosa et al., 2022), an enhancement in both charts' structure is always sought-after in SPC due to the importance of monitoring small process shifts in the industries (Ali, 2020; Li et al., 2024; Nawaz et al., 2021). Yashchin (1989), for instance, proposed to assign weights to all past samples in the CUSUM structure, just like the EWMA. The weighted CUSUM chart outperforms the standard CUSUM in detecting small shifts (Shu et al., 2011).

The CUSUM charts as discussed previously in this section are designed based on a specific shift size. Zhao et al. (2005) argued that in practice, the exact value of any shift to occur in a process is typically unknown and may vary within a certain range

than the predicted one. Thus, Zhao et al. (2005) proposed a dual CUSUM (DCUSUM) chart to simultaneously monitor shifts in the process. The chart combines two CUSUM charts where an out-of-control condition is signaled when either of the CUSUM charts signals. The findings revealed that the DCUSUM chart surpasses the standard CUSUM and CSC charts. Meanwhile, Jiang et al. (2008) introduced an adaptive CUSUM (ACUSUM) chart which performs more superior than the adaptive EWMA (AEWMA) chart by Capizzi and Masarotto (2003). Both adaptive charts make use of a parameter adjustment on the standard charts.

The use of run rules schemes was introduced by Riaz et al. (2011) in the CUSUM control structure for monitoring shifts in the mean. In their study, three run rules were proposed, Rule 1: $T(1,1,a,\infty)$, Rule 2: $T(2,3,b,\infty)$ and Rule 3: $T(4,5,c,\infty)$. Rule 1 is designed to detect large shifts, relying on a single point falling above or below the centerline. Rule 2 focuses on smaller shifts and requires two out of three consecutive points falling outside of the centerline. Rule 3 requires four out of five consecutive points falling outside of the centerline. The approach yields better ARL_1, which can quickly detect a shift in a process compared to the standard CUSUM and EWMA charts. It was also claimed to outperform the ARL_1 of the enhanced CUSUM based on the FIR and weighted approaches upon small to moderate shifts. Yet, the run rule schemes as commonly seen in the Shewhart's application (Shan & Huang, 2021; Shongwe & Malela-Majika, 2022) shall be applied carefully since the boast in the detection may come at the cost of increasing the false alarm rates (Koutras, 2007; Lu et al., 2020; Yeganeh & Shadman, 2021). Abbas et al. (2011) proceeded to apply

the run rule schemes in discussing the performance of the EWMA chart in which they claimed to now improve the sensitivity of the chart for small shifts.

Recently, Abbas et al. (2013a) introduced a new chart for process location. The chart retains the salient features from both CUSUM and EWMA as it was constructed by integrating the EWMA chart statistics into the CUSUM original control structure. As a result, this newly introduced chart; known as mixed EWMA-CUSUM (MEC), claimed to surpass the original memory-type control charts in monitoring very small shifts in the process. Abbas et al. (2013b) focused on combining both the CUSUM and EWMA charts known as CS-EWMA to monitor shifts in process dispersion. The CS-EWMA chart plots the cumulative sum of the exponentially weighted moving averages to signal a change when a process is out-of-control. When comparing the CS-EWMA chart's performance against the standard CUSUM and EWMA charts based on the ARL, it was shown to be superior for both small and large shifts in the process dispersion.

Ajadi et al. (2016) enhanced the performance of the MEC control chart with various FIR features, known as the MEC head start (MECHS), MEC fast initial response (MECFIR), and the MEC with the combination of the FIR and head start (HS) features denoted as MECFIRHS. They also proposed the MEC with run rules (MECRR) chart via 2/3 run rule schemes. The proposed charts are then compared with existing charts, including the standard CUSUM and EWMA, the FIR CUSUM and EWMA, as well as the CUSUM and EWMA with 2/3 run rule schemes. The comparisons showed that the proposed charts are superior in a smaller shift detection than the existing charts.

Following the success demonstrated by Abbas et al. (2013a) and Abbas et al. (2013b), Zaman et al. (2015) proposed an inverted version of the MEC control chart; nowadays known as a mixed CUSUM-EWMA (MCE) control chart. The MCE control chart was shown to be just as effective as the standard CUSUM and EWMA charts but better than the standard Shewhart $\bar{X}$ chart across magnitudes of shifts. In their work, Zaman et al. (2015) claimed that the inverted version of the MEC chart outperforms the original version in detecting various magnitudes of shifts, δ, starting from $\delta = 0.5\sigma$ if the MCE chart is designed for $\lambda \geq 0.5$. Thus, meeting the demand of fast detection of small process shifts in many areas of SPC. Measured in a standard deviation unit, a small shift is defined to be less than 1.5σ (Montgomery., 2009; Alwan et al., 2023). For moderate and large shifts, δ is usually set at $1\sigma \leq \delta \leq 2\sigma$ and $\delta > 2\sigma$, respectively.

While the Shewhart chart is known to be effective when δ is large, Zaman et al. (2015) have shown that the proposed MCE control chart can outrun the Shewhart's performance for varying choices of λ unlike seen in the MEC chart's performance. This ARL finding was supplemented with the standard deviation run length (SDRL). Notably, across a wide range of λ used in designing the charts, the difference in the SDRLs between the MCE and MCE charts diminishes when $\delta \geq 1.25\sigma$.

Continuing their previous work on monitoring process location, Zaman et al. (2016) then focused on process dispersion. The MCE chart control structure now centered on the transformation of the sample variance via three different approaches, yielding three

new MCE charts denoted as MCE-*T*, MCE-*J*, and MCE-*V*. The findings revealed that the performance of the three charts is superior by rapidly detecting the shifts process dispersion when compared to the following dispersion charts: S^2-EWMA (Castagliola, 2005), CUSUM-S^2 (Castagliola et al., 2009), and CS-EWMA (Abbas et al., 2013b).

Most recently, Abbas (2018) proposed a newer version of the memory-type control chart known as homogeneously weighted moving average (HWMA) chart. Unlike the EWMA chart, the HWMA chart assigns equal weight to the previous samples and claims to surpass the performance of the standard CUSUM, EWMA and MEC charts when designed with a small λ value. Yet, the practice of assigning equal importance to the past samples is claimed to be biased, especially at the beginning of the process monitoring (Knoth et al., 2021, 2023).

The improvement in the performance of the memory-type charts over the Shewhart chart is laudable. Moreover, the recent MEC and MCE control charts offer an advantage over the standard CUSUM and EMWA charts upon relatively small changes in the process. Yet, they are still confined to the normality assumption as these standard charts use the sample mean and the sample standard deviation in their control structure, making them highly susceptible to the presence of outliers (Chaudhary et al., 2023).

2.5 Approaches upon Deviation from the Normality Assumption

Continuous works in SPC have been concentrated on limiting the effect of outliers; focusing on balancing the Type I and Type II errors on charts' performance. The following subsections explain the works involved in detail.

2.5.1 Nonparametric Control Charts

To accommodate many practical situations that usually involve non-normal data, works concentrating on a distribution-free method, i.e., a nonparametric chart, have been explored in SPC. Earlier on, many works concentrated on modifying the Shewhart chart to not be restricted to the normality assumption. For instance, Amin et al. (1995) proposed a nonparametric control chart for the Shewhart based on sign test statistics. Later, Chakraborti et al. (2009) proposed two nonparametric Shewhart control charts to monitor process location which limits are constructed via two specified order statistics in Phase I data. The detection in Phase II employs some runs-type signaling rules. The chart statistic can be any order of statistic in Phase II data; the median is used in the study for its simplicity and robustness. The results show that the proposed approaches are robust regarding the ARL performance, supplemented by the SDRLs.

Chakraborti and Wiel (2008) also applied the Mann-Whitney Statistic on the nonparametric Shewhart chart and observed that it is superior to the parametric Shewhart chart, which is based on the sample mean, when the underlying process follows heavy-tailed and skewed distributions. Moreover, Jones-Farmer et al. (2009) proposed to use a mean-rank signal in signaling an out-of-control process via the

Shewhart chart. Their study strictly focuses on the use of a control chart in Phase I for getting representative samples to be used for estimating the Shewhart's limit later. When comparing the mean-rank chart with the Shewhart $\bar{X}$ chart via the Monte Carlo simulation, the nonparametric chart always signals better across normal and skewed distributions.

Mukherjee et al. (2019) constructed nonparametric EWMA and CUSUM charts based on the Wilcoxon rank-sum, Hogg-Fisher-Randle (HFS), and precedence test statistics for monitoring process location. These nonparametric charts were identified as NPEWMA and NPCUSUM, respectively, and showed superior performance over the standard charts, particularly in detecting small and moderate shifts under skewed distributions. Additionally, Abbas et al. (2020) introduced the nonparametric double EWMA chart by utilizing the Wilcoxon signed-rank statistic for monitoring process location. Their chart displayed an improved out-of-control performance when compared to these nonparametric charts: the EWMA sign chart, as well as the CUSUM and EWMA signed rank charts. Meanwhile, Yue and Liu (2022) opted for a progressive approach for monitoring a change in process dispersion. Their more recent work extended the progressive approach for a chart to simultaneously monitor process location and dispersion parameters.

Many works on the nonparametric control charts focus on ranking information among observations (Hawkins & Deng, 2010; Jones-Farmer et al., 2009; Li et al., 2010; Zou et al., 2012). Some of the nonparametric control charts are based on data categorization and category data analysis (Qiu & Li, 2011).

However, the nonparametric charts are claimed to be less efficient (i.e., fail to signal out-of-control conditions), compared to their parametric counterparts, and less popular among control chart practitioners due to failure of incorrect non-rejection of untrue null hypothesis (Smajdorova & Noskievicova, 2016).

To balance a good control of the false alarm rates while maintaining charts' capability to fast detect an out-of-control condition, robust approaches have been tackled by many SPC researchers.

2.5.2 Robust Control Charts

As discussed in the previous section, nonparametric control charts pose some limitation. Thus, a robust approach is favored in SPC since with non-rigid distributional assumption, it is still considered to be part of the parametric models and thus, retaining its merits (Huber, 1981).

Focusing on the robust approach, Langenberg and Iglewicz (1986) recommended estimating process parameters of the Shewhart chart in Phase I via the trimmed mean of subgroup averages and trimmed mean of subgroup ranges. This robust approach was subsequently shown to be less affected by outliers than the standard Shewhart $\bar{X}$ chart. Meanwhile, Rocke (1992) suggested control limits defined by the mean of the subgroup interquartile ranges in constructing the Shewhart charts for monitoring location and dispersion, separately. Both location and dispersion robust charts were claimed to be good in detecting occasional outliers.

Meanwhile, Hawkins (1993) proposed to winsorize the observations in Phase I in limiting the effect of outliers on the parameter estimation. A winsorized approach focuses on limiting the effect of outlier, rather than eliminating it. The identified outliers that are supposedly trimmed will now be replaced by the highest and lowest end of the 'clean' data (Dixon & Tukey, 1968; Tukey & McLaughlin, 1963). Thus, keeping the original number of observations. Dixon and Tukey (1968), and Rivest (1994) claimed that this approach works well under skewed distributions. The approach was first taken by Hawkins (1993) in SPC by winsorizing the subgroup mean and range to limit the effect of outliers on the CUSUM chart's performance. This work concentrates on making the CUSUM chart performs well in signaling out-of-control conditions while still maintaining the occurrences of the false alarm to the nominal value under non-normality.

Focusing on robustifying the Shewhart control structure, Abu-Shawiesh and Abdullah (1999) applied robust estimators, namely, the Hodges–Lehmann (*HL*) for the location parameter and the Shamos-Bickel-Lehmann (*SBL*) for the scale parameter. Both the *HL* and *SBL* estimators have 29% *BP*, thus, giving the Shewhart chart a good performance under heavy-tailed distributions. Notably, the robust chart performance is getting better with a large sample size when tails become heavier, unlike the standard Shewhart chart.

Abu-Shawiesh (2009) focused on the sample median and the median absolute deviation about sample median (*MADn*) for estimating the Shewhart limit. By replacing the classical estimators with the robust estimators, the chart which was tested under various non-normal distributions, indicates the ability to control Type I and

Type II error, unlike the standard Shewhart $\bar{X}$ chart. Similarly, Wu et al. (2002) employed several robust scale estimators, namely the *MADn*, average absolute deviation to the median (*AADM*), and median of average absolute deviation (*MAAD*) to estimate the process dispersion in the Shewhart $\bar{X}$ chart. These robust estimators were again proved to limit the effect of outliers on the control chart's performance. Focusing on monitoring dispersion in the process, Abu-Shawiesh (2008) employed the median absolute deviation (*MAD*) in a Shewhart chart. Similarly, Adekeye (2012) used the *MAD* to construct control limits for the Shewhart $\bar{X}$ chart and Shewhart *S* chart. In both works, the robustification improves the detection capability of the Shewhart charts upon violation of the normality assumption.

The application of the *MAD* or *MADn* is popular in SPC as a pairing for robust location estimators in Phase I, or in constructing a dispersion chart since this robust scale estimator is highly unaffected by the outliers. Sindhumol et al. (2016) claimed that the *MAD* can provide a better estimate when compared to the Gini's Mean Difference (*G*) which is another robust scale estimator. Between these two robust scale estimators, a control chart for monitoring mean shift shows a better control of the false alarm rate in the presence of outliers when the *MAD* was used in Phase I to estimate the process dispersion (Sindhumol et al., 2016).

The use of robust statistics in SPC is not only commendable in Phase I but also in the Phase II when applications involve memory-type charts. A memory-type chart is specifically designed to detect a difference in the mean of a process. Thus, a user is focusing on an upward or downward shift in the process mean until it eventually causes the mean value to be out-of-control. Therefore, as argued by Rocke (1989),

"outliers in the subgroup should not cause a signal to occur since they do not directly represent a shift in the mean". Therefore, in limiting the effect of outliers on the chart statistic, a robust statistic is favored in place of the sample mean in Phase II. It is worth to note that the robust work in Phase I focuses on parameter estimation when Phase I data are non-normal. Meanwhile, the robust statistic employed in Phase II concentrates on the calculation of the chart statistic when Phase II data are non-normal. Several notable studies that focus on robustifying the memory-type charts on both phases are discussed next.

Nazir et al. (2016) substituted several robust location estimators such as trimmed mean, *HL*, tri-mean, midrange, and median, in the plotting statistics of the CUSUM, EWMA, and MEC control charts. These memory-type charts were then tested for normal and contaminated normal distributions. Assessments via the ARL and varying percentiles of the run length (RL) distribution reveal that no chart was found to satisfactorily perform the best in all conditions. However, their study concluded that the EWMA chart with the median estimator consistently performs the best across most of the conditions specified.

The advantage of using the median charts, i.e., charts that focus on the sample median in its plotting statistics, over the standard chart as well as other robust control charts has been demonstrated by many researchers. See for examples, Abdul-Rahman et al., (2018, 2021), Ahmad et al., (2014), Mim et al. (2023), Noor et al. (2023, 2024), Park (2009), and Yang et al. (2010). However, since the distribution of the sample median is unknown, constructing a median control chart typically relies on a simulation in deriving the standard error of the estimator.

Most recently, Abbas et al. (2018) proposed a mixed control chart that is based on the EWMA and dual CUSUM (DCUSUM) charts for monitoring process location. Known as mixed EWMA DCUSUM, the chart was constructed with five different estimators, namely mean, median, midrange, tri-mean and *HL*, and evaluated based on the ARL under normal and contaminated data. The finding shows that the proposed chart, when constructed with the robust tri-mean estimator, is the most superior among others. Even though the charts based on the *HL* and median estimators are less superior to the tri-mean chart under contaminated data, they are still better than the mean chart. Abdul-Rahman et al. (2018) proposed the EWWA chart using the *MOM* estimator which is claimed to gain good control of the false alarm rate (supported by the robust ARL_0) under heavily skewed distribution while maintaining quick detection under various skewness levels. In their subsequent work, i.e., Abdul-Rahman et al. (2020), the same good performance is observed when integrating the robust estimator into the CUSUM control structure. Recently, Noor et al. (2024) published a finding on the MEC chart under the *g*-and-*h* distribution, emphasizing that the *MOM* estimator offers a robust performance to the chart under in-control and out-of-control conditions, not only when data are skewed but also heavy-tailed.

2.6 Robust Estimators

The classical estimators, i.e., the sample mean and sample standard deviation, are highly susceptible to the effect of outliers. Thus, in the context of SPC, outliers may appear in Phase I and/or Phase II, causing the performance of the standard control chart to deteriorate as discussed in Section 2.3. Notable robust works as introduced in Section 2.4 attested to the superiority of the robust statistics over the classical estimators. This is due to a high breakdown point (*BP*) and bounded influence function possessed by robust statistics.

2.6.1 Properties of Robust Estimators

The robustness of a statistical procedure is commonly assessed via the *BP* (Raymaekers & Rousseeuw, 2023), statistical efficiency and influence function (Hampel, 1986). The concept of BP was introduced by Hampel (1968) and Hampel (1971) who defined the *BP* as the percentage of outliers or contaminated data that would cause a calculation for an estimator in a finite sample to deviate significantly from the parameter value. The same explanations were given by Donoho (1982) and elaborated by Donoho and Huber (1983). Geyer (2006) introduced a concept known as the finite sample *BP* for an estimator which describes the proportion of data that can be assigned arbitrary values without causing a significant decline in the estimator's performance. Typically, this *BP* is expressed as a function of a sample size, *n*. To simplify this concept into a single numerical value, Geyer (2006) also introduced the concept of the asymptotic *BP*. The asymptotic *BP* represents the limit of the finite sample *BP* as *n* approaches infinity. Since then, the *BP* has been used to evaluate the robustness of scale, regression, and other situations (Alshqaq & Abuzaid, 2023; Dibal

& Dallah, 2021; Fan et al., 2023; Fishbone & Mili, 2023; Liu et al., 2023; Lopuhaa, 2023).

Donoho and Huber (1983) defined the *BP* of T at X is ε^*, as $\varepsilon^*(X,T) = inf\{\varepsilon: b(\varepsilon;X,T) = \infty\}$, where $X = (x_1, x_2, \dots, x_n)$ be a fixed sample of size n, $T = \{T_n\}_{n=1,n=2,}$ ... be an estimator with values in some Euclidean space, ε^* is the smallest value of $\varepsilon = \frac{m}{n}$ with replacing an arbitrary subset of size m of the sample by arbitrary values $Y = (y_1, y_2, \dots, y_m)$, $b(\varepsilon;X,T) = sup|T(X') - T(X)|$ with $T(X)$ be its value at sample X. Following that, the *BP* for the sample mean is $\frac{1}{n}$. In other words, a single outlier can significantly disrupt the estimation of this estimator. Conversely, the *BP* of the sample median in a finite sample is $\frac{n-1}{2n}$.

Another robust property is the influence function that was introduced by Hampel in 1968. For an estimator to be robust, its influence function must be bounded, meaning it limits the impact of outliers (Hampel, 1974). According to De Menezes et al. (2021), the influence function, ψ, represents the impact of outliers, often measured as a multiple of the standardized residual, ξ, on the estimator. The influence function is the first derivative of function ρ with respect to the ξ, and can be defined as $\psi(\xi) = \frac{\partial\rho(\xi)}{\partial\xi}$. The classical mean has unbounded influence functions, meaning that a single outlier can affect the mean.

The efficiency refers to the performance of an estimator in fitting the data when the errors follow a different distribution than expected, usually assumed as normal distribution (De Menezes et al., 2021). The smaller the variance in its sampling

distribution, the more efficient is the estimator (Serfling, 2009). The classical mean is the most efficient location estimator for the normal distribution but not the best location estimator when the assumptions are not met. The loss efficiency of classical estimators when all assumptions are not satisfied is estimated to be in the range 5% to 50% (Hampel, 1986). The robust estimator is more resistant to departure of normality and the presence of outliers.

2.6.2 Robust location estimators

Notably, the asymptotic *BP* of the sample mean is 0%. Meanwhile, the asymptotic *BP* of the sample median is 50%, which is the highest possible *BP* for location (Acharya et al., 2022; Santhanasamy & Abdul-Rahman, 2022). A *BP* of 50% implies that the sample median can tolerate up to 50% of outliers in the dataset before its calculation is disrupted. Another robust estimator with 50% *BP* is the *M*-estimator of location which was introduced by Huber (1981). Yet, despite gaining significant attention in various fields, including statistics, economics, and machine learning, due to its capability to handle data containing outliers, the *M*-estimator does not produce a unique solution, which may pose a disadvantage to practitioners (Crisp & Burridge, 1993). Alternatively, Wang et al., (2007) introduced a weighted randomly trimmed means as the robust location estimator and proved that the estimator possesses the highest breakdown point as the sample median. This robust location estimator is recommended upon a heavy-tailed distribution while the Huber's *M*-estimator is seen as more suitable for the light-tailed distribution (Wang et al., 2007).

Other notable robust estimators commonly used in SPC have a *BP* that hovers between 0% and 50%. For instance, the (k/n)-trimmed mean which averages the data except for *k* smallest and *k* largest observation is noted with the *BP* of $(k\ +\ 1)/n$, while the *BP* of the *HL* is 29% (Rousseeuw & Verboven, 2002). With a lower *BP*, the *HL* and the trimmed mean are more susceptible to the outliers and thus, considered to be less robust than the sample median.

Often, it is recommended to remove or provide less weightage to the outliers in the dataset so that its effect on the parameter estimation can be minimized (Sindhumol et al., 2016). Proposed by Tukey (1948), the trimmed mean estimator, as briefly discussed, focuses on symmetric trimming in removing outliers from the dataset (Tukey, 1948). However, the trimmed mean estimator focuses on the symmetric trimming. Thus, this robust approach works best only when outliers appear on both tails of the distribution. Another alternative to the trimmed mean estimator is the scaled deviation trimmed mean proposed by Wu and Zuo (2009) which is recommended upon a light-tail symmetric distribution. However, this robust location estimator still assumes the symmetric trimming approach in eliminating outliers. For asymmetric trimming, the *MOM* estimator, which was proposed by Wilcox and Keselman (2003a), is more effective. This robust estimator uses trimming criteria based on the sample median and the *MADn* (thus, yielding a 50% *BP*) to flag outliers on either side (or both) of the tails. The identified outliers will be removed before averaging the remaining observations. Therefore, without outliers as in normal distribution, *MOM* becomes the classical mean estimator. This makes the *MOM* estimator flexible and can adapt to the presence or absence of outliers.

The *MOM* estimator is also claimed to possess better efficiency, i.e., smaller standard error, when compared to the 20% trimmed means when outliers are very common (Wilcox, 2003).

Later, Haddad et al. (2013) proposed a winsorized version of the *MOM*, known as the *WMOM* estimator, to limit the effect of outliers on the multivariate version of the Shewhart chart for process location. Rather than excluding the outliers in averaging the dataset, the *WMOM* replaces the identified outliers based on the *MOM* trimming criteria with the smallest and largest value in the 'clean' dataset. Thus, like the *MOM*, the *WMOM* possesses a 50% *BP* as its trimming criteria are based on the sample median and the *MADn.*

2.6.3 Robust scale estimators

Median absolute deviation (*MAD*) was proposed by Hampel (1974). Implemented in numerous applications, the *MAD* has the highest *BP* for the scale, i.e., 50%, which is double of interquartile range (IQR) *BP* (Rousseeuw & Croux, 1993). This high *BP* compensates for its drawback, i.e., only 37% of efficiency under normality as opposed to 64% by the sample median when data are highly contaminated (Rousseeuw & Croux, 1993). The *MAD* is frequently compared to the *G* estimator as discussed briefly in section 2.4.2. The *G* estimator was introduced by Gini (1912) and noted with an extremely high efficiency at 98% (David, 1981). With 50% *BP*, the *G* estimator is very robust unlike the sample standard deviation (Saeed & Kamal, 2016). While the *MAD* is more popular due to the highest *BP* and simple structure of the estimator. the application of the *G* estimator as a scale measure

has been discussed positively by Ceriani and Verme (2012), Riaz and Saghirr (2007), and Yitzhaki and Lambert (2012).

2.7 Summary of Research Work in SPC

Sections 2.1 – 2.5 discussed the application of the robust methods within the context of SPC. The discussion concentrated on the negative influence of outliers on the ARL performance and how the robust statistics can mitigate their effect in process monitoring. The significance of the robust methods extends beyond their application in SPC since the methods are not restricted to the underlying distributional assumption. Thus, they can work well across many data scenarios and applications.

In SPC, the performance of the standard charts deteriorates as data deviate from normal. Comparison between the robust charts and their standard counterparts under heavy-tailed, skewed distribution, or contaminated distributions indicates that in the majority of the situations, the robust charts supersede the detection capability of the standard charts. Yet, in SPC, finding a good balance between the Type I and Type II errors is still an ongoing study. This is due to the unpredictable nature of the underlying process.

Getting the balance ARL chart ($ARL_0 > ARL_1$) is always the goal in SPC as it indicates that the chart can quickly signal shifts in the process. Yet, if $ARL_0 \approx 370$ is desirable, how far can we allow the ARL_0 to deviate from its nominal value under non-normality before conceding that the chart is no longer robust. This issue was noted by Woodall (2017) who also emphasized that the control of the false alarm rate has always been important in SPC research.

Thus, the key implementation to a reliable control chart is via the robust ARL_0. Without it, the chart's detection capability is questionable as noted in the work by Human et al. (2011) and Abdul-Rahman (2020). Therefore, constructing a reliable control chart that passes the ARL evaluation is important before applying it in real practice since 'controlling' the ARL_0 can only be done theoretically but not in practice.

CHAPTER THREE
RESEARCH METHODOLOGY

3.1 Introduction

The focus of this study is on the monitoring of process location via two distinct memory-type charts known as the mixed EWMA-CUSUM (MEC) and the mixed CUSUM-EWMA (MCE). By employing three locations estimators with the highest possible breakdown point (*BP*), namely the median, modified one-step M-estimator (*MOM*), and winsorized *MOM* (*WMOM*), six new robust memory-type control charts were produced as listed in Table 3.1. Notations in the third column of Table 3.1 are used throughout the thesis, henceforth.

Table 3.1

The Proposed Control Charts

Control Chart	Location Estimator	Proposed Control Charts
MEC	median	$MEC_{\tilde{X}}$
	MOM	MEC_{MOM}
	WMOM	MEC_{WMOM}
MCE	median	$MCE_{\tilde{X}}$
	MOM	MCE_{MOM}
	WMOM	MCE_{WMOM}

Unlike the Shewhart control chart, which is categorized under the memory-less control chart, and thus, less sensitive in detecting small process shifts ($\delta \leq 1.5$) (Montgomery, 2009), the MEC and MCE charts are claimed to perform well under this scenario (Nazir et al. 2015; Zaman et al., 2015). Thus, focusing on the small and moderate shift detection, the six newly proposed robust charts (in Table 3.1) were designed and assessed based on the ARL under in-control and out-of-control states via Monte Carlo simulation studies. Figure 3.1 depicts the flowchart of the simulation study.

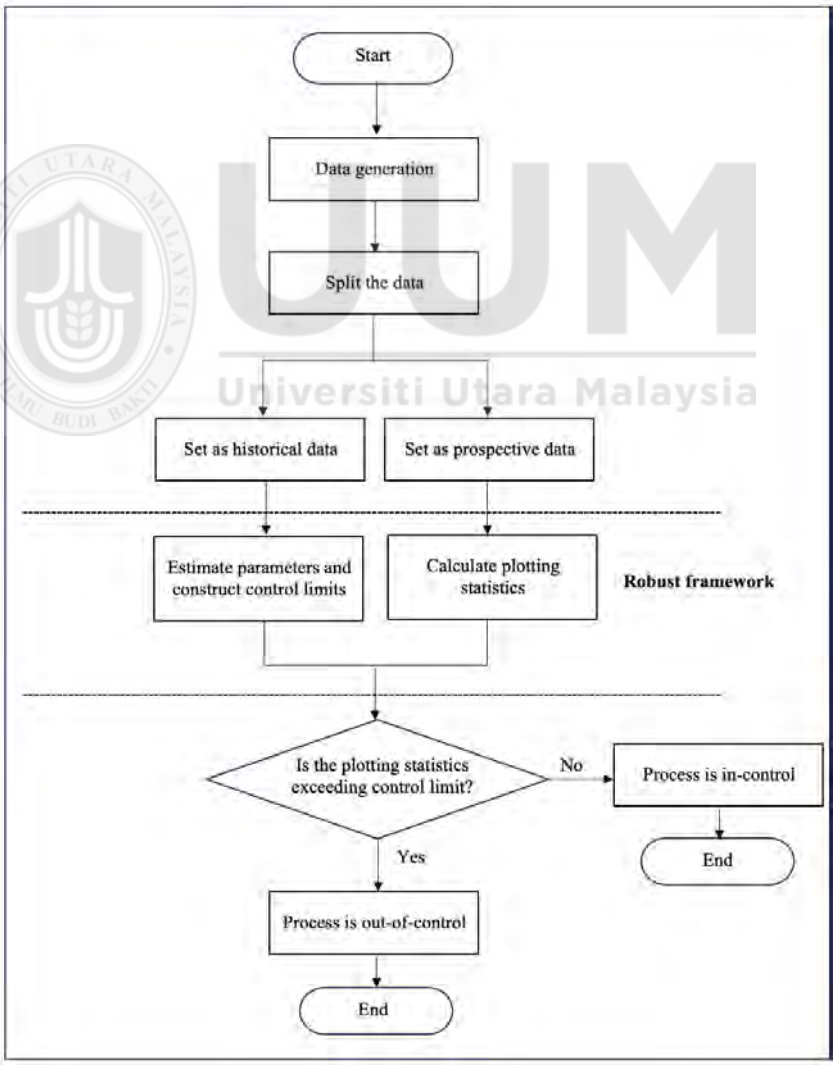

Figure 3.1 Flowchart of the Simulation Study

3.2 Construction of the Memory-Type Control Charts

The subsequent subsections focus on the structure of the MEC and MCE charts for monitoring process location. To equip the reader with the structure of the charts, the discussion starts with the two original memory-type charts, namely the CUSUM and EWMA.

3.2.1 CUSUM $\hat{\theta}$ control chart

The CUSUM chart involves two chart statistics, namely C_i^+ and C_i^-, for detecting an upward shift and a downward shift in the process location, respectively. Both are defined as follows (Montgomery, 2009):

$$C_i^+ = max\left[0, \left(\hat{\theta}_i - \theta_0\right) - K_{\hat{\theta}} + C_{i-1}^+\right], \quad \text{for } i = 1, 2, 3, \ldots, m \tag{3.1}$$

and

$$C_i^- = max\left[0, -\left(\hat{\theta}_i - \theta_0\right) - K_{\hat{\theta}} + C_{i-1}^-\right], \quad \text{for } i = 1, 2, 3, \ldots, m \tag{3.2}$$

where i = the sample number, m = the subgroup number, $\hat{\theta}$ = estimator of location parameter θ, θ_0 = in-control location parameter, $K_{\hat{\theta}}$ = reference value, and $H_{\hat{\theta}}$ = control limit.

The initial value of the chart statistics is usually set at 0 ($C_0^+ = 0,\ C_0^- = 0$) (Abbas et al., 2013a). The chart signals an out-of-control condition when either of the C_i^+ or C_i^- exceeds the $H_{\hat{\theta}}$. Typically, the parameters $K_{\hat{\theta}}$ and $H_{\hat{\theta}}$ are standardized as in Equations (3.3) and (3.4) so that they are not influenced by the standard deviation of

the sampling distribution (Abdul-Rahman, 2020).

$$K_{\hat{\theta}} = k \times \sigma_{\hat{\theta}} \tag{3.3}$$

and

$$H_{\hat{\theta}} = h \times \sigma_{\hat{\theta}} \tag{3.4}$$

where $\sigma_{\hat{\theta}}$ is the standard deviation of $\hat{\theta}$, and *k* and *h* are the constants that are chosen to satisfy a pre-determined ARL_0, respectively. A common practice is to set *k* at half of the standard deviation of $\hat{\theta}$ to make the chart responsive to small and moderate shifts in the process mean (Montgomery, 2009) and derive the *h* corresponding to the chosen *k* value to achieve the pre-determined ARL_0, say 370, under normality.

It shall be noted that the description used for the *i*, *m*, $\hat{\theta}$, and $\sigma_{\hat{\theta}}$ are carried through, henceforth.

3.2.2 EWMA $\hat{\theta}$ control chart

The EWMA control structure is defined as (Roberts, 1959):

$$Z_i = \lambda\hat{\theta}_i + (1-\lambda)Z_{i-1} \qquad \text{for } i = 1, 2, 3, \ldots, m \tag{3.5}$$

$$UCL_i = \theta_0 + L_{\hat{\theta}}\sqrt{Var(\hat{\theta})\frac{\lambda}{2-\lambda}(1-(1-\lambda)^{2i})} \tag{3.6}$$

$$LCL_i = \theta_0 - L_{\hat{\theta}}\sqrt{Var(\hat{\theta})\frac{\lambda}{2-\lambda}(1-(1-\lambda)^{2i})} \tag{3.7}$$

where $L_{\hat{\theta}}$ is a positive constant that determines the width of the EWMA control limits and λ is the smoothing constant that takes a value between 0 and 1 $(0 < \lambda \leq 1)$. The initial value, Z_0, is typically set at θ_0, i.e., in-control location parameter. The Z_i in Equation (3.5) is compared against the upper control limit (UCL) and the lower control limit (LCL) as defined in Equations (3.6) and (3.7). The constant $L_{\hat{\theta}}$ are chosen based on the specified λ to achieve the pre-determined ARL_0 under normality.

The control limits specified by Equations (3.6) and (3.7) are time-varying limits. When i in Equation (3.6) and (3.7) are approaching infinity $(i \to \infty)$, the control limits become asymptotic limits. Thus, UCL_i and LCL_i become:

$$UCL_i = \theta_0 + L_{\hat{\theta}}\sqrt{Var(\hat{\theta})\frac{\lambda}{2-\lambda}} \tag{3.8}$$

$$LCL_i = \theta_0 - L_{\hat{\theta}}\sqrt{Var(\hat{\theta})\frac{\lambda}{2-\lambda}}. \tag{3.9}$$

3.2.3 MEC $\widehat{\theta}$ control chart

Introduced by Abbas et. al (2013a), the MEC chart integrates the EWMA chart statistic (defined in Equation (3.5)) into the CUSUM control structure (defined in Equations (3.1) and (3.2)). The MEC chart statistics are defined as:

$$MEC_i^+ = max\left[0, (Z_i - \theta_0) - K_{z_i} + MEC_{i-1}^+\right], \quad \text{for } i = 1, 2, 3, \ldots, m \tag{3.10}$$

and

$$MEC_i^- = max\left[0, -(Z_i - \theta_0) - K_{z_i} + MEC_{i-1}^-\right], \quad \text{for } i = 1, 2, 3, \ldots, m \tag{3.11}$$

where the initial values, MEC_0^+ and MEC_0^-, are usually set at 0; analogous to the CUSUM chart. The MEC chart's variance is defined as:

$$Var(Z_i) = \sigma_{z_i}^2 \left[\frac{\lambda}{2-\lambda}\left(1 - (1-\lambda)^{2i}\right)\right] \tag{3.12}$$

where $\lambda \in (0, 1]$. The standardized of K_{z_i} and H_{z_i}, which are the reference value and control limits of the chart, respectively, are the function of the standard error of the chart.

$$K_{z_i} = k \times \sqrt{Var(Z_i)} \tag{3.13}$$

and

$$H_{z_i} = h \times \sqrt{Var(Z_i)}. \tag{3.14}$$

Notably, when *i* in Equation (3.9) is approaching infinity ($i \to \infty$) , $Var(Z_i)$ becomes:

$$Var(Z_i) = \sigma_{\hat{\theta}}^2 \left[\frac{\lambda}{2-\lambda}\right] \tag{3.15}$$

Thus, both K_{z_i} and H_{z_i}, become:

$$K_{z_i} = k \times \sigma_{\hat{\theta}} \sqrt{\frac{\lambda}{2-\lambda}} \tag{3.16}$$

and

$$H_{z_i} = h \times \sigma_{\hat{\theta}} \sqrt{\frac{\lambda}{2-\lambda}}\,. \tag{3.17}$$

The values of *h* and λ, paired with a fixed value of *k*, need to be derived to achieve the pre-determined ARL_0. Typically, $k = ½$ is employed to carry the salient features of the CUSUM for fast detection of small and moderate shifts (refer to Section 3.2.1).

Like the CUSUM chart, the MEC_i^+ (in Equation (3.10)) detects an upward shift in the mean until the value shifts to out-of-control. A similar explanation goes for the MEC_i^- (in Equation (3.11)) but for a downward shift in the mean. Both are compared against $H_{\hat{\theta}}$, and if either of the MEC_i^+ or MEC_i^- exceeds H_{z_i}, the process is deemed out-of-control. Otherwise, the process is in statistical control.

3.2.4 MCE $\widehat{\theta}$ control chart

The MCE control chart was introduced by Zaman et. al (2015) by integrating the CUSUM statistics (defined in Equations (3.1) and (3.2) into the EWMA control structure (defined in Equations (3.5) – (3.7)). The structure of the MCE chart, which is constructed based on two chart statistics, can be said analogous to the reversed version of the MEC chart. The MCE chart has two chart statistics, namely MCE_i^+ and MCE_i^-, for detecting an upward shift and a downward shift in the process location, respectively. Both are defined as follows:

$$MCE_i^+ = (1-\lambda)MCE_{i-1}^+ + \lambda C_i^+, \quad \text{for } i = 1, 2, 3, \ldots, m \tag{3.18}$$

and

$$MCE_i^- = (1-\lambda)MCE_{i-1}^- + \lambda C_i^-, \quad \text{for } i = 1, 2, 3, \ldots, m. \tag{3.19}$$

The CUSUM statistic, C_i^+ and C_i^-, are defined as in Equations (3.1) and (3.2). Following the EWMA chart, the smoothing constant that determines the weight of the samples is set at: $\lambda \in (0, 1]$ and the initial values, MCE_0^+ and MCE_0^-, are taken to be equal to target mean value θ_0, as in the EMWA (i.e., $MCE_0^+ = MCE_0^- = \theta_0$).

Recalling the EWMA control structure as discussed in Section 3.2.2, the control limits of the MCE chart (UCL and LCL) follow the EWMA which are time-varying up to a specific value of *i* and become constant as $i \to \infty$. The MEC control limits are defined as follows:

$$UCL_i = \mu_{c_i} + K_c \sigma_{c_i} \sqrt{\frac{\lambda}{2-\lambda}(1-(1-\lambda)^{2i})} \tag{3.20}$$

where K_c is a positive constant that determines the width of the control limit; and μ_{c_i} and σ_{c_i} are mean and standard error, respectively.

If $i \to \infty$, the time-varying limit in Equation (3.20) becomes an asymptotic limit as defined below:

$$UCL_i = \mu_{c_i} + K_c \sigma_{c_i} \sqrt{\frac{\lambda}{2-\lambda}}\,. \tag{3.21}$$

The MEC chart signals an out-of-control condition when either of the MCE_i^+ or MCE_i^- defined in Equations (3.18) and (3.19), respectively, exceeds the UCL_i. The K_c is typically chosen for specified values of λ and k to achieve the pre-determined ARL_0 under normality.

The following section explains on the robust location estimators ($\hat{\theta}$) employed in this study.

3.2.5 Description of The Location Estimators

In this study, $\hat{\theta}_i$ in the MEC and MCE charts were estimated with the following robust location estimators, namely the median, modified one-step *M*-estimator (*MOM*), and winsorized *MOM* (*WMOM*) for monitoring process location. These median based location estimators possess the highest possible *BP* for location (50%) as discussed in Section 2.5.2 of Chapter 2. For a comparison, the classical mean is included where it was used to construct the standard MEC and MCE chart.

Suppose for a random sample of size n, $X = \{X_1, X_2, \dots, X_n\}$, then the location estimator $(\hat{\theta})$ can be defined as:

i. Mean

For a comparison purpose, the sample mean is included and can be computed as:

$$\hat{\theta} = \sum_{i=1}^{n} \frac{X_i}{n} . \tag{3.22}$$

Unlike the rest of the chosen robust estimators, the sample mean possesses 0% *BP* as discussed in Section 2.5.1 of Chapter 2. Thus, its computation can easily be corrupted when data are non-normal.

ii. Median

The sample median is defined as (Abdul-Rahman et al., 2021):

$$\hat{\theta} = \begin{cases} X_{\frac{n+1}{2}}, & \text{if } n \text{ is odd} \\ \frac{1}{2}\left(X_{\frac{n}{2}} + X_{\frac{n+2}{2}}\right), & \text{if } n \text{ is even.} \end{cases} \tag{3.23}$$

iii. Modified one-step m-estimator (*MOM*)

The *MOM* can be computed as (Wilcox & Keselman, 2003a).

$$\hat{\theta} = \frac{\sum_{i=i_1+1}^{n-i_2} X_{(i)}}{n-i_1-i_2} \tag{3.24}$$

where

$X_{(i)}$ = *i*th ordered observation

i_1 = number of observations X_i such that $(X_i - M) < -K(MAD_n)$

i_2 = number of observations X_i such that $(X_i - M) > K(MAD_n)$.

Equation (3.24) defines the trimming criteria based on *M* = median and *MADn* = 1.4826 $med_i|x_i - med_j x_j|$. The constant 1.4826 is applied in the *MADn* formula to ensure that this scale estimator remains consistent when the underlying distribution follows normal (Rousseeuw & Hubert, 2018).

A common practice is to set $K = 2.24$ to achieve high efficiency under normality when n is less than 100 (Wilcox & Keselman, 2003b). Using the *MOM* estimator, it is possible to trim a different number of observations in each tail or even, no trimming involves when the underlying distribution is normal. When data are symmetric heavy-tailed, the *MOM* will trim the data symmetrically, analogous to the usual trimmed mean estimator.

iv. Winsorized *MOM* (*WMOM*)

The *WMOM* estimator was proposed by Haddad et al. (2013) who defined it as:

$$\hat{\theta} = \frac{\sum_{i_1}^{n_j} W_{ij}}{n_j} \tag{3.25}$$

where

W_{ij} = the *i*th ordered observations in group *j* (after replacing outliers flagged in Equation 3.24)

n_j = number of observations for group *j*.

The construction of the winsorized sample is defined as follows:

$$W_{ij} = \begin{cases} X_{(i_1+1)j}, & \text{if } X_{ij} \leq X_{(i_1+1)j} \\ X_{ij}, & \text{if } X_{(i_1+1)j} < X_{ij} < X_{(n-i_2)j} \\ X_{n_j-i_2}, & \text{if } X_{ij} \geq X_{(n-i_2)j} \end{cases} \tag{3.26}$$

where

X_{ij} = the *i*th ordered observations in group *j* (before replacing outliers)

i_1 = total number of smaller outliers in the data

i_2 = total number of larger outliers in the data.

Defined in Equation (3.26), $X_{ij} \leq X_{(i_1+1)j}$ and $X_{ij} \geq X_{(n_j-i_2)j}$ are for determining the lower and upper winsorized values, respectively. That is, the values to replace the outliers flagged by the *MOM*'s trimming criteria in Equation (3.23) earlier. Following the winsorizing process, the 'clean' data ($\overline{W}_{ij}$) is obtained and used to get an average as defined in Equation (3.25).

3.2.5.1 Unknown parameter cases

In this study, the in-control parameters of the process were assumed to be unknown. Thus, the location parameter was estimated based on Phase I data which might not be representative of the process (i.e., contains outliers).

Specifically, Phase I involved two series of simulation procedures. The first series was for determining the standard deviation of the sampling distribution of the location estimator, $\sigma_{\widehat{\theta}}$, based on 10^6 iterations. The second series involves 10^4 trials of subgroup, *m*, in-control Phase I with sample size, *n*, to estimate the process mean, $\widehat{\theta}$. Let the Phase I data be represented by $Y_{ij} = \{Y_{11}, \ldots, Y_{nm}\}$ where $i = 1,2, \ldots n$ and $j = 1,2, \ldots m$. We assume that Y_{ij} to be independent and identically distributed (*i.i.d*)

following an unknown distribution W which has a mean θ_0 and a standard deviation $\sigma_{\hat{\theta}}$, $Y_{ij} \sim W(\theta_0, \sigma_{\hat{\theta}})$. The θ_0, was estimated using the mean of $\hat{\theta}$, given by:

$$\hat{\theta}_0 = \frac{\sum_{j=1}^{m} \hat{\theta}_j}{m}. \tag{3.27}$$

In Phase I of this study, θ_0 was estimated to isolate the effect of estimating the location parameter on the proposed MEC and MCE charts. This approach was emphasized by Schoonhoven et al. (2011) and later by Abdul-Rahman (2020) in their simulation studies when studying the performance of control charts for process location when parameters of the process are unknown.

3.3 Variables Manipulated

The investigation of the performance of the newly proposed robust memory-type control charts was conducted by manipulating several variables frequently discussed in SPC and commonly encountered in real practice. The following subsections focus on those variables, namely the types of distribution, design shifts (δ^*), sample sizes (n), and shift sizes (δ). Those variables were selected due to their influence on the ARL performance of the memory-type charts as illustrated later.

3.3.1 Types of Distribution

When a process fails to follow the normality assumption, the ARL value of the chart can vary substantially as discussed in Sections 2.2 and 2.3. The severity of the situation depends on the types of distribution, or the level of contamination observed in the data. Thus, in this study, *g*-and-*h* distributions were chosen to mimic normal and non-normal

distributions while analyzing their impact on the ARL performances of the newly proposed robust charts in Table 3.1.

The *g*-and-*h* distribution was introduced by Tukey (1977) which can be derived through transformations of the standard normal distribution. This transformation process allows statisticians to capture symmetric, heavy tails, and skewed data to varying degrees based on *g* and *h* values (Yan & Genton, 2019a, 2019b). Therefore, the *g*-and-*h* distribution has gained considerable attention in statistical modeling (Mondal et al., 2022), simulation studies (Astivia & Edward, 2022), and distributional shape analysis (Jorge & Boris, 1984). The *g*-and-*h* distribution has been utilized in a range of disciplines including environmental science, economics, finance, and more areas of application (Ley, 2015).

The *g*-and-*h* distribution captures the non-normality through the *g* and/or *h* parameters, as it is aptly name. Let $Z \sim N(0,1)$ denote a standard normal random variable. To generate data for the *g*-and-*h* distributions, the following steps are adhered to:

i. Generate a standard normal variate, Z_{ij}.

ii. Convert the standard normal variates to random variables as follows:

$$Y_{ij} = \begin{cases} \frac{\exp(gZ_{ij})-1}{g} \exp\left(hZ_{ij}^2/2\right), & g \neq 0 \\ Z_{ij}\exp\left(hZ_{ij}^2/2\right), & g = 0. \end{cases} \tag{3.28}$$

The parameters g and h control the skewness and kurtosis, respectively. When $g = 0$ and $h = 0$, $Y_{ij} = Z_{ij}$, represents a standard normal distribution. As h gets larger, the tails of the distribution become heavier. The same goes for g which controls the skewness. Following Wilcox (2022), four g-and-h distributions were specified as in Table 3.2 to capture possible non-normal data scenarios in SPC, that is, symmetric but heavy-tails, skewed, and skewed with heavy-tails. Henceforth, the notations in the first column of Table 3.2 are used when describing each of the chosen g-and-h distributions.

Table 3.2

The Chosen g-and-h Distribution

Distribution	**(*g*, *h*)**	**Description**
G0H0	(0, 0)	Normal distribution
G0H0.5	(0, 0.5)	Symmetric heavy-tailed distribution
G0.5H0	(0.5, 0)	Skewed normal-tailed distribution
G0.5H0.5	(0.5, 0.5)	Skewed heavy-tailed distribution

To illustrate the non-normal shape assumed by each of the chosen g-and-h distributions, their probability density functions (PDFs) and the cumulative distribution functions (CDFs) are given in the form of graphs as illustrated in columns 2 and 3 of Table 3.3. Column 1 of the table illustrates the skewness ($\hat{\gamma}_1$) and kurtosis ($\hat{\gamma}_2$) values for the respective g-and-h distribution. Row 4 of Table 3.3 is an

extreme non-normal data scenario as indicated by $\hat{\gamma}_1$ and $\hat{\gamma}_2$. Represented by G0.5H0.5, this extreme data condition was included in assessing the newly proposed robust charts' performance. The idea is that, if the proposed robust control charts can balance the Type I and Type II errors under this extreme non-normality, they shall perform well under a lesser condition in real practice.

Table 3.3

PDF and CDF of the g-and-h Distribution

Parameters	**PDF**	**CDF**
	Normal	
$g = 0$ $h = 0$ $\hat{\gamma}_1 = -0.0298$ $\hat{\gamma}_2 = 2.9834$	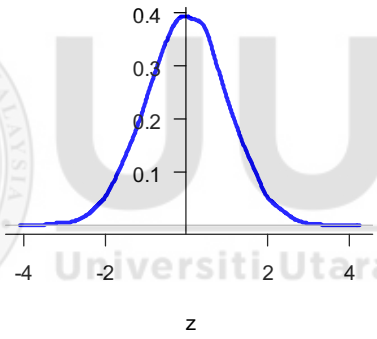	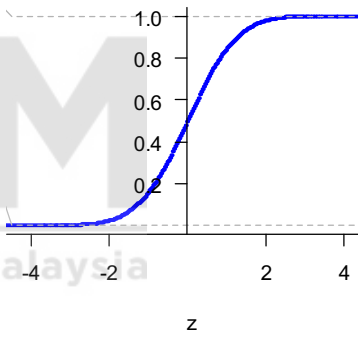
	Symmetric heavy-tailed	
$g = 0$ $h = 0.5$ $\hat{\gamma}_1 = 1.7030$ $\hat{\gamma}_2 = 332.0013$	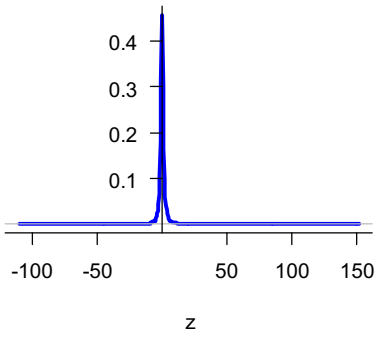	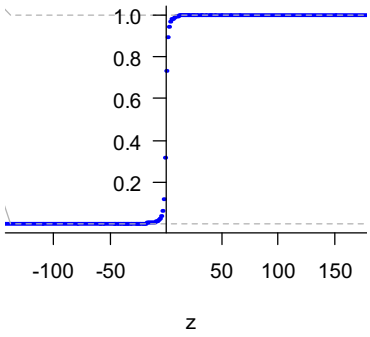

Skewed normal-tailed

$g = 0.5$

$h = 0$

$\hat{\gamma}_1 = 1.6191$

$\hat{\gamma}_2 = 7.6453$

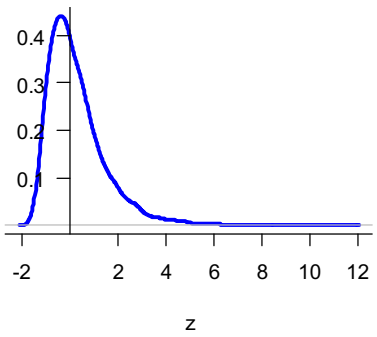

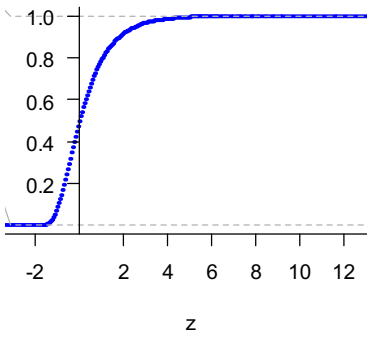

Skewed heavy-tailed

$g = 0.5$

$h = 0.5$

$\hat{\gamma}_1 = 35.1766$

$\hat{\gamma}_2 = 2080.646$

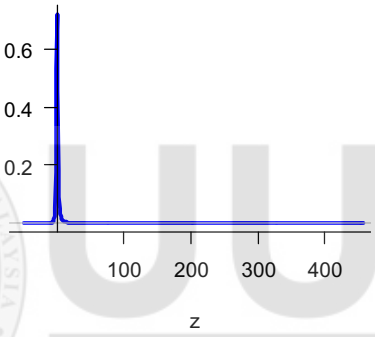

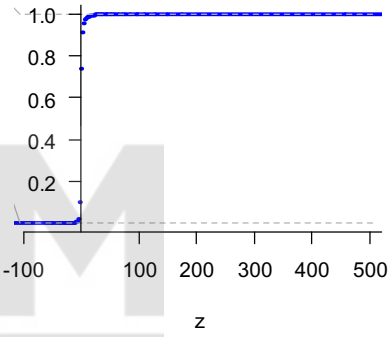

3.3.2 Sample Sizes

The selection of the sample size (n) is important for effective process monitoring. To study the effect of n on the ARL, this study focused on small and moderate n, i.e., $n = 5$ and 9, respectively. According to Montgomery (2009), it is common practice to opt for sample sizes of 4, 5 or 6. Moreover, Teoh et al. (2013) highlighted the benefits of employing small to moderate sample sizes in industrial environments. This approach can effectively minimize costs, reduce time requirements, and reduce inspection processes. Moreover, in various industries, $n = 5$ is the most common

sample size utilized in process monitoring because it can easily be attained, practical and give minimum variation within subgroups (Swamidass, 2000).

3.3.3 Design Shifts

The memory-type charts offer flexibility to the practitioners, unlike the Shewhart chart. That is, the memory-type charts can be designed (or tuned) to any shift that is expected to occur in the process. For instance, based on prior information, a process always exhibits a small change in mean value, say $\delta = 0.75$, after a long run. A memory-type chart can be designed relative to this size of shift so that it can quickly signal a change in the process when this size of shift occurs.

It is important to note the actual shift that occurs may vary from what the chart is designed for. For instance, an MEC chart can be designed for $\delta = 0.75$ but suddenly, a much smaller shift, say $\delta = 0.25$, occurs in the process. Will the chart fail to detect this relatively small shift? This question would be tackled in Chapter 4 when assessing the ARL performance of the proposed memory-type charts.

In this study, all six newly proposed robust memory-type charts were designed for the optimal detection of small and moderate shifts to accommodate their importance in SPC (refer to Section 2.3 of Chapter 2). The design shifts used are specified in Table 3.4 (Crowder, 1989; Lucas & Saccucci, 1990).

Table 3.4

Design Shifts (δ^*)

δ^*	Description
0.5	Small design shift
1	Moderate design shift

3.3.4 Shift Sizes

To assess the effectiveness of the proposed robust control charts in detecting process shifts, δ, (which are measured in standard error units), this study considered various magnitudes of shifts. The range of δ investigated in this study is displayed in Table 3.5.

Table 3.5

Shift Size (δ)

δ	Description	State of the process
0	No shift	In-control
0.25, 0.5, 0.75	Small shift	Out-of-control
1, 1.5, 1.75	Moderate shift	
2, 3	Large shift	

Following Abdul-Rahman et al. (2020), the chosen range of δ enables us to illustrate the effect of small, moderate, and large shifts on the ARL values of the proposed robust memory-type charts. For $\delta \neq 0$, the charts' capability to signal out-of-control conditions would be assessed. Meanwhile, $\delta = 0$ would allow us to monitor the occurrences of false alarms across all four *g*-and-*h* distributions and thus, able to gauge the charts' capability to control the Type I error as the data deviate from normal.

For the reader's convenience, the following notations are used, henceforth:

- δ^* is the design shift (Section 3.3.3)
- δ is the actual shift (Section 3.3.4).

3.4 Simulation Procedures

3.4.1 Optimal Parameter Derivation

The design of the investigated MEC and MCE charts involves derivations of the optimal parameters. For the MEC chart, the parameters are *h*; and for the MCE charts, they are *Kc*. In this study, the optimal parameters were derived via Monte Carlo simulation studies according to the specified design shifts (δ^*) in Section 3.3.3.

In this study, the location parameter was assumed to be unknown and thus, needed to be estimated using the Phase I data. The following steps were followed through in deriving the optimal parameters for the MEC charts when the nominal ARL_0 was set at 370.

1. Fixed n.
2. Fixed $ARL_0 \approx 370$ when the process is in-control $(\delta = 0)$ and G0H0.
3. Set the design shift, $\delta^* = 1.0$.
4. Set the smoothing constant, $\lambda = 0.13$.
5. Set the reference value, $k = 0.5$.
6. Determine the optimal parameter, h such that the value yields $ARL_0 \approx 370$ for the chart.

To derive the optimal parameters for the MCE charts, Steps 1 – 5 in the MEC charts were adhered to. Now, Step 6 differs from before, i.e., the optimal parameter, K_c, needs to be derived such that the yields $ARL_0 \approx 370$ for the MCE chart.

Note that the value of δ^* specified in Step 3 dictates the value of λ in Step 4. The value of λ for pertinent to δ^* can be referred to Crowder (1989). Figure 3.2 presents the flowchart of designing the MEC and MCE charts.

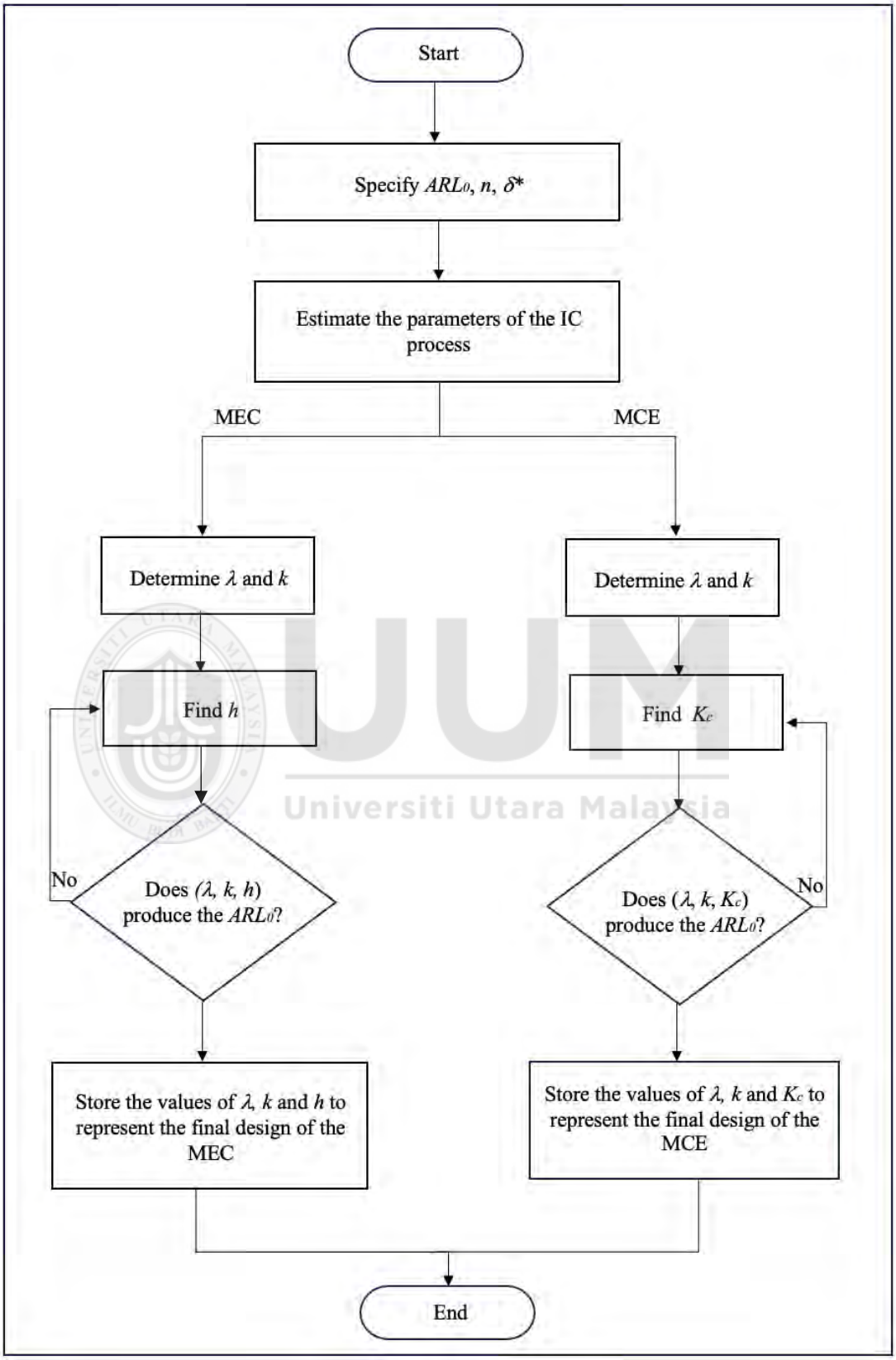

Figure 3.2. The Flowchart to Derive Optimal Parameters of the MEC and MCE Charts

3.5 Data Generation

The simulation procedures defined in Section 3.4 were executed using SAS software for Windows version 9.4. To assess the effect of non-normality on the investigated charts under in-control and out-of-control states, data from the four *g*-and-*h* distributions as specified in Table 3.2 were generated in Phase I and Phase II (refer to Section 3.4).

A standard normal variate, Z_i was generated. Specifically, the random-number function, RANNOR, in SAS, was employed to generate a random number following a standard normal distribution with $\mu = 0$ and $\sigma^2 = 1$. The generated random numbers were simulated with a seed number set to 33333. The next process involved transforming Z_i into a random variable, Y_{ij} using *g*-and-*h* distributions as defined in Equation (3.28).

3.6 Measure of Control Chart Performance

All investigated charts were evaluated using the ARL value. Specifically, the ARL_0 was used to assess the in-control robustness, while the ARL_1 was used to measure the detection capability.

In this study, Bradley's stringent criterion of robustness was used to assess the ARL_0 (Bradley, 1978). A statistical procedure is deemed robust if its false alarm rate ($\hat{\alpha}$) falls within this robust interval $[0.9\alpha, 1.1\alpha]$ (Bradley, 1978). Thus, for a pre-determined $ARL_0 = 370$, the α is equivalent to 0.0027 $\left(\alpha = \frac{1}{370}\right)$ as discussed in Section 1.3 of

Chapter 1. This yields a stringent robust criterion defined as [0.00243, 0.00297] which is equivalent to [337, 412].

The investigated charts are considered robust when its ARL_0 falls between 337 to 412 when data are non-normal. The most robust chart is the chart with the closest value to 370. Moreover, a chart with the smallest ARL_1 under a specified condition is the most efficient chart in signaling an out-of-control condition.

3.7 ARL Simulation

The ARL represents the average number of sample plots on a chart before a signal is given (Atalay et al., 2020). Here, the ARL was derived via Monte Carlo simulation in SAS. The following explains the ARL simulation involved in the study.

3.7.1 ARL simulation procedure for the MEC $\widehat{\theta}$ control chart

1. Determine the optimal parameters (λ, k, h).
2. Select one of the four underlying process distributions (specified in Table 3.2), and establish the size of the in-control Phase I data, Y_i where $i = m \times n, m = 50$.
3. Generate the in-control Phase I data. Utilize Equation (3.27) to compute $\hat{\theta}_0$ based on the data, and pair it with $\sigma_{\hat{\theta}}$.
4. Generate n observations from subgroup m, based on the selected distribution (which matches the Phase I distribution). Subsequently, calculate the chart statistics, MEC_i^+ and MEC_i^-, using Equation (3.10) and (3.11), respectively and set $MEC_0^+ = MEC_0^- = 0$.

5. If both MEC_i^+ and MEC_i^- are less than H_{z_i}, increase the run-length counter.
6. Repeat Steps 3 and 4 until either MEC_i^+ and MEC_i^- are greater than or equal to H_{z_i}. At this point, a signal is given, and the corresponding run length equals to *i.* Do for all δ.
7. Repeat Steps 3 to 6 for 10^4 iterations. These 10^4 independent run-lengths were used to determine the mean of the RL, i.e., the ARL.

Note that Step 1 outlines in the ARL simulation above, i.e., determining the values for λ, k, and h, follows Steps 2 – 7 that were explained in Subsection 3.4. Moreover, Step 3 outlines in the ARL simulation above considered $\delta = 0$ to get an in-control data, i.e., no shift in the process. In step 6, various values of $\delta = \{0.25, 0.5, 0.75, 1, 1.5, 1.75, 2, 3\}$ was integrated into equation 3.28, such that, $\hat{\theta}_i = \hat{\theta} + Y_{ij}$ to get out-of-control data.

3.7.2 ARL simulation procedure for the MCE $\hat{\theta}$ control chart

1. Determine the optimal parameters (λ, k, K_c).
2. Select one of the four underlying process distributions (specified in Table 3.2), and establish the size of the in-control Phase I data, Y_i where $i = m \times n, m = 50$.
3. Generate the in-control Phase I data. Utilize Equation (3.27) to compute $\hat{\theta}_0$ based on the data, and pair it with $\sigma_{\hat{\theta}}$.
4. Generate n observations from subgroup m, based on the selected distribution (which matches the Phase I distribution). Subsequently,

calculate the chart statistics, MCE_i^+ and MCE_i^-, using Equation (3.18) and (3.19), respectively and set $MEC_0^+ = MEC_0^- = \hat{\theta}_0$.

5. If both MCE_i^+ and MCE_i^- are less than UCL_i, increase the run-length counter.
6. Repeat Steps 3 and 4 until either MCE_i^+ and MCE_i^- are greater than or equal to UCL_i. At this point, a signal is given, and the corresponding run length equals to i. Do for all δ.
7. Repeat Steps 3 to 6 for 10^4 iterations. These 10^4 independent run-lengths were used to determine the mean of the RL, i.e., the ARL.

As in the MEC chart, Step 1 outlines in the ARL simulation for the MCE chart, i.e., determining the values for λ, k, and K_c, follows Steps 2 – 7 that were explained in Subsection 3.4. Moreover, Step 3 outlines in the ARL simulation above considered $\delta = 0$ to get an in-control data, i.e., no shift in the process. In step 6, various values of $\delta = \{0.25, 0.5, 0.75, 1, 1.5, 1.75, 2, 3\}$ was integrated into equation 3.28, such that, $\hat{\theta}_i = \hat{\theta} + Y_{ij}$ to get out-of-control data.

In Section 3.2.5.1, process dispersion in Phase I was assumed known to isolate the effect of estimating process location in this study. However, sampling distribution of robust estimators is hardly attainable (Relles & Rogers, 1977). Thus, in employing the chosen median based estimators, their standard error ($\sigma_{\hat{\theta}}$) in Step 3 of the ARL simulation were simulated based on 10^9 samples of size n from the relevant g-and-h distribution when $\delta = 0$.

3.8 Real Data Analysis

The performance of all investigated charts was validated using water quality and manufacturing data. For water quality data, two meteorological variables were involved which are, (i) total suspended solids (TSS) (in milligrams/Liter, mg/L) and dissolved oxygen concentration (DOC) (in milligrams/Liter, mg/L). This water quality dataset concentrated on Pengkalan Sungai Udang station in Selangor, Malaysia. Both meteorological variables, i.e., the TSS and DOC, are part of the water quality index (WQI) assessment and thus, crucial in determining the quality of the process. The dataset was acquired from the Selangor Maritime Gateway (SMG) and the Malaysian National Water Quality Standard (NWQS). From both variables, 560 observations were collected and grouped into 80 samples, each with a sample size of 7 (n = 7).

After validating the real data using TSS and DOC data, the manufacturing data from medical specialties company were applied to enhance the validity of the study. Specifically, the balloon catheter dataset of synergy XD everolimus-eluting platinum chromium coronary stent system were used which consist of variables namely, marker band length, marker band diameter, bond diameter and tip to proximal marker band. For this study, the marker band length of size 49mm were chosen because this variable was found to be easily failed while measuring using marker band inspection and result in significant variation between samples. For manufacturing data, the variable is the marker band length (mm) consist of 375 observations collected and grouped into 75 samples, each with a sample size of 5 (n = 5).

The first half of the dataset was used to construct the control limits (Phase I), and the latter half was used to monitor the out-of-control samples (Phase II). The findings would be used to identify the best performance from the MEC and MCE control charts and most importantly, to check if the results corroborated with findings in the simulation studies.

CHAPTER FOUR
RESULTS OF ANALYSIS

4.1 Introduction

This chapter focuses on the in-control and out-of-control performances of two distinct memory-type control charts, namely the mixed EWMA-CUSUM (MEC) and mixed CUSUM-EWMA (MCE) charts. Six robust memory-type charts for process location were constructed using three median based location estimators. Their performances were assessed based on the average run length (ARL) and subsequently compared against their standard counterparts.

Several variables were manipulated to study the strengths and weaknesses of the proposed charts, which include types of distribution (by *g*-and-*h* distributions), sample sizes (n), actual shift sizes (δ) and design shifts (δ^*), in mimicking frequently encountered conditions in real practice. Based on these four variables, 128 conditions were generated and used to evaluate the performances of the investigated charts based on the ARL via a Monte Carlo simulation study. The findings are depicted in tables in the forms of ARL_0 and ARL_1 and discussed in detail in this chapter.

All investigated charts were designed to produce an $ARL_0 \approx 370$ under normality; a distribution represented by G0H0 in this study. The first evaluation of each type of chart in this chapter concentrates on how far the ARL_0 of the investigated charts deviate from the nominal value when the underlying process follows G0H0.5, G0.5H0, and G0.5.H0.5. Respectively, these three distributions represent the symmetric heavy-tailed, skewed normal-tailed, and skewed heavy-tailed distributions. The ARL_0

produced by each chart under these three non-normal data across n = {5, 9} and δ = 0 when they were designed for δ^* = {0.5, 1} determines the ability of the charts to control the Type I error.

In Section 3.6 of Chapter 3, the ability of the charts to control Type I error is gauged based on the Bradley's stringent criterion of robustness defined by [0.9 α, 1.1 α]. For a pre-determined ARL_0 = 370 which is equivalent to α = 0.0027 $\left(\alpha = {}^{1}/_{370}\right)$, the investigated chart is considered robust when the $\hat{\alpha}$ falls between 0.00243 and 0.00297, where the upper and lower boundaries are included. Thus, this study, which focuses on the ARL performance, concludes that a chart is robust if it can produce an ARL_0 within [337, 412] under non-normality.

The second evaluation of each type of chart in this chapter concentrates on the ARL_1 for δ = {0.25, 0.5, 0.75, 1, 1.5, 2, 3} across all four *g*-and-*h* distributions. A chart with the smallest ARL_1 across the investigated conditions is deemed to be the most effective chart in signaling out-of-control conditions.

The following sections are organized based on the types of memory-type charts under investigation. Section 4.2 focuses on the MEC control charts' performances under the in-control state (based on the ARL_0), followed by the out-of-control performance (based on the ARL_1). Similarly, Section 4.3 focuses on the MCE control charts' performances under both states of the process. In Section 4.4, all charts investigated under the MEC and MCE are compared in terms of the ARL_0 and ARL_1. The comparison includes the performance of the Shewhart $\bar{X}$ chart to support the claim that memory-type charts are allegedly better than memory-less charts.

4.2 MEC Charts

Four MEC control charts were investigated in this study. Three of them are the robust MEC charts based on the median, *MOM*, and *WMOM* estimators. Referring to Table 3.1 in Chapter 3, the notations for the robust charts are $MEC_{\tilde{X}}$, MEC_{MOM}, and MEC_{WMOM}, respectively. These robust MEC charts were compared against the standard chart based on the sample mean ($MEC_{\bar{X}}$).

The construction of the four MEC charts started with the optimal parameter derivation, i.e., the reference value (k) and the decision limit (h) as discussed in Section 3.4.1 of Chapter 3, under normality (G0H0). The optimal parameter values are listed in Table 4.1.

Table 4.1

Optimal Parameters of the MEC Chart for $ARL_0 \approx 370$

			Charts			
n	λ	δ^*	$MEC_{\bar{X}}$	$MEC_{\tilde{X}}$	MEC_{MOM}	MEC_{WMOM}
5	0.05	0.5	*h = 107.6*	*h = 107.91*	*h = 107.61*	*h = 108.63*
5	0.13	1	*h = 36.61*	*h = 37*	*h = 36.74*	*h = 37.51*
9	0.05	0.5	*h = 107*	*h = 107.74*	*h = 107.59*	*h = 107.98*
9	0.13	1	*h = 37*	*h = 36.78*	*h = 36.87*	*h = 36.87*

The following hypotheses are adhered to in assessing the MEC charts' performances where the charts were specifically designed to signal a shift in the process location when the process is out-of-control. The hypotheses are:

H_0: The process is in-control, i.e., $\theta = \theta_0$

H_1: The process is out-of-control, i.e., $\theta \neq \theta_0$

where $\theta =$ mean, and θ_0 = in-control location parameter.

4.2.1 ARL_0

A Type I error occurs when the H_0 is falsely rejected with no special cause exists in the process (i.e., the process is in-control). This section analyzes the occurrences of the Type I error when the newly proposed robust MEC charts were subjected to the three non-normal *g*-and-*h* distributions under an in-control state. Via the simulation study, this in-control state was produced by setting $\delta = 0$.

The ARL_0 of the investigated MEC charts for $n = \{5, 9\}$ are presented in Tables 4.2 and 4.3, respectively. Specifically, $\delta^* = \{0.5, 1\}$ are shown in the first column of the tables followed by the values of ARL_0 for the $MEC_{\bar{X}}$, $MEC_{\tilde{X}}$, MEC_{MOM}, and MEC_{WMOM}. As discussed in Section 3.3.4 of Chapter 3, the two design shifts are of interest due to the importance of small shifts detection in SPC.

The *g*-and-*h* distributions were used to study the effect of skewness and/or heavy tails on the ARL_0. Specifically, G0H0.5, G0.5H0, and G0.5H0.5 where each refers to the symmetric heavy-tailed, skewed normal-tailed, and skewed heavy-tailed distributions,

respectively, were employed in this study. The ARL_0 results for all four MEC charts are shown in Tables 4.2 and 4.3.

Table 4.2

ARL_0 for the MEC Charts when n = 5

δ^*	Distribution	Charts			
		$MEC_{\bar{X}}$	$MEC_{\tilde{X}}$	MEC_{MOM}	MEC_{WMOM}
0.5	G0H0	370.05	370.05	370.79	370.80
	G0H0.5	771.11	370.47	372.79	370.96
	G0.5H0	369.75	364.77	359.40	362.39
	G0.5H0.5	1471.99	378.23	374.10	363.86
1	G0H0	369.61	369.82	369.79	369.58
	G0H0.5	948.99	371.07	374.40	374.52
	G0.5H0	368.32	370.31	371.42	371.06
	G0.5H0.5	1667.37	382.85	362.88	367.37

Table 4.3

ARL_0 for the MEC Charts when n = 9

δ^*	Distribution	Charts			
		$MEC_{\bar{X}}$	$MEC_{\tilde{X}}$	MEC_{MOM}	MEC_{WMOM}
0.5	G0H0	369.42	370.37	368.82	370.09
	G0H0.5	820.62	372.08	377.22	367.73
	G0.5H0	365.66	367.92	363.78	373.06
	G0.5H0.5	2464.16	368.39	368.57	367.08
1	G0H0	369.44	370.35	370.89	369.49
	G0H0.5	1052.48	371.10	372.93	370.90
	G0.5H0	379.08	367.21	371.62	371.25
	G0.5H0.5	2845.33	366.45	375.96	366.39

Tables 4.2 and 4.3 highlight the ARL_0 values that fall within the Bradley's stringent criterion which requires the value to be between 337 to 412 including both lower and upper boundaries. From both tables, all charts yield an $ARL_0 \approx 370$ under G0H0, as they were designed to produce under normality. Concerning the three non-normal distributions taken into consideration in this study, i.e., G0H.5, G.5H0, and G.5H.5, the ARL_0 of all robust control charts ($MEC_{\tilde{X}}$, MEC_{MOM}, and MEC_{WMOM}) fall within the stringent criterion. More importantly, their ARL_0 do not deviate much from the nominal value even under an extreme data condition (G0.5H0.5). This is not true for the standard MEC chart ($MEC_{\bar{X}}$) which only exhibits good control of ARL_0 under G0.5H0. It shall be emphasized that the $MEC_{\bar{X}}$ fail to control the false alarm rate when outliers were captured in heavy-tailed distributions.

Under G0H0.5 and G0.5H0.5, the $MEC_{\bar{X}}$ produces higher ARL_0 than the nominal value (370) for both n. Their ARL_0 are far exceeding the upper limit of the stringent criterion. To illustrate, when the $MEC_{\bar{X}}$ was designed based on $\delta^* = 0.5$ and $n = 5$, its ARL_0 = 2464.16, which is approximately 6.7 times higher than the nominal value as shown in Table 4.2 for G0.5H0.5. Increasing the δ^* and n in designing the chart pushes the ARL_0 further away from the stringent criterion as illustrated in Table 4.3. As the ARL_0 and the false alarm rate are inversely related, this large ARL_0 exhibits by the $MEC_{\bar{X}}$ indicates an incredibly small false alarm rate. This is not ideal as the statistical power of the chart would be affected as discussed in Section 4.2.2.

4.2.2 ARL_1

A Type II error occurs when the H_0 fails to be rejected when a special cause(s) exists in the process (i.e., the process is out-of-control). The efficiency of a control chart in signaling out-of-control conditions decreases as the Type II error increases (i.e., $1 - \beta$ where β is the Type II error).

This section analyzes the occurrences of the efficiency of the MEC charts when the newly proposed robust MEC charts were subjected to the three non-normal *g*-and-*h* distributions under an out-of-control state. Via the simulation study, this out-of-control state was produced by setting $\delta = \{0.25, 0.5, 0.75, 1, 1.5, 2, 3\}$. The impact of non-normality on the MEC charts' capability to detect this various magnitude of shifts was discussed based on the ARL_1.

Four distinct tables, each displaying one of the *g*-and-*h* distributions, are used to list the results. The *n* is shown in the first column of every table, followed by δ^*. The third column focuses on the actual shift that may occur in the process, i.e., δ. The last four columns list the ARL_1 values for the specific pair of δ^* and *n.* Ideally, it could be hard to single out a chart with the smallest ARL_1 for each investigated condition since we have a total of 128 conditions. Thus, the aim here is to find a chart that can maintain small ARL_1 values consistently across the investigated scenarios.

a. G0H0

Table 4.4 shows the ARL_1 performance of the four MEC charts under normality. The results show that the chart designed for $\delta^* = 0.5$ has the largest ARL_1 for small shifts ($0.25 \leq \delta \leq 0.7$), while the chart designed for $\delta^* = 1$ is the best for all δ values. An increase in n leads to an improved detection of out-of-control conditions for all four MEC charts, regardless of the design. This is shown by a decreasing value in the ARL_1. However, when $n = 5$ and $\delta = 0.25$, the ARL_1 of the MEC_{WMOM}, as italicized in Table 4.4, is larger than the other charts. As expected, with an increase in n, the $MEC_{\bar{X}}$ outperforms the robust charts under normality in detecting the smallest shift under investigation, i.e., $\delta = 0.25$ for $n = 9$.

b. G0H0.5

In Table 4.5, the ARL_1 correspond to the $MEC_{\bar{X}}, MEC_{\tilde{X}}, MEC_{MOM}$, and MEC_{WMOM} under symmetric heavy-tailed distribution are listed. The result shows that by increasing n from 5 to 9, the values of the ARL_1 can be decreased. Hence, a better detection of out-of-control conditions. This is true for all charts under each respective δ^*. More importantly, when n is large, the ARL_1 of all MEC charts are comparable across small process shifts, irrespective of δ^*. However, for $n = 5$ and $\delta = 0.25$, the ARL_1 of the MEC_{WMOM} is slightly affected. The italicized ARL_1 of the MEC_{WMOM} is the largest among the investigated charts. On the other hand, the ARL_1 of the $MEC_{\bar{X}}$ (in bold) exhibit smaller values except for $n = 9$ and $\delta^* = 1$. Under this design, the MEC_{MOM} yields smaller ARL_1 than the rest of the charts. The claim is supported by the values in bold in Table 4.5.

Table 4.4

ARL_1 of the MEC Charts for G0H0 Distribution

			Charts			
n	δ^*	δ	$MEC_{\bar{X}}$	$MEC_{\tilde{X}}$	MEC_{MOM}	MEC_{WMOM}
5	0.5	0.25	57.4233	57.6721	57.9755	*58.0681*
		0.5	32.3803	32.358	32.2952	32.5305
		0.75	24.3139	24.4304	24.3303	24.485
		1	19.9896	20.0494	19.9981	20.1275
		1.5	15.2903	15.3212	15.2942	15.3995
		2	12.6365	12.6553	12.6447	12.7289
		3	9.6897	9.7119	9.6951	9.7568
	1	0.25	37.2868	37.4978	37.1556	*38.2665*
		0.5	32.3803	32.358	32.2952	32.5305
		0.75	12.5781	12.6622	12.6085	12.78
		1	10.1606	10.2236	10.1877	10.3203
		1.5	7.6285	7.686	7.6472	7.7563
		2	6.2565	6.2938	6.2636	6.3493
		3	4.8388	4.8782	4.8479	4.9018
9	0.5	0.25	**43.7733**	44.1136	44.0715	44.1106
		0.5	26.2343	26.3046	26.3265	26.3544
		0.75	19.8334	19.9498	19.9228	19.9663
		1	16.3952	16.441	16.4645	16.4927
		1.5	12.5419	12.6053	12.5906	12.6136
		2	10.3656	10.4087	10.3984	10.4373
		3	7.9789	7.9973	7.9896	7.9998
	1	0.25	25.9735	25.8084	25.9451	25.8538
		0.5	13.7853	13.7535	13.7585	13.7903
		0.75	10.2063	10.1406	10.1582	10.1791
		1	8.3088	8.2792	8.2853	8.2672
		1.5	6.2696	6.2402	6.2507	6.2561
		2	5.1225	5.1064	5.1076	5.1212
		3	3.9961	3.994	3.9952	3.9948

Table 4.5

ARL_1 of the MEC Charts for G0H0.5 Distribution

			Charts			
n	δ^*	δ	$MEC_{\bar{X}}$	$MEC_{\tilde{X}}$	MEC_{MOM}	MEC_{WMOM}
		0.25	**55.7716**	57.8502	57.6178	*58.3458*
		0.5	32.7493	32.3581	32.2826	32.5013
		0.75	24.3453	24.4009	24.3386	24.5025
	0.5	1	**19.9764**	20.0478	20.0088	20.1393
		1.5	15.2703	15.3071	15.2885	15.3817
		2	12.6563	12.6603	12.6416	12.7183
		3	9.8069	9.7229	9.6981	9.7556
5						
		0.25	**36.3416**	37.6629	37.5713	*37.9341*
		0.5	17.3877	17.4988	17.4459	17.6981
		0.75	12.6103	12.6649	12.6216	12.7805
	1	1	10.126	10.2038	10.1857	10.306
		1.5	7.7897	7.6799	7.6389	7.7551
		2	6.1297	6.282	6.2619	6.3338
		3	4.9624	4.8911	4.8624	4.922
		0.25	**43.9238**	44.0871	44.2294	44.1574
		0.5	26.4951	26.3148	26.2782	26.3973
		0.75	19.8596	19.9466	19.9293	19.9859
	0.5	1	16.6486	16.4613	16.4394	16.4767
		1.5	12.5302	12.6222	12.5906	12.6152
		2	10.2783	10.4072	10.3992	10.4289
		3	7.998	7.9978	7.991	8.0011
9						
		0.25	*26.1591*	25.877	25.895	**25.8163**
		0.5	13.7305	13.791	13.7908	13.7819
		0.75	10.1872	10.148	10.1693	10.165
	1	1	8.2738	8.2952	8.2917	8.284
		1.5	6.1377	6.2385	6.2563	6.252
		2	5.0304	5.0979	5.1036	5.1056
		3	3.9982	3.993	3.9938	3.994

c. G0.5H0

The value of ARL_1 for the $MEC_{\bar{X}}$, $MEC_{\tilde{X}}$, MEC_{MOM}, and MEC_{WMOM} charts under skewed normal-tailed distribution are presented in Table 4.6. The effect of utilizing small sample sizes (specifically $n = 5$ in this study) in detecting a relatively small shift in the process, $\delta = 0.25$, is the worst on the $MEC_{\tilde{X}}$ chart. The impact is lessened as δ increases beyond 0.75, i.e., when the magnitude of shifts is moderate and large. Notably, for the smallest size of shift observed in this study ($\delta = 0.25$), the ARL_1 of the MEC_{MOM} is slightly affected as n increases (italicized values in Table 4.6) but outperforms the other charts for the rest of the small shifts. For moderate and large shifts, i.e., $\delta \geq 0.75$, all charts perform comparably.

d. G0.5H0.5

Focusing on an extreme case whereby both skewness and heavy-tailed are observed in the data. Table 4.7 shows the ARL_1 values of all charts when G0.5H0.5. The result clearly shows that there is a significant difference in the performance of the $MEC_{\bar{X}}$ when compared to the robust MEC charts for relatively small shifts in the study, i.e., $\delta = \{0.25, 0.5\}$. Except for $n = 5$, $\delta^* = 0.5$ and $\delta = 0.25$, this standard chart performs the worst as indicated by the italicized values. From the results, increasing n while designing the chart for a larger δ^* can lead to better detection by the proposed charts. With the addition to the bold values in Table 4.7 that suggest the MEC_{WMOM} is the most efficient in signaling a very small change in the process, this robust chart also performs consistently well across other small values of δ when compared to the rest of the investigated charts. It is crucial to note that, the difference among the charts' performance is significant when the shift is relatively small, i.e., $\delta \leq 0.5$.

Meanwhile, for moderate and large shifts ($0.75 \leq \delta \leq 3$), all charts perform similarly.

The analyses across all four *g*-and-*h* distributions on the newly proposed robust MEC charts against their standard counterpart conclude that the standard chart ($MEC_{\bar{X}}$) chart is not effective at detecting process shifts, especially for skewed and extreme non-normal distributions. When designed for a quick detection of moderate shifts ($\delta^* = 1$), the $MEC_{\bar{X}}$ loses its ability to signal small shifts in the location which becomes worse under skewed and heavy-tailed distributions. Across the non-normal distributions observed, the $MEC_{\bar{X}}$ yield large ARL_1 across both n, δ^*, and data distribution in most of the conditions specified. Conversely, the three robust MEC charts are superior to the $MEC_{\bar{X}}$ chart. The $MEC_{\tilde{X}}$, MEC_{MOM}, and MEC_{WMOM} can quickly detect a change in the data under non-normality, especially when a small shift occurs in the process. Under the extreme data distribution (G0.5H0.5), the MEC_{MOM} and MEC_{WMOM} perform similarly for moderate shifts when designed for $\delta^* = 0.5$. However, when $\delta^* = \delta = 1$, the MEC_{WMOM} is the best across both n. That is, the MEC_{WMOM} is the most efficient for the shift it is designed to detect.

Table 4.6

ARL_1 of the MEC Charts for G0.5H0 Distribution

			Charts			
n	δ^*	δ	$MEC_{\bar{X}}$	$MEC_{\tilde{X}}$	MEC_{MOM}	MEC_{WMOM}
		0.25	58.3907	*58.5201*	57.7659	**55.918**
		0.5	32.2639	32.4264	32.3091	**31.9695**
		0.75	24.3031	24.3881	24.3639	24.2342
	0.5	1	20.0038	20.0584	20.0224	19.9883
		1.5	15.2868	15.3091	15.2887	15.3136
		2	12.6367	12.6557	12.6343	12.6797
		3	9.6839	9.7144	9.6877	9.7334
5						
		0.25	37.6736	*38.3764*	37.5049	**35.4651**
		0.5	17.409	17.5037	17.5108	17.4043
		0.75	12.6186	12.659	12.6193	12.6994
	1	1	10.1471	10.2304	10.17	10.2264
		1.5	7.6342	7.6844	7.6391	7.711
		2	6.2563	6.2863	6.2652	6.3199
		3	4.8363	4.8638	4.845	4.8932
		0.25	43.7372	44.1839	*44.2179*	**43.4809**
		0.5	26.1936	26.2797	26.3085	26.1419
		0.75	19.8707	19.9498	19.9374	19.892
	0.5	1	16.3851	16.4597	16.4374	16.4305
		1.5	12.5428	12.5962	12.5973	12.6003
		2	10.3731	10.4191	10.4037	10.4132
		3	7.9662	7.9802	7.984	7.9855
9						
		0.25	25.9382	25.8481	*26.0739*	**25.444**
		0.5	13.7891	13.7515	13.7537	13.708
		0.75	10.1996	10.1311	10.1817	10.1209
	1	1	8.3093	8.2839	8.2792	8.2594
		1.5	6.2629	6.2401	6.2591	6.2346
		2	5.1061	5.0987	5.0991	5.090
		3	3.9895	3.9871	3.9892	3.9911

Table 4.7

ARL_1 of the MEC Charts for G0.5H0.5 Distribution

			Charts			
n	δ^*	δ	$MEC_{\bar{X}}$	$MEC_{\tilde{X}}$	MEC_{MOM}	MEC_{WMOM}
		0.25	57.7078	*58.7546*	58.7422	**55.9965**
		0.5	*33.4925*	32.3743	32.5065	32.0692
		0.75	24.3665	24.393	24.3578	24.2031
	0.5	1	20.0034	20.0572	**19.991**	**19.9502**
		1.5	15.2836	15.3104	15.2962	15.2909
		2	12.7832	12.6653	12.6513	12.6746
		3	9.9033	9.7349	9.7085	9.7426
5						
		0.25	*42.4726*	38.7902	38.5031	**36.3152**
		0.5	*18.6151*	17.5717	17.4657	17.3207
		0.75	*13.0525*	12.6705	12.6188	12.6406
	1	1	10.3018	10.2123	10.1766	10.2043
		1.5	7.7539	7.6794	7.6482	7.7035
		2	6.0406	6.2826	6.2595	6.3107
		3	4.9685	4.8878	4.8672	4.9069
		0.25	*46.1313*	44.2827	44.2061	**42.7723**
		0.5	26.3144	26.3103	26.2725	**25.9913**
		0.75	19.8215	19.9544	19.9456	19.7653
	0.5	1	16.3485	16.4624	16.4625	16.3756
		1.5	12.6176	12.6045	12.5872	12.5582
		2	10.1364	10.4155	10.3994	10.3976
		3	7.9939	7.9807	7.9755	7.9763
9						
		0.25	*27.6188*	25.8908	26.2369	**24.8487**
		0.5	13.9225	13.7901	13.7518	13.5839
		0.75	10.3488	10.143	10.1702	10.0811
	1	1	8.112	8.2818	8.2874	8.2285
		1.5	6.0243	6.2328	6.2426	6.2173
		2	4.9986	5.0835	5.086	5.0737
		3	3.9975	3.9849	3.9852	3.9812

4.3 MCE Charts

Four MEC control charts based on the sample mean, median, *MOM*, and *WMOM* were designed and assessed in this section. They are denoted as $MCE_{\bar{X}}$, $MCE_{\tilde{X}}$, MCE_{MOM}, and MCE_{WMOM}, respectively. The hypotheses in assessing the performances of these charts under the ARL_0 and ARL_1 are as defined in Section 4.2.

Table 4.8 lists the optimal parameter, K_c, of the $MCE_{\bar{X}}$, $MCE_{\tilde{X}}$, MCE_{MOM}, and MCE_{WMOM} chart that were derived for n = {5, 9}. The smoothing constant, λ is determined based on the chosen δ^* = {0.5, 1} following

Table 4.8

Optimal Parameters of the MCE Charts for $ARL_0 \approx 370$

			Charts			
n	λ	δ^*	$MCE_{\bar{X}}$	$MCE_{\tilde{X}}$	MCE_{MOM}	MCE_{WMOM}
5	0.05	0.5	$K_c = 6.5605$	$K_c = 6.0599$	$K_c = 6.1815$	$K_c = 6.2806$
5	0.13	1	$K_c = 4.7750$	$K_c = 4.3533$	$K_c = 4.4855$	$K_c = 4.5103$
9	0.05	0.5	$K_c = 7.4511$	$K_c = 6.8482$	$K_c = 7.1118$	$K_c = 7.3039$
9	0.13	1	$K_c = 5.5710$	$K_c = 5.0227$	$K_c = 5.2828$	$K_c = 5.4132$

4.3.1 ARL_0

The ARL_0 values shown in Tables 4.9 - 4.10 are based on the n = {5, 9} when the underlying process data follows the g-and-h distributions. All the MCE charts used in this study were designed for $ARL_0 \approx 370$ under normality, i.e., G0H0. The in-control performance of the MCE charts was then investigated when the underlying distribution deviates from normal, that is, when G0H0.5, G0.5H0, and G0.5H0.5. In Tables 4.9 and 4.10, the performance of the charts that complies with the Bradley's stringent criterion of robustness, i.e., [337, 412] is indicated by the highlighted ARL_0. The robust MCE charts can control the false alarm rate according to the Bradley's stringent criterion under G0H0.5 for certain conditions only. A thorough comparison of the MEC and MCE charts is given at this chapter's conclusion.

From Tables 4.9 and 4.10, designing the robust MCE charts with either $\delta^* = 0.5$ and $\delta = 1$, can limit the effects of outliers on the design structures of the charts whereby they can still control the false alarm rate under non-normal data scenarios. In contrast, the standard MCE chart ($MCE_{\bar{X}}$), may produce large values of ARL_0 under heavy-tailed cases (G0H0.5 and G0.5H0.5). As shown in Tables 4.9 and 4.10, the ARL_0 for the $MCE_{\bar{X}}$ under heavy-tailed cases are much higher than the pre-determined value of 370. This can negatively affect the power, i.e., the shift detection capability of the chart, as discussed in the subsequent section.

Table 4.9

ARL_0 for the MCE Charts when n = 5

δ^*	Distribution	Charts			
		$MCE_{\bar{X}}$	$MCE_{\tilde{X}}$	MCE_{MOM}	MCE_{WMOM}
0.5	G0H0	370.07	369.92	369.95	370.05
	G0H0.5	4969.67	352.49	420.67	448.80
	G0.5H0	233.65	176.47	211.58	214.06
	G0.5H0.5	7019.21	214.23	249.71	256.89
1	G0H0	370.02	370.07	369.93	369.82
	G0H0.5	4624.08	305.17	371.56	369.46
	G0.5H0	189.08	145.12	183.36	177.94
	G0.5H0.5	6906.74	175.32	205.45	207.62

Table 4.10

ARL_0 for the MCE Charts n = 9

δ^*	Distribution	Charts			
		$MCE_{\bar{X}}$	$MCE_{\tilde{X}}$	MCE_{MOM}	MCE_{WMOM}
0.5	G0H0	370.33	370.02	370.02	370.02
	G0H0.5	5118.65	320.92	426.71	513.36
	G0.5H0	242.08	184.25	239.70	244.90
	G0.5H0.5	7113.52	187.14	228.24	254.43
1	G0H0	370.12	370.02	370.11	369.95
	G0H0.5	4744.94	286.43	385.55	447.21
	G0.5H0	196.59	156.22	209.77	203.97
	G0.5H0.5	7055.53	153.25	189.74	213.87

4.3.2 *ARL1*

The four *g*-and-*h* distributions are covered in the *ARL1* findings where the results are organized following the table layout specified in this section.

a. G0H0

The *ARL1* values for each of the four MCE charts ($MCE_{\bar{X}}$, $MCE_{\tilde{X}}$, MCE_{MOM} and MCE_{WMOM}) are listed in Table 4.11 following data normally distributed. The results show that the *ARL1* values are consistent when $\delta > 0.5$. However, when a small *n* is employed for monitoring $\delta < 0.5$, there is a fluctuation in the control chart performance, with MCE_{MOM} and $MCE_{\bar{X}}$ turning out as the least effective methods. Both robust charts show larger *ARL1* values when compared to the other investigated MCE charts as italicized in Table 4.11. This suggests that under these circumstances, the MCE_{MOM} and $MCE_{\bar{X}}$ have less power in detecting small shifts. Generally, a change in *n* and δ^* has the same impact for all the charts. As the *n* increases from 5 to 9, the *ARL1* values decrease significantly when the charts were designed for $\delta^* = 0.5$. Moreover, an increase *n* is shown to enhance the performance of control charts especially for a relatively small change in the process ($\delta \leq 0.5$). On the other hand, the bold values in Table 4.11 present smaller *ARL1* for the $MCE_{\tilde{X}}$ and MEC_{WMOM} when compared to the other MCE charts, irrespective of δ^*.

Table 4.11

ARL_1 of the MCE Charts for G0H0 Distribution

			Charts			
n	δ^*	δ	$MCE_{\bar{X}}$	$MCE_{\tilde{X}}$	MCE_{MOM}	MCE_{WMOM}
5	0.5	0.25	*28.285*	**27.1063**	*28.3735*	27.665
		0.5	6.999	7.0191	7.1392	**6.9455**
		0.75	4.25	4.4242	4.4397	4.3352
		1	3.42	3.5718	3.5791	3.4955
		1.5	2.635	2.7979	2.8088	2.7205
		2	2.111	2.2203	2.2208	2.1666
		3	1.998	2.0001	2	1.9997
		0.25	*42.025*	40.6295	*43.0593*	**40.1805**
		0.5	9.218	**8.7358**	9.2424	8.8618
		0.75	3.819	3.8373	3.9653	3.8379
	1	1	2.63	2.7202	2.731	2.6719
		1.5	1.983	2.0475	2.0595	2.0179
		2	1.635	1.7822	1.7952	1.6991
		3	1.033	1.0713	1.0796	1.0495
		0.25	16.96	**15.9278**	16.9205	16.9741
		0.5	4.488	4.6185	4.6323	4.5771
		0.75	3.156	3.3383	3.3041	3.2151
	0.5	1	2.583	2.756	2.7183	2.6439
		1.5	2.028	2.0745	2.0614	2.0411
		2	1.985	1.9995	1.9986	1.9955
		3	1.213	1.5735	1.5025	1.3265
9						
		0.25	26.673	**24.4725**	26.8084	26.0821
		0.5	4.921	4.8153	*5.0463*	4.9134
		0.75	2.511	2.5886	2.5863	2.5497
	1	1	1.989	2.0732	2.0692	2.0247
		1.5	1.409	1.5593	1.5486	1.4579
		2	1.043	1.0908	1.0847	1.0543
		3	1	1	1.0000	1

b. G0H0.5

For the symmetric heavy-tailed distributions (G0H0.5), the findings are presented in Table 4.12. The $MCE_{\bar{X}}$ control chart displays the largest ARL_1 values across all n and δ, suggesting poor shift detection capability, as indicated by the italicized values. Contrarily, all robust MCE charts consistently yield small values of ARL_1 for all n and δ. The $MCE_{\tilde{X}}$ chart shows the best performance among all the robust MCE charts with the smallest ARL_1 values in bold. This result suggests that the robust MCE charts are best to detect small shifts in symmetric heavy-tailed distributions when compared to the $MCE_{\bar{X}}$ chart. The ARL_1 values for the robust MCE charts remain stable despite a change in n and δ. Unexpectedly, the $MCE_{\tilde{X}}$ chart performs the best when the shifts are relatively small $\delta \leq 1$ and can be considered the best at $\delta = 0.5$.

c. G0.5H0

Table 4.13 presents the results for G0.5H0 which is a skewed normal-tailed distribution. For $n = 5$, the $MCE_{\bar{X}}$ control chart shows the largest ARL_1 across both δ^*. When n increases from 5 to 9, the $MCE_{\bar{X}}$ shows the highest ARL_1 values across both δ^*, given by the italicized values. This suggests a poor shift detection. On the other hand, the $MCE_{\tilde{X}}$ chart shows the best performance and consistently produces a much smaller ARL_1 for both n and δ utilized in the study than the rest of the MCE charts.

Table 4.12

ARL_1 of the MCE Charts for G0H0.5 Distribution

			Charts			
n	δ^*	δ	$MCE_{\bar{X}}$	$MCE_{\tilde{X}}$	MCE_{MOM}	MCE_{WMOM}
		0.25	*2447.888*	**41.6979**	46.8074	50.9045
		0.5	*42.253*	**8.2627**	8.6868	8.7433
		0.75	*12.61*	**5.028**	5.219	5.249
	0.5	1	*9.834*	**4.0575**	4.1841	4.2507
		1.5	*8.282*	3.1165	3.198	3.2127
		2	*6.129*	2.7677	2.8842	2.9052
		3	*5.004*	2.0142	2.0279	2.031
5						
		0.25	*3217.882*	**63.3546**	74.8538	76.2744
		0.5	*955.602*	**12.5394**	14.0416	14.2362
		0.75	*20.801*	**4.4012**	4.7233	4.7276
	1	1	*9.989*	**3.0943**	3.2314	3.248
		1.5	*5.733*	2.1931	2.2669	2.2775
		2	*4.779*	1.9981	2.0125	2.0161
		3	*4.057*	1.4551	1.6868	1.7019
		0.25	*1774.465*	**19.3528**	22.5912	26.0661
		0.5	*15.782*	**4.9942**	5.204	5.4423
		0.75	*9.906*	**3.5329**	3.6813	3.8158
	0.5	1	*7.82*	**2.9778**	3.0791	3.1501
		1.5	*6.013*	2.1843	2.298	2.4301
		2	*5.01*	2.0047	2.0102	2.0195
		3	*4.002*	1.9392	1.9846	1.9943
9						
		0.25	*2901.115*	**31.628**	38.1524	46.1582
		0.5	*285.697*	**5.2957**	6.0281	6.4173
		0.75	*8.796*	**2.7461**	2.8958	3.0064
	1	1	*6.041*	**2.1692**	2.2558	2.3082
		1.5	*4.354*	1.8053	1.8981	1.9495
		2	*3.976*	1.2147	1.3576	1.5115
		3	*3*	1.001	1.0036	1.0055

Table 4.13

ARL_1 of the MCE Charts for G0.5H0 Distribution

			Charts			
n	δ^*	δ	$MCE_{\bar{X}}$	$MCE_{\tilde{X}}$	MCE_{MOM}	MCE_{WMOM}
		0.25	*34.624*	**28.0118**	30.2872	30.1997
		0.5	*8.501*	7.5523	7.7945	7.7748
		0.75	4.716	4.5674	4.6577	4.5983
	0.5	1	3.753	3.6543	3.7296	3.6825
		1.5	2.922	2.8735	2.9197	2.8734
		2	2.393	2.326	2.3926	2.3337
		3	2	1.9981	1.9994	1.9993
5						
		0.25	*42.373*	**35.0015**	39.413	37.5749
		0.5	*11.651*	**9.8228**	10.6478	10.3831
		0.75	4.493	4.12	4.2607	4.1873
	1	1	2.93	2.8117	2.8881	2.8539
		1.5	2.083	2.0422	2.0804	2.0608
		2	1.888	1.8519	1.8882	1.8486
		3	1.157	1.0857	1.1529	1.0961
		0.25	*20.535*	**16.8715**	18.4085	19.1788
		0.5	*5.066*	4.772	4.8915	4.8836
		0.75	3.458	3.3752	3.4362	3.4132
	0.5	1	2.878	2.8143	2.8573	2.8392
		1.5	2.12	2.0722	2.1125	2.0951
		2	1.999	1.9974	1.999	1.9988
		3	1.812	1.7137	1.7881	1.7417
9						
		0.25	*28.51*	**22.7873**	26.7697	26.4923
		0.5	*6.066*	**5.1688**	5.5566	5.603
		0.75	2.763	2.6528	2.7113	2.6947
	1	1	2.135	2.0691	2.1173	2.1004
		1.5	1.726	1.6456	1.7036	1.6684
		2	1.165	1.099	1.1487	1.1244
		3	1	1	1	1

d. G0.5H0.5

The findings for G0.5H0.5 are summarized in Table 4.14. The findings follow an almost similar pattern as observed under G0H0.5. Again, the $MCE_{\bar{X}}$ control chart exhibits worse performance, i.e., the largest value of ARL_1 across all n and δ (italicized values in Table 4.14). Even with an increase in n, there is not much difference in the ARL_1 performance of the standard chart. For example, there is just as slight decrease in the ARL_1 value in detecting $\delta = 0.25$ which is observed for $\delta^* = 1$ when increasing the n from 5 to 9.

In contrast, all three robust charts ($MCE_{\tilde{X}}$, MCE_{MOM}, and MCE_{WMOM}) consistently produce small ARL_1 across all n and δ. The bold values in Table 4.14 indicate the smallest ARL_1 for the $MCE_{\tilde{X}}$, which performs better than the other investigated robust MCE charts. This indicates that the robust MCE charts can still quickly detect shifts despite far deviation in the normality assumption. For both n, the performance of the MCE_{MOM} and MCE_{WMOM} improves as δ^* increases, i.e., smaller ARL_1. This is true for small shifts, i.e., $0.25 \leq \delta \leq 0.5$. Moreover, the MCE_{MOM} is the next best chart followed by the MCE_{WMOM}.

Table 4.14

ARL_1 of the MCE Charts for G0.5H0.5 Distribution

			Charts			
n	δ^*	δ	$MCE_{\bar{X}}$	$MCE_{\tilde{X}}$	MCE_{MOM}	MCE_{WMOM}
		0.25	*6512.278*	**44.269**	49.149	50.5071
		0.5	*652.723*	**9.2207**	9.616	9.8837
		0.75	*33.331*	5.2523	5.429	5.5242
	0.5	1	*21.278*	4.229	4.3446	4.431
		1.5	*15.71*	3.2156	3.313	3.3865
		2	*12.993*	2.9025	2.9473	2.9652
		3	*9.999*	2.0159	2.0409	2.0675
5						
		0.25	*6881.463*	**57.4109**	65.8081	66.4383
		0.5	*5520.929*	**14.9059**	16.653	16.9199
		0.75	*320.486*	**4.8075**	5.0824	5.1931
	1	1	*24.564*	3.2333	3.3711	3.4181
		1.5	*12.899*	2.2884	2.3934	2.4394
		2	*9.986*	1.9909	2.0055	2.0078
		3	*7.508*	1.7611	1.8664	1.8964
		0.25	*5871.863*	**20.3336**	23.2598	27.4094
		0.5	*46.154*	**5.1167**	5.3582	5.7123
		0.75	*21.006*	3.6135	3.7548	3.9669
	0.5	1	*15.827*	3.011	3.1042	3.2343
		1.5	*12.39*	2.2414	2.3898	2.6269
		2	*10.045*	2.0008	2.0041	2.0191
		3	*7.998*	1.9594	1.9843	1.9958
9						
		0.25	*6469.581*	**28.9977**	34.9416	40.4806
		0.5	*3472.864*	**5.8619**	6.4293	7.4136
		0.75	*27.641*	2.8326	2.9599	3.1504
	1	1	*13.25*	2.1838	2.272	2.4018
		1.5	*9.079*	1.861	1.9191	1.9646
		2	*7.932*	1.2975	1.4773	1.7175
		3	*5.996*	1.0005	1.0007	1.0029

4.4 Comparison of the MEC and MCE Charts

In this section, the ARL performances of the investigated MEC and MCE charts are compared with respect to several shifts observed in the process. Three values of shifts (δ) are taken into consideration for comparison purposes. They are, (i) $\delta = 0$ (no shift), $\delta = 0.5$ (small actual shift), and $\delta = 1$ (moderate actual shift). Tables 4.15 to 4.17 display the ARL values corresponding to the abovementioned δ values. Each table is dedicated to a specific *g*-and-*h* distribution and presents the ARL values corresponding to the specific combination of *n*, δ^* and δ. To further emphasize the strength of the proposed robust memory-type charts, this study includes the ARL performance of the Shewhart $\bar{X}$ control with 3-sigma control limits, listed on the final column of each table. Henceforth, the Shewhart chart is denoted by $\bar{X}$. Since the $\bar{X}$ cannot be designed, i.e., tuned, for a specific magnitude of shifts due to its reliance on fixed control limits and the sample mean as the estimator (Haridy & Benneyan, 2024), the ARL values for this chart when $n = \{5, 9\}$ are displayed repeatedly across the two design shifts ($\delta^* = \{0.5, 1\}$). These δ^* were used to design the MEC and MCE chart for $ARL_0 \approx 370$; analogous to the Shewhart chart with 3-sigma limits.

The comparison among the MEC charts ($MEC_{\bar{X}}$, $MEC_{\tilde{X}}$, MEC_{MOM}, and MEC_{WMOM}), MCE charts ($MCE_{\bar{X}}$, $MCE_{\tilde{X}}$, MCE_{MOM}, and MCE_{WMOM}), and $\bar{X}$ chart are based on the ARL_0 and ARL_1. As mentioned before, the ARL_0 assesses the in-control robustness of the chart. Meanwhile, the ARL_1 evaluates the capability of the chart to quickly detect shifts in the process. Ideally, a good chart has a large value of ARL_0 and small ARL_1. In the following tables, the ARL_0 results are listed under $\delta = 0$ (no shift). When $\delta \neq 0$, the results are referred to the ARL_1.

a. G0H0

Table 4.15 compares the ARL of the nine charts under G0H0. When $\delta = 0$, all ARL_0 values are as expected, i.e., 370, as the charts were designed to have. For $\delta \neq 0$, the following are observed. The MCE charts in general, exhibit superior performances (i.e., smaller ARL_1) when compared to the MEC charts when a change in the process is small, i.e., $\delta = 0.5$. However, it is important to note that the effectiveness of these MEC and MCE charts differs based on the *n*. It has been observed that in both sample sizes, the MCE charts can effectively detect small process shifts ($0.25 \leq \delta \leq 0.5$), judging by the smallest ARL_1 values for both δ^*. Overall, the MCE charts consistently outperform the MEC charts, across all conditions in this study. This is due to the design of their control structure, which enhances sensitivity and enables faster detection of process shifts. In contrast, the MEC charts are comparatively less efficient in detecting shifts when data follows a normal distribution.

It is important to note that the shift detection capability of the investigated charts, including the $\bar{X}$, increases with a larger value of *n*. When *n* increases, the MCE charts show better out-of-control performances compared to the MEC charts. When the actual shift size is aligned with the design shift, i.e., ($\delta = \delta^*$), the MCE_{WMOM} demonstrates the capability to detect a small shift even when *n* is small. Specifically, the MCE_{WMOM} displays the smallest ARL_1 for small δ value ($0.25 \leq \delta \leq 0.5$). Thus, highlighting the MCE_{WMOM} efficiency. However, as *n* increases, the performance of the $MCE_{\bar{X}}$ chart exceeds the MCE_{WMOM} in performance. Notably, $MCE_{\bar{X}}$ stands out as the best choice for detecting a small shift ($\delta = 0.5$) faster even when it was designed for a moderate shift detection ($\delta * = 1$).

Table 4.15

ARL of the MEC and MCE Charts for G0H0 Distribution

			MEC				**MCE**				$\overline{X}$
n	δ^*	δ	$MEC_{\bar{X}}$	$MEC_{\tilde{X}}$	MEC_{MOM}	MEC_{WMOM}	$MCE_{\bar{X}}$	$MCE_{\tilde{X}}$	MCE_{MOM}	MCE_{WMOM}	
5		0	370.05	370.05	370.79	370.80	370.07	369.92	369.95	370.05	369.68
	0.5	0.5	32.3803	32.358	32.2952	32.5305	6.999	7.0191	7.1392	6.9455	37.75
		1	19.9896	20.0494	19.9981	20.1275	3.42	3.5718	3.5791	3.4955	4.76
		0	369.61	369.82	369.79	369.58	370.02	370.07	369.93	369.82	369.68
	1	0.5	32.3803	32.358	32.2952	32.5305	9.218	8.7358	9.2424	8.8618	37.75
		1	10.1606	10.2236	10.1877	10.3203	2.63	2.7202	2.731	2.6719	4.76
9		0	369.42	370.37	368.82	370.09	369.42	370.37	368.82	370.09	369.96
	0.5	0.5	26.2343	26.3046	26.3265	26.3544	4.488	4.6185	4.6323	4.5771	16.41
		1	16.3952	16.441	16.4645	16.4927	2.583	2.756	2.7183	2.6439	2.06
		0	369.44	370.35	370.89	369.49	370.12	370.02	370.11	369.95	369.96
	1	0.5	13.7853	13.7535	13.7585	13.7903	4.921	4.8153	*5.0463*	4.9134	16.41
		1	8.3088	8.2792	8.2853	8.2672	1.989	2.0732	2.0692	2.0247	2.06

b. G0H0.5

The ARL for all charts under G0H0.5 is listed in Table 4.16. The main focus is to identify a control chart that maintains the ARL_0 value within the Bradley's stringent criterion while consistently producing high ARL_1 (i.e., good detection capability). As mentioned previously, the Bradley's stringent criterion is set at [337, 412]. The values highlighted in Table 4.16 correspond to the ARL_0 that falls within the robust criteria.

For a small design shift ($\delta^* = 0.5$), all the robust MEC charts ($MEC_{\bar{X}}$, MEC_{MOM}, and MEC_{WMOM}) demonstrates remarkable in-control robustness and consistently yields small ARL_1 values for $\delta > 0$. These consistent detection capabilities are evident in both n. For a moderate design shift ($\delta^* = 1.0$), the ranking of charts varies depending on the n. For $n = 5$, the MCE_{MOM} displays the robust in-control performance with $ARL_0 = 371.56$ and consistent detection capability across δ. Despite this, making it the most robust chart under symmetric heavy-tailed distributions. For $n = 9$, the MEC_{WMOM} chart not only maintains consistency in providing quick detection for $\delta > 0$, but it emerges as the most robust chart.

In conclusion, the MEC charts have illustrated their robustness and detection capability across varying settings, and the MCE chart has displayed consistent detection capabilities with different levels of robustness across the conditions specified. It has been noted that the ARL_0 of the $MEC_{\bar{X}}$ and $MCE_{\bar{X}}$ is comparatively less robust than other charts under investigation. However, Table 4.16 demonstrates that the MEC_{MOM} exhibits greater detection power than the MEC_{WMOM} chart, particularly when the actual shift is relatively small.

The $\bar{X}$ fails to meet the Bradley's stringent criterion as shown by the ARL_0 for $\delta = 0$ in Table 4.16. Even with an increase in n, the ARL_0 value does not approach the expected 370. Consequently, its detection capability is not worth pursuing for discussion as it is consistently being outperformed by the MEC and MCE charts.

c. G0.5H0

G0. 5H0 denotes the impact of non-normality on skewness. Table 4.17 lists the ARL results. The ARL highlighted for $\delta = 0$ indicates that all ARL_0 generated by the MEC charts under investigation fall within the Bradley's stringent criterion. In contrast, none of the ARL_0 for MCE charts falls within the stringent criterion, suggesting that the MCE charts under this investigation are not robust. The level of robustness exhibited by the MEC varies based on the δ^* which exhibits better in-control robustness, i.e., an improved ARL_0, when designed for small shift ($\delta^* = 0.5$).

When the value of δ^* is set to 0.5, the MEC chart emerges as the best choice to be used due to its combined robustness and consistent high detection. Specifically, the $MEC_{\bar{X}}$ is identified as the top performer for $n = 5$, and MEC_{WMOM} for $n = 9$, respectively. For $\delta^* = 1$ and $n = 5$, the $MEC_{\tilde{X}}$ is recognized as the most robust, exhibiting consistent quick detection and robust ARL_0 values. For $n = 9$, the MEC_{WMOM} chart is deemed the most suitable chart to be used.

Table 4.16

ARL of the MEC and MCE Charts for G0H0.5 Distribution

			MEC				**MCE**				$\bar{X}$
n	δ^*	δ	$MEC_{\bar{X}}$	$MEC_{\tilde{X}}$	MEC_{MOM}	MEC_{WMOM}	$MCE_{\bar{X}}$	$MCE_{\tilde{X}}$	MCE_{MOM}	MCE_{WMOM}	
5	0.5	0	771.11	370.47	372.79	370.96	4969.67	352.49	420.67	448.80	222.29
		0.5	32.7493	32.3581	32.2826	32.5013	42.253	8.2627	8.6868	8.7433	152.70
		1	19.9764	20.0478	20.0088	20.1393	9.834	4.0575	4.1841	4.2507	35.64
	1	0	948.99	371.07	374.40	374.52	4624.08	305.17	371.56	369.46	222.29
		0.5	17.3877	17.4988	17.4459	17.6981	955.602	12.5394	14.0416	14.2362	152.70
		1	10.126	10.2038	10.1857	10.306	9.989	3.0943	3.2314	3.248	35.64
9	0.5	0	820.62	372.08	377.22	367.73	5118.65	320.92	426.71	513.36	241.86
		0.5	26.4951	26.3148	26.2782	26.3973	15.782	4.9942	5.204	5.4423	116.77
		1	16.6486	16.4613	16.4394	16.4767	7.82	2.9778	3.0791	3.1501	2.48
	1	0	1052.48	371.10	372.93	370.90	4744.94	286.43	385.55	447.21	241.86
		0.5	13.7305	13.791	13.7908	13.7819	285.697	5.2957	6.0281	6.4173	116.77
		1	8.2738	8.2952	8.2917	8.284	6.041	2.1692	2.2558	2.3082	2.48

Table 4.17

ARL of The MEC and MCE Charts for G0.5H0 Distribution

			MEC				MCE				$\bar{X}$
n	δ^*	δ	$MEC_{\bar{X}}$	$MEC_{\tilde{X}}$	MEC_{MOM}	MEC_{WMOM}	$MCE_{\bar{X}}$	$MCE_{\tilde{X}}$	MCE_{MOM}	MCE_{WMOM}	
5		0	369.75	364.77	359.40	362.39	233.65	176.47	211.58	214.06	126.23
	0.5	0.5	32.2639	32.4264	32.3091	31.9695	8.501	7.5523	7.7945	7.7748	23.34
		1	20.0038	20.0584	20.0224	19.9883	3.753	3.6543	3.7296	3.6825	5.20
	1	0	368.32	370.31	371.42	371.06	189.08	145.12	183.36	177.94	126.23
		0.5	17.409	17.5037	17.5108	17.4043	11.651	9.8228	10.6478	10.3831	23.34
		1	10.1471	10.2304	10.17	10.2264	2.93	2.8117	2.8881	2.8539	5.20
9		0	365.66	367.92	363.78	373.06	242.08	184.25	239.70	244.90	164.54
	0.5	0.5	26.1936	26.2797	26.3085	26.1419	5.066	4.772	4.8915	4.8836	13.55
		1	16.3851	16.4597	16.4374	16.4305	2.878	2.8143	2.8573	2.8392	2.24
	1	0	379.08	367.21	371.62	371.25	196.59	156.22	209.77	203.97	164.54
		0.5	13.7891	13.7515	13.7537	13.708	6.066	5.1688	5.5566	5.603	13.55
		1	8.3093	8.2839	8.2792	8.2594	2.135	2.0691	2.1173	2.1004	2.24

d. G0.5H0.5

Table 4.18 presents a comparison of ARL performance among the nine charts for G0.5H0.5. This distribution holds particular significance as it provides insights into the charts' behavior under extreme data distribution, i.e., i.e., high kurtosis and skewness. The findings indicate that employing the standard charts is not advisable, as these standard charts fail to maintain the ARL_0 values within the acceptable range of 337 to 412, making their effectiveness in detecting shifts dubious. The MCE charts are more likely to be impacted than the MEC chart under this scenario, judging by the ARL_0 of the MCE charts. Notably, $\bar{X}$ struggles to control the ARL_0 within the acceptable range with the worst performances when $\delta \neq 0$.

It is important to emphasize that the MEC charts constructed based on robust estimators, as shown in this section, can perform reliably when dealing with extreme non-normality when designing for an optimal small shift detection, i.e., $\delta^* = 0.5$. That is, a robust ARL_0 can be achieved (as highlighted in yellow) when these robust charts were designed specifically based on $\delta^* = 0.5$. Thus, ensuring reliable small shift detection as the charts are intended for.

When $n = 5$, it has been observed that the MEC_{WMOM} demonstrates exceptional performance in robustness and consistently high detection. On the other hand, when $n = 9$, the MEC_{MOM} is identified as the most robust chart. As n increases, the ARL_0 of both robust charts exhibit significant improvement and move toward the nominal value (370). Hence, the MEC_{WMOM} is selected for its most robust and consistently high detection for $n = 5$, and MEC_{MOM} is chosen for $n = 9$.

Table 4.18

ARL of the MEC and MCE Charts G0.5H0.5 Distribution

			MEC				**MCE**				$\overline{X}$
n	δ^*	δ	$MEC_{\bar{X}}$	$MEC_{\tilde{X}}$	MEC_{MOM}	MEC_{WMOM}	$MCE_{\bar{X}}$	$MCE_{\tilde{X}}$	MCE_{MOM}	MCE_{WMOM}	
5	0.5	0	1471.99	378.23	374.10	363.86	7019.21	214.23	249.71	256.89	819.77
		0.5	33.4925	32.3743	32.5065	32.0692	652.723	9.2207	9.616	9.8837	403.42
		1	20.0034	20.0572	19.991	19.9502	21.278	4.229	4.3446	4.431	108.12
	1	0	1667.37	382.85	362.88	367.37	6906.74	175.32	205.45	207.62	819.77
		0.5	18.6151	17.5717	17.4657	17.3207	5520.929	14.9059	16.653	16.9199	403.42
		1	10.3018	10.2123	10.1766	10.2043	24.564	3.2333	3.3711	3.4181	108.12
9	0.5	0	2464.16	368.39	368.57	367.08	7113.52	187.14	228.24	254.43	770.42
		0.5	26.3144	26.3103	26.2725	25.9913	46.154	5.1167	5.3582	5.7123	263.44
		1	16.3485	16.4624	16.4625	16.3756	15.827	3.011	3.1042	3.2343	4.46
	1	0	2845.33	366.45	375.96	366.39	7055.53	153.25	189.74	213.87	770.42
		0.5	13.9225	13.7901	13.7518	13.5839	3472.864	5.8619	6.4293	7.4136	263.44
		1	8.112	8.2818	8.2874	8.2285	13.25	2.1838	2.272	2.4018	4.46

Throughout this study, which covers the MEC and MCE charts, it is evident that the specification of δ^* is crucial as it has an impact on the robustness and detection capabilities of these memory-type charts, as demonstrated in this chapter. Notably, the robust MEC charts demonstrate high robustness against non-normality when designed for an optimal detection of small shift, i.e., $\delta^* = 0.5$.

4.5 Real Data Application

To demonstrate the application of the investigated MEC and MCE chart on real data, the charts were applied to water quality data from Selangor Maritime Gateway (SMG) and the Malaysian National Water Quality Standard (NWQS), and manufacturing data from medical specialties company.

4.5.1 MEC and MCE Charts on DOC and TSS data

Figures 4.1 and 4.2 illustrate line charts that were constructed for hourly TSS and DOC data, respectively from 27th June 2023 until 22nd July 2023. For this study, 560 data values from TSS and DOC data were selected. An increasing trend can be observed for the TSS, starting in July as depicted in Figure 4.1. Meanwhile, in Figure 4.2, the highest data values in the DOC data are observed in June.

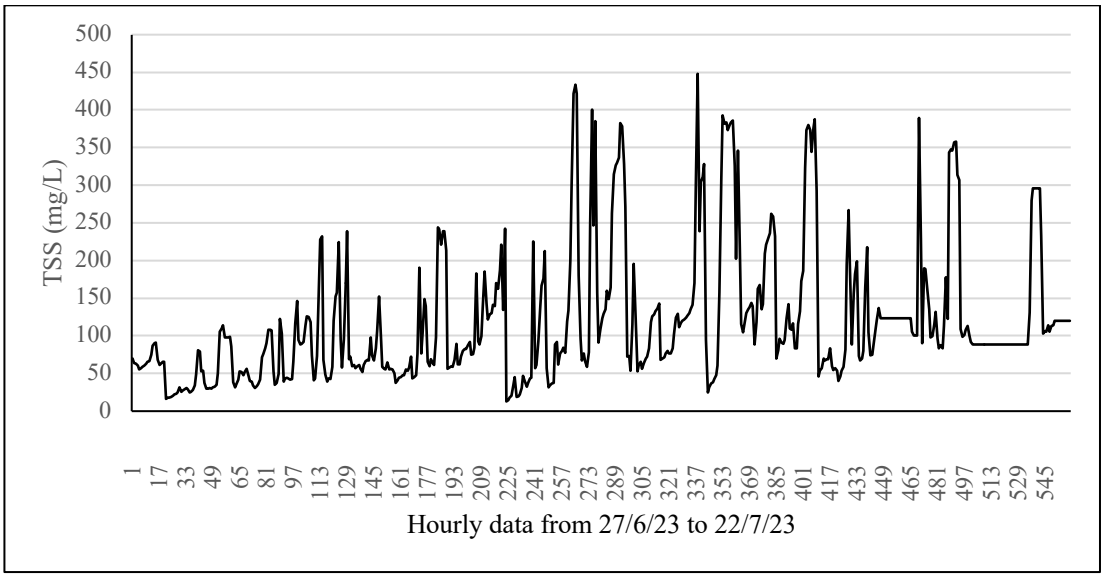

Figure 4.1 Line Chart of TSS Data

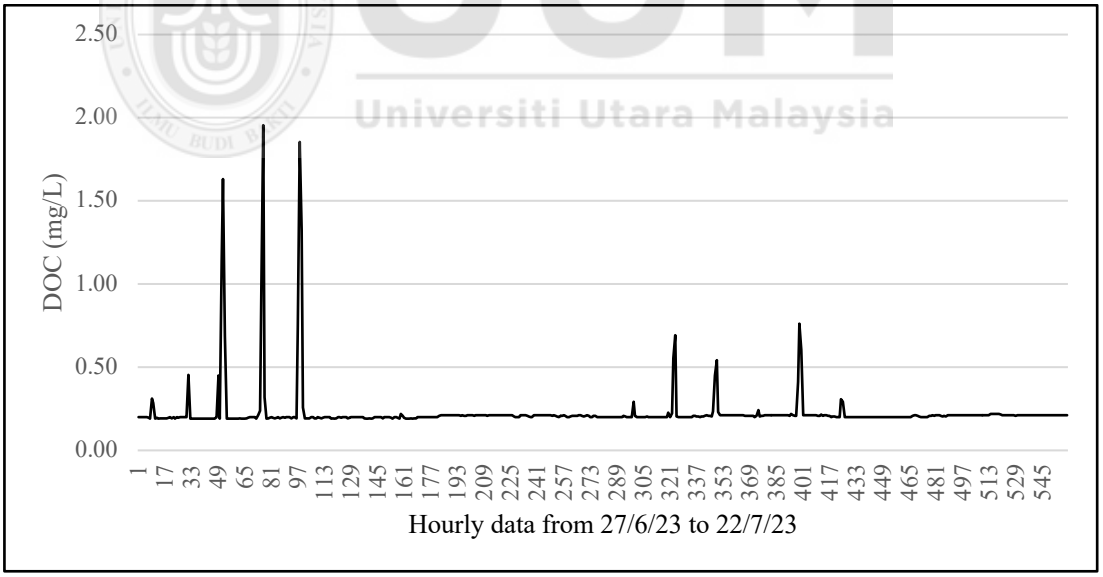

Figure 4.2 Line Chart of DOC Data

Table 4.19 shows the estimator values for TSS and DOC data. Based on the result, the values of mean for TSS and DOC are higher than their respective median values, indicating that the distribution shape is right-skewed. Since the distribution is skewed, the mean is not the best estimator of central tendency, as it is in influenced by extreme values. Therefore, the median-based estimators i.e., median, *MOM*, and *WMOM* are more appropriate for accurately representing the central tendency of the data.

Table 4.19

Estimator Values of TSS and DOC Data

		Estimator			
		Mean	**Median**	***MOM***	***WMOM***
Data	TSS	119.53	88.75	88.0228	104.5449
	DOC	0.2253	0.2025	0.2029	0.2043

Figures 4.3 and 4.4 show the normality test using the Kolmogrov-Smirnov test on TSS and DOC for the 560 data values. With p-value < 0.01, both TSS and DOC data are concluded to be non-normally distributed at 5% significance level, making them suitable to be applied on the newly proposed robust MEC and MCE charts in this study.

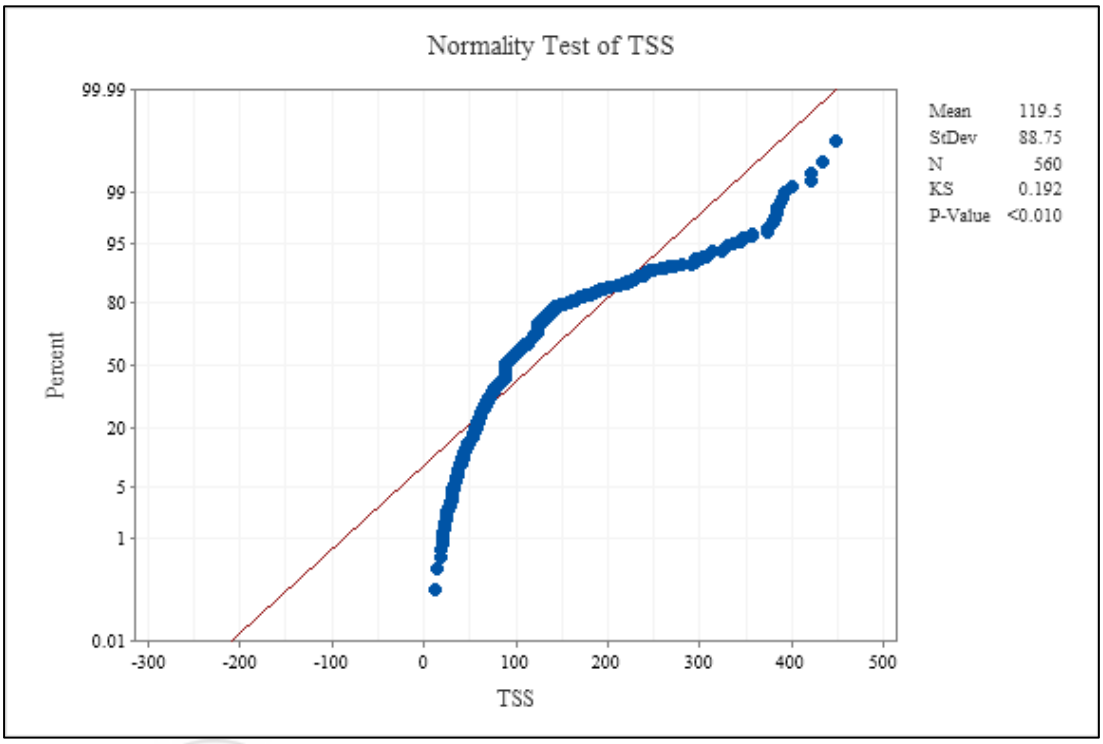

Figure 4.3 Normality Test of the TSS Data

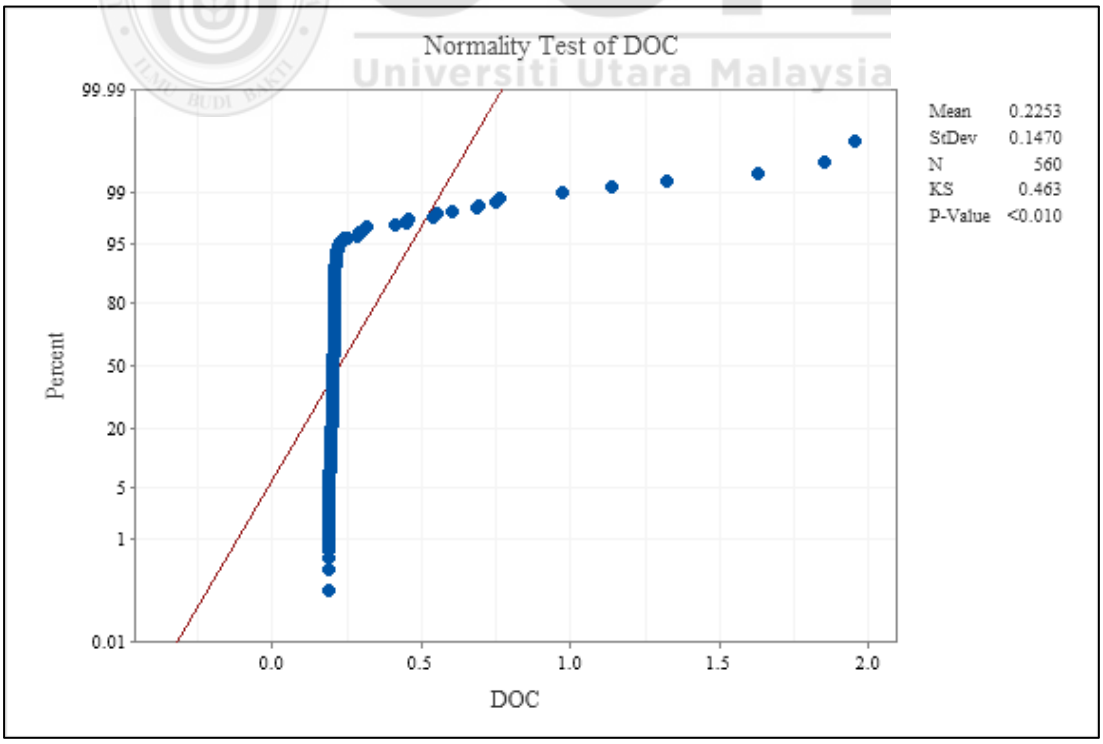

Figure 4.4 Normality Test of the DOC Data

Following the normality test, the 560 data values of the TSS and DOC data were grouped into 80 samples (m = 80), each with a sample size of 7 (n = 7) as presented in Figures 4.5 and 4.6. This rational subgrouping value, i.e., n = 7, was opted in this real data analysis due to the similar characteristics exhibited by the TSS and DOC data within a seven-hourly period. For example, observations taken between 12 am to 7 am vary with the next cycle (7 am – 1 pm) which could be attributed to the varying temperature in day versus night. Thus, to minimize the variation within the subgroup while maximizing the variation between the subgroups, n = 7 was chosen.

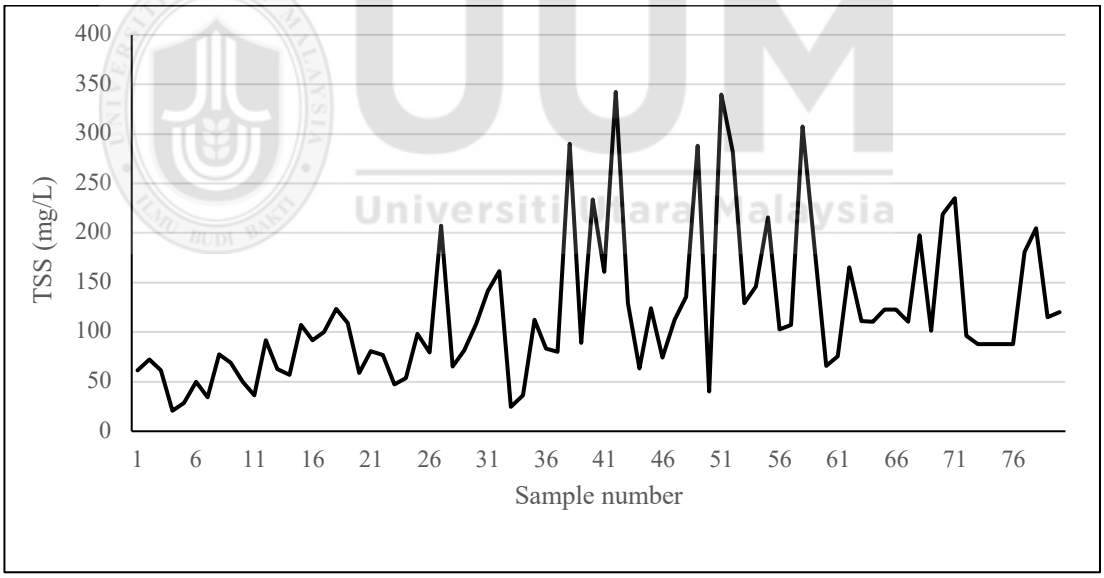

Figure 4.5 Line Chart for 80 Samples of TSS Data

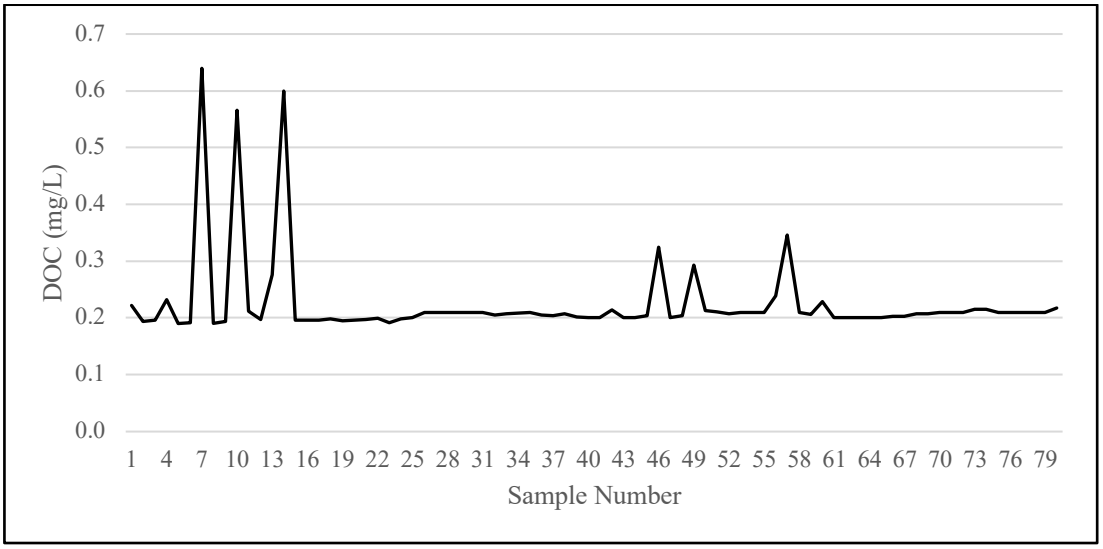

Figure 4.6 Line Chart for 80 Samples of DOC Data

The first half of the dataset was used to construct the control limits (Phase I) and the latter half was used to monitor the out-of-control samples (Phase II). For n = 7 and λ = 0.13 and k = 0.5 (as in the simulation study), the optimal parameters of the MEC and MCE charts were derived and listed in Tables 4.20 – 4.21.

Table 4.20

Optimal Parameters of the MEC Chart for $ARL_0 \approx 370$

			Charts			
n	λ	δ^*	$MEC_{\bar{X}}$	$MEC_{\tilde{X}}$	MEC_{MOM}	MEC_{WMOM}
7	0.13	1	$h = 36.54$	$h = 36.65$	$h = 36.68$	$h = 36.9$

Table 4.21

Optimal Parameters of the MCE Chart for $ARL_0 \approx 370$

			Charts			
n	λ	δ^*	$MCE_{\bar{X}}$	$MCE_{\tilde{X}}$	MCE_{MOM}	MCE_{WMOM}
7	0.13	1	$K_c = 5.21$	$K_c = 4.732$	$K_c = 4.942$	$K_c = 5.032$

The outcomes of the proposed MEC and MCE charts can be observed in Figures 4.7 to 4.22. For the MEC charts, both statistics, MEC_i^+ and MEC_i^-, are plotted against the control limit, H, while for MCE charts, both statistics, MCE_i^+ and MCE_i^-, are plotted against the control limit, UCL_i.

Figures 4.7 to 4.10 illustrate the output of the MEC charts for the TSS data. The $MEC_{\bar{X}}$, as presented in Figure 4.7, shows no out-of-control samples. Meanwhile, Figure 4.8 indicates 8 out-of-control samples (samples 23 to 30) for the robust $MEC_{\tilde{X}}$. Lastly, Figures 4.9 and 4.10 show the output for the robust MEC_{MOM} and MEC_{WMOM} with 7 out-of-control samples (samples 24 to 30). This implies that all the robust charts ($MEC_{\tilde{X}}, MEC_{MOM}, MEC_{WMOM}$) are quicker than the $MEC_{\bar{X}}$ chart in detecting a change in the TSS data. The findings from both the simulation analysis and real data analysis consistently indicate that all robust charts ($MEC_{\tilde{X}}, MEC_{MOM}, MEC_{WMOM}$) exbibit superior performance in detecting shifts under non-normal data condition compared to the $MEC_{\bar{X}}$ chart.

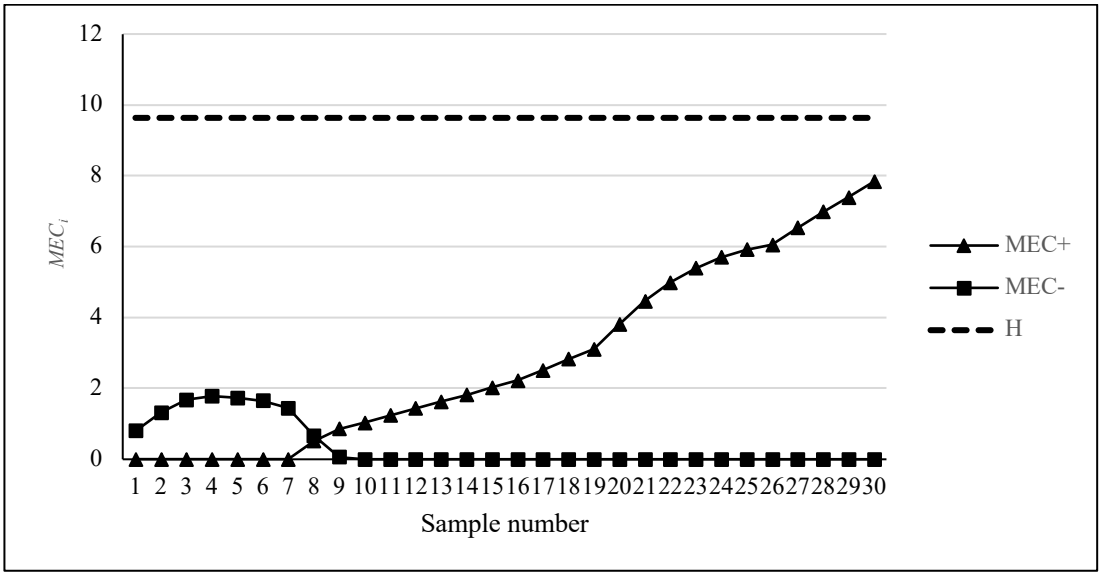

Figure 4.7. $MEC_{\bar{X}}$ Chart for the TSS Data

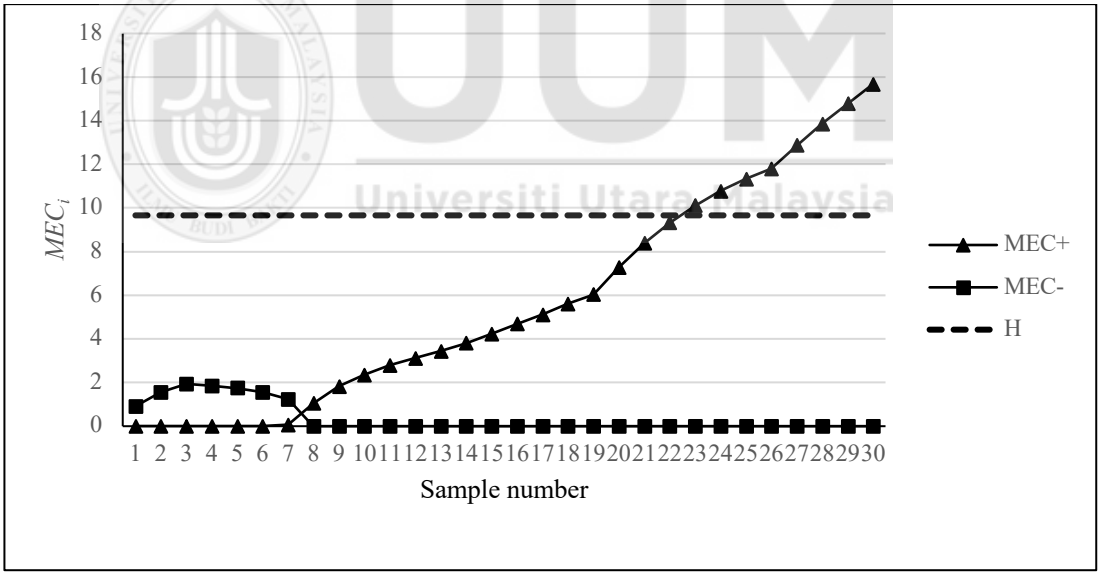

Figure 4.8. $MEC_{\tilde{X}}$ Chart for the TSS Data

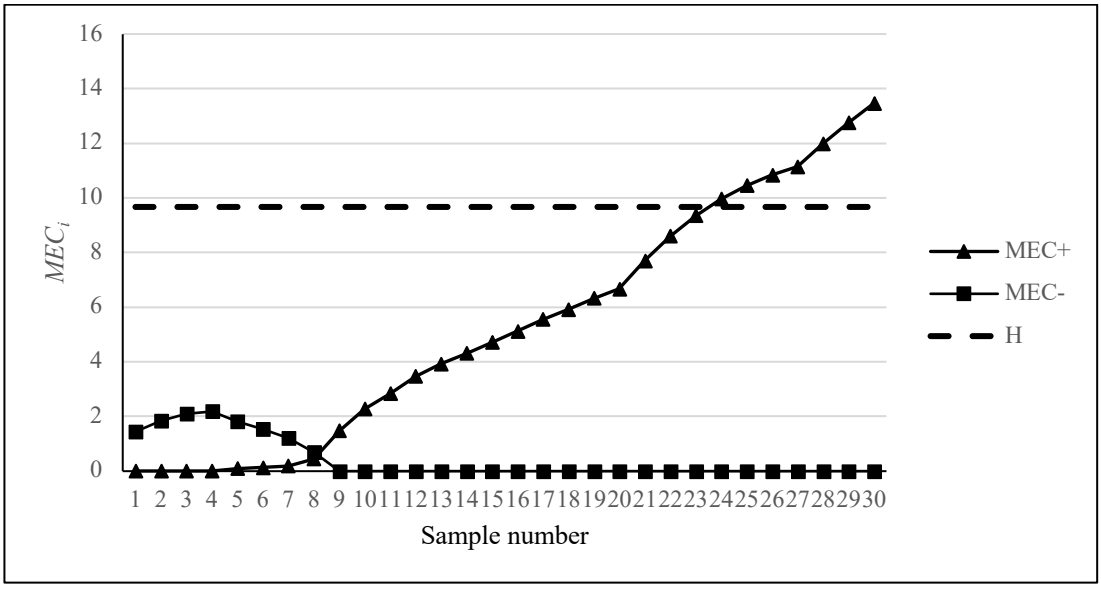

Figure 4.9 MEC_{MOM} Chart for the TSS Data

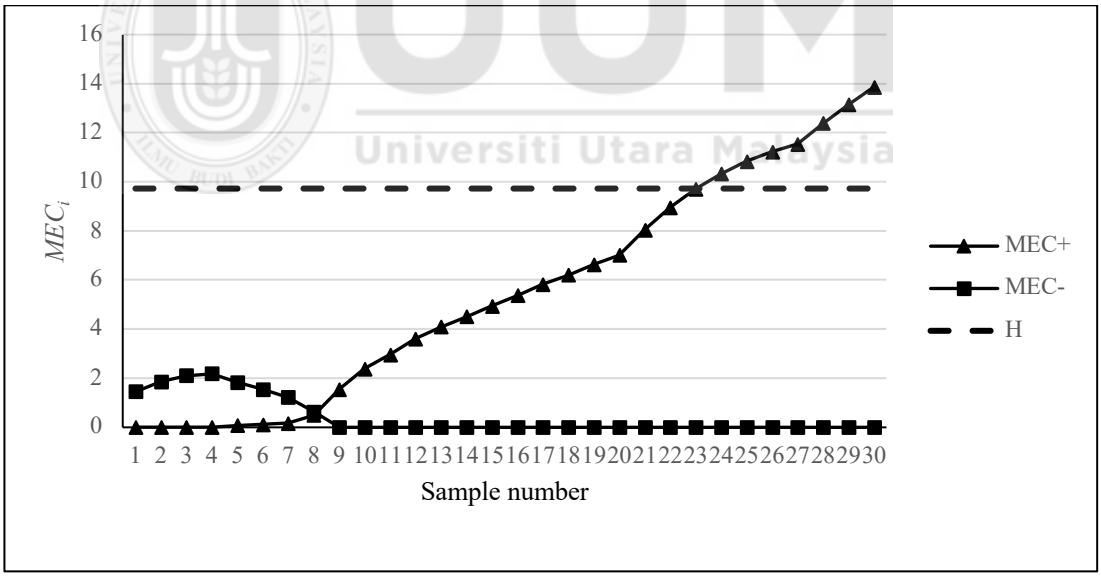

Figure 4.10 MEC_{WMOM} for the TSS Data

Figures 4.11 - 4.14 illustrate the output of MCE charts for the TSS data which show no out-of-control samples for all investigated MCE charts. This finding contrasts with the results obtained from MEC charts, where all robust charts $(MEC_{\tilde{X}}, MEC_{MOM}, MEC_{WMOM})$ demonstrated superior sensitivity to shifts in non-normal data compared to $MEC_{\bar{X}}$ chart. Furthermore, this finding aligns with the simulation results, which similarly indicated that the MCE charts are less sensitive in detecting shifts compared to MEC charts.

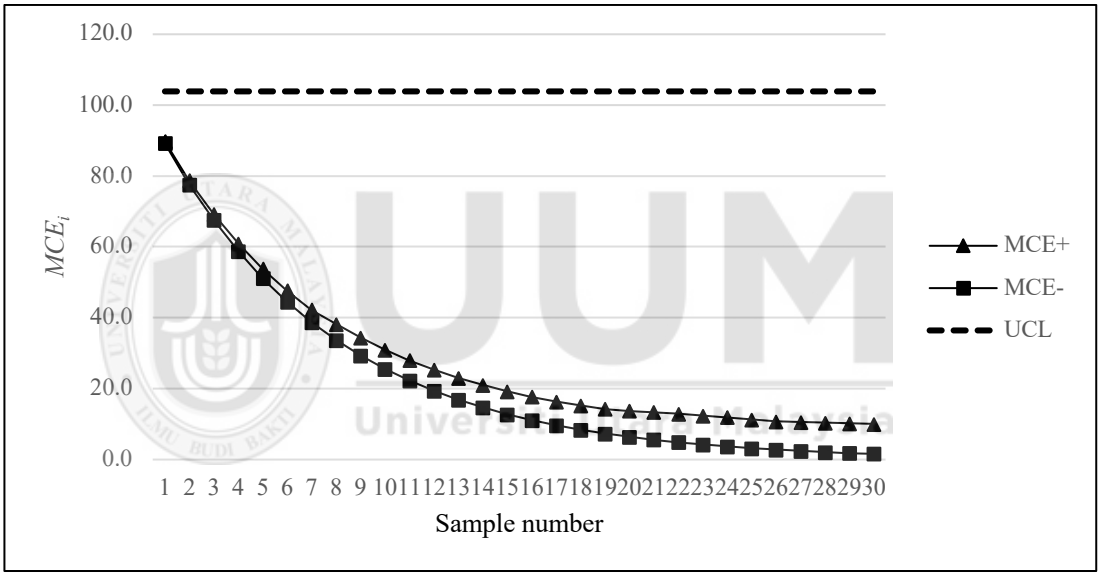

Figure 4.11 $MCE_{\bar{X}}$ Chart for the TSS Data

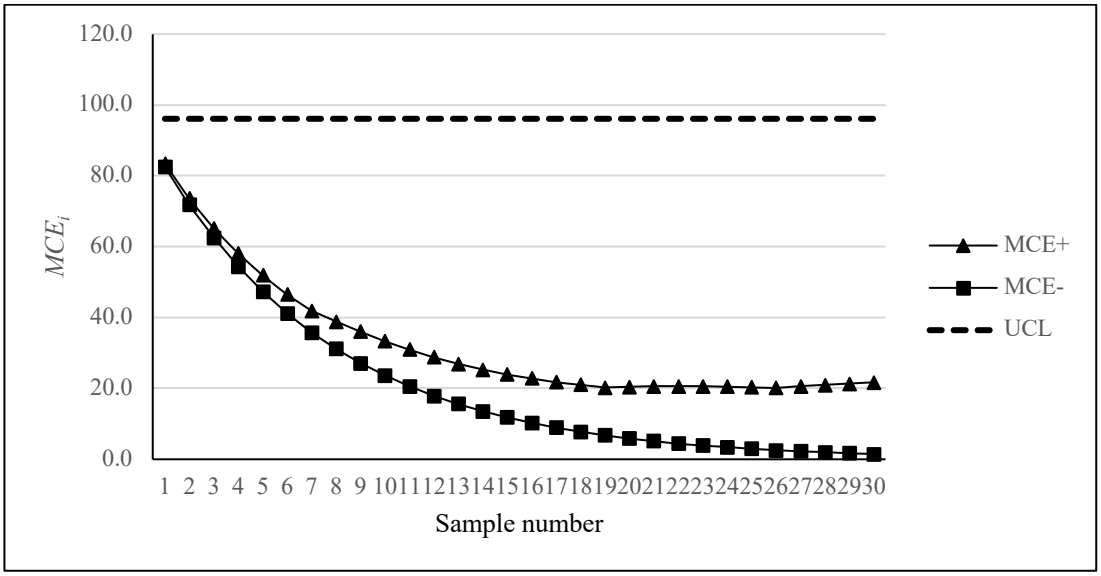

Figure 4.12 $MCE_{\tilde{X}}$ Chart for the TSS Data

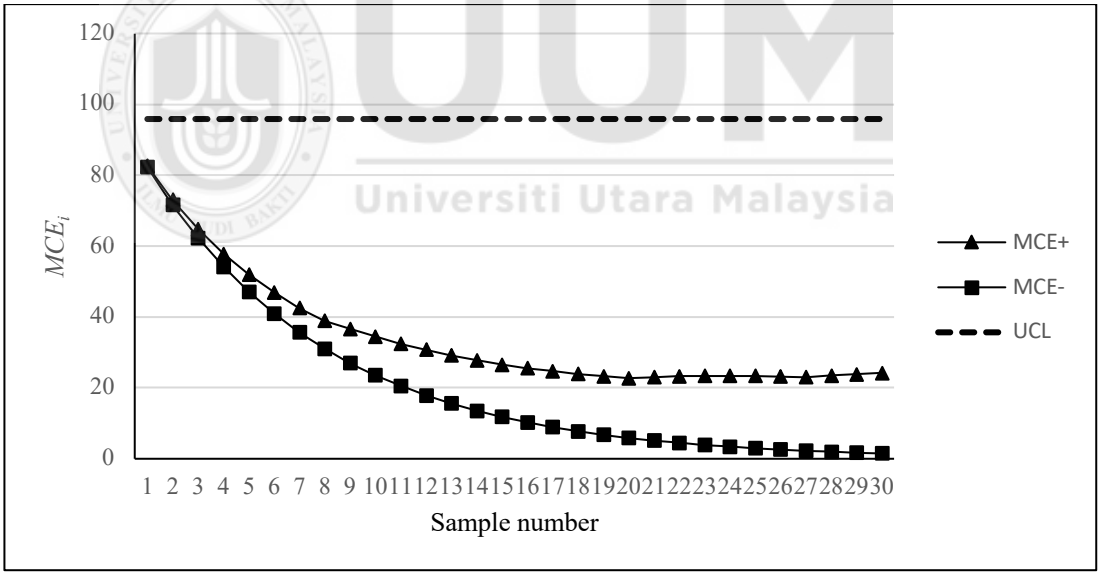

Figure 4.13 MCE_{MOM} Chart for the TSS Data

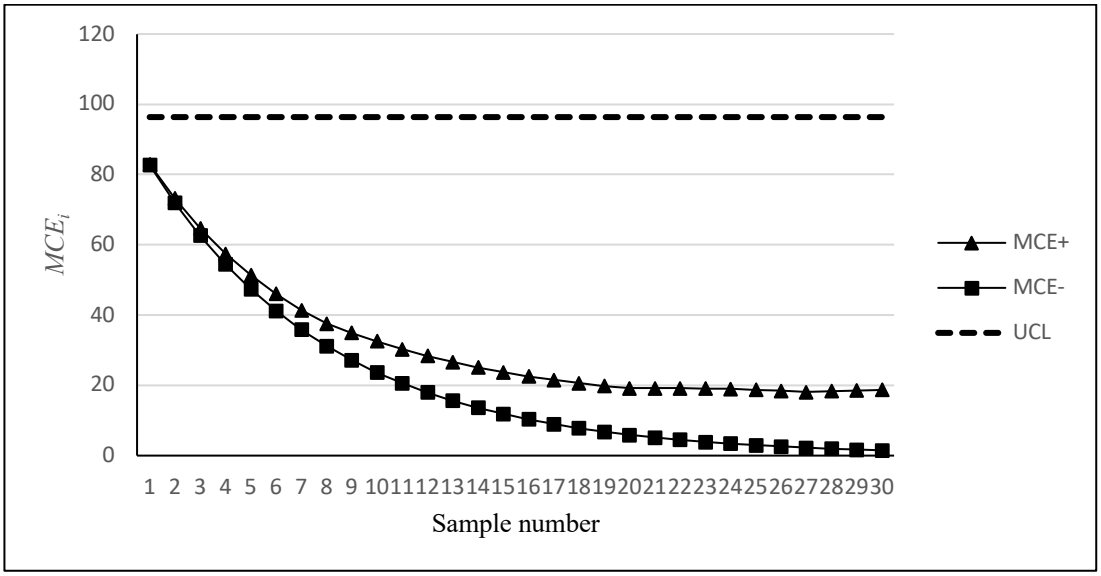

Figure 4.14 MCE_{WMOM} Chart for the TSS Data

Figures 4.15 to 4.18 illustrate the output of the MEC charts for the DOC data. The $MEC_{\bar{X}}$, as presented, in Figure 4.15 shows 23 out-of-control samples (samples 8 to 30) for the MEC_i^-, while no out-of-control samples were identified for the MEC_i^+. Meanwhile, all the robust MEC charts ($MEC_{\tilde{X}}$, MEC_{MOM}, and MEC_{WMOM}) in Figures 4.16 to 4.18 consistently indicated 30 out-of-control samples (samples 1 to 30) for the MEC_i^- and no out-of-control samples for the MEC_i^+. This implies that the proposed robust charts are more sensitive to changes in the DOC data when compared to the $MEC_{\bar{X}}$ chart.

The charts show more out-of-control samples for the MEC_i^- compared to the MEC_i^+. The difference may be due to the external factors, such as temperature changes between day and night, which can affect the process behavior during each cycle.

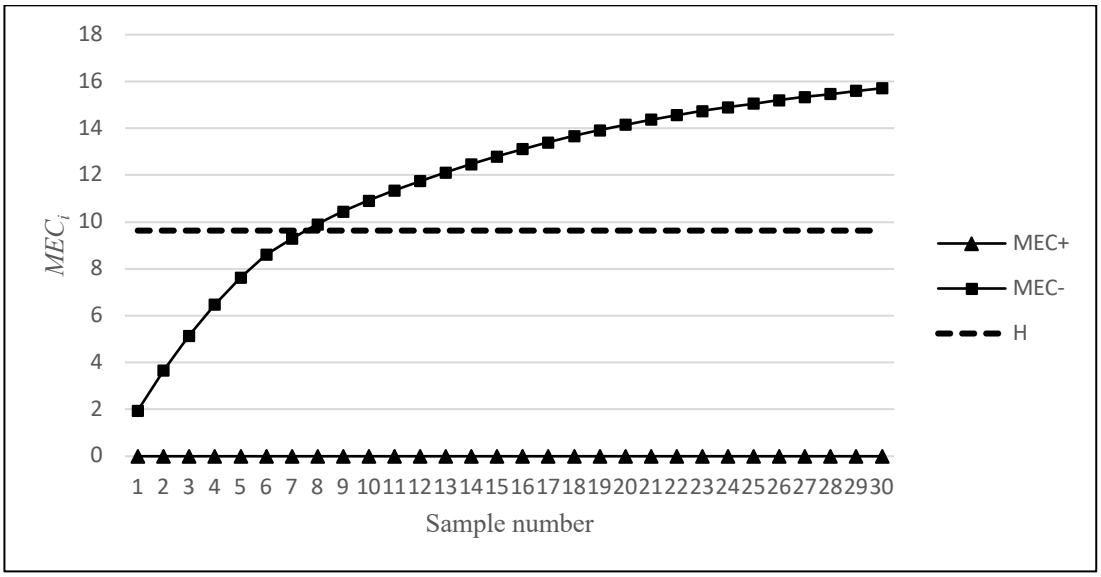

Figure 4.15 $MEC_{\bar{X}}$ Chart for the DOC Data

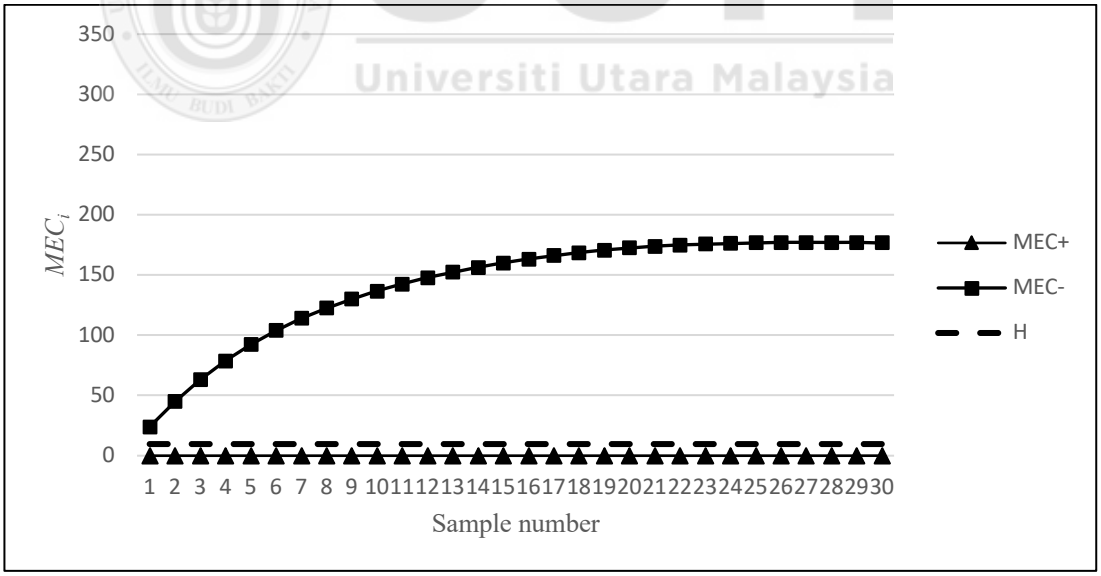

Figure 4.16 $MEC_{\tilde{X}}$ Chart for the DOC Data

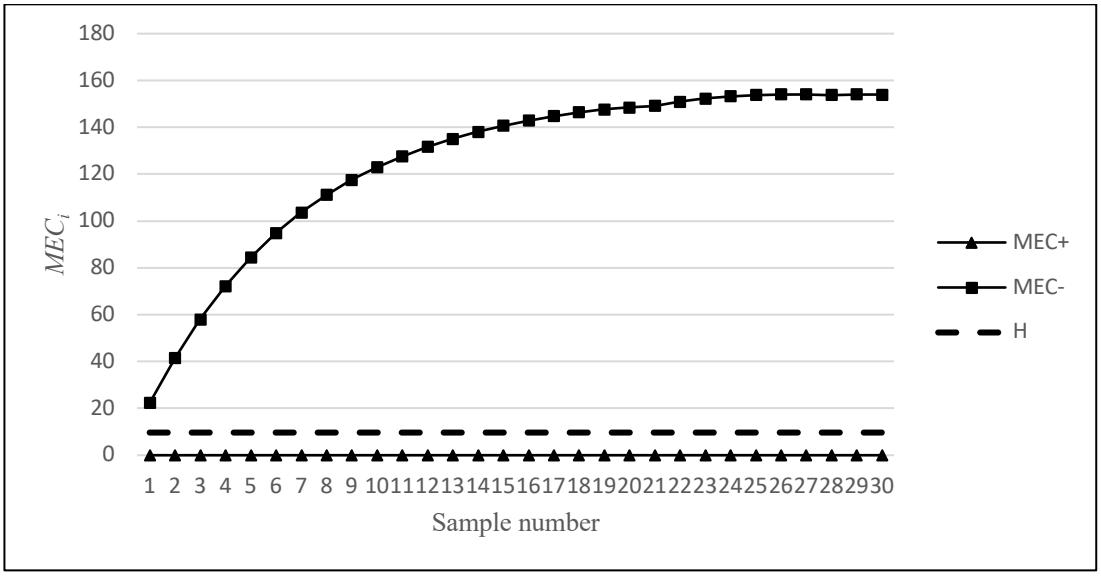

Figure 4.17 MEC_{MOM} Chart for the DOC Data

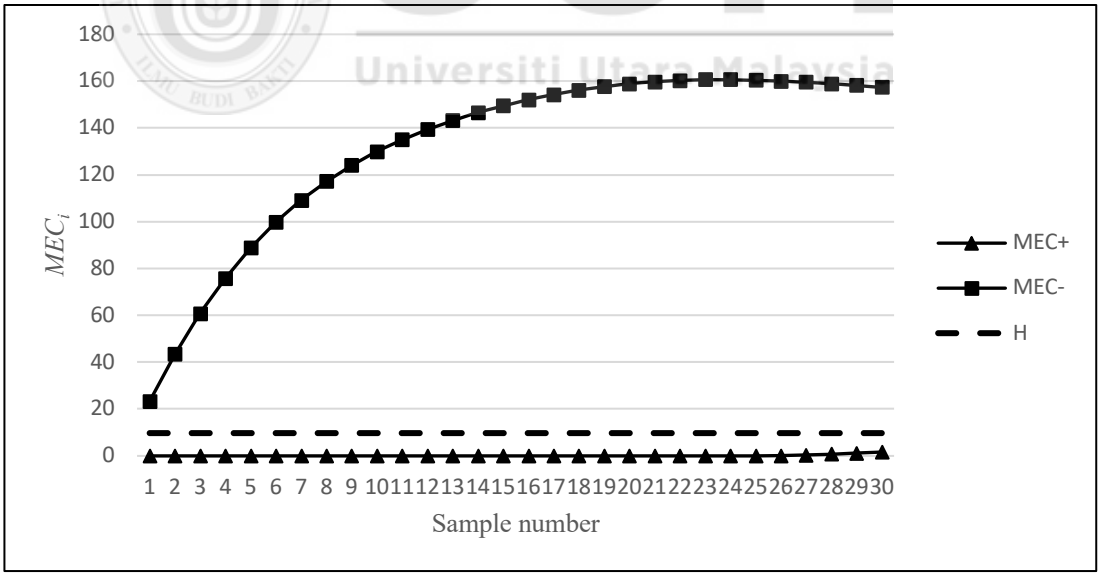

Figure 4.18 MEC_{WMOM} Chart for the DOC Data

Figures 4.19 to 4.22 illustrate the output of the MCE charts for the DOC data. The $MCE_{\bar{X}}$ and $MCE_{\tilde{X}}$ charts, as presented in Figure 4.19 and 4.20, shows no out-of-control samples. Meanwhile, the robust MCE_{MOM} chart in Figure 4.21 indicates 25 out-of-control samples (samples 6 to 30) for the increasing trend and eight (8) out-of-control samples (samples 23 to 30) for the decreasing trend. The robust MCE_{WMOM} in Figure 4.22 indicates 24 out-of-control samples (samples 7 to 30) for the increasing trend and seven (7) out-of-control samples (samples 24 to 30) for the decreasing trend. This implies that the MCE_{MOM} MCE_{WMOM} charts are more sensitive to the changes in the DOC data, unlike the $MCE_{\bar{X}}$ and $MCE_{\tilde{X}}$ charts.

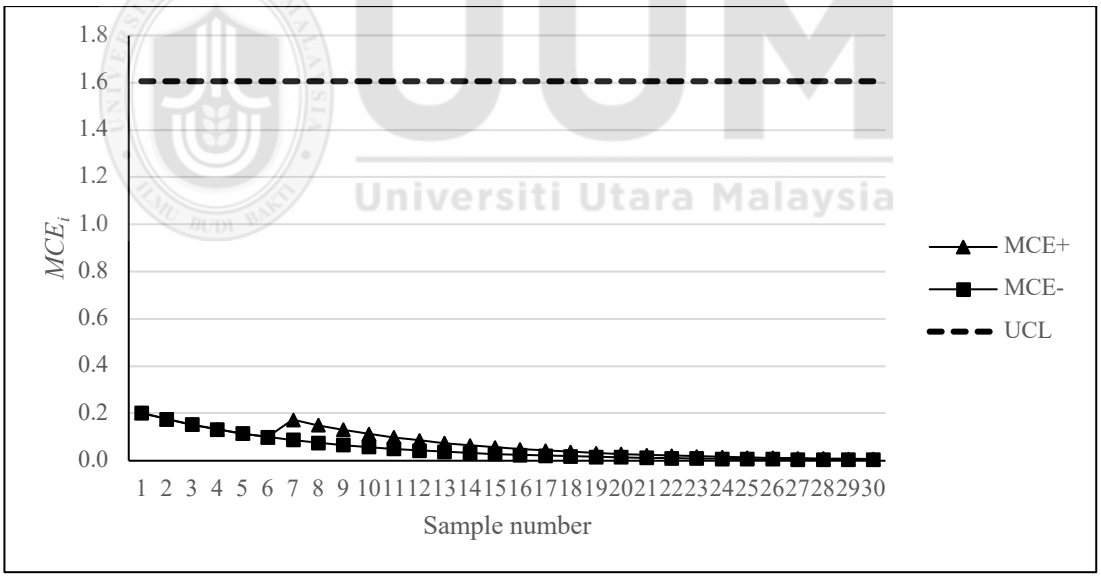

Figure 4.19 $MCE_{\bar{X}}$ Chart for the DOC Data

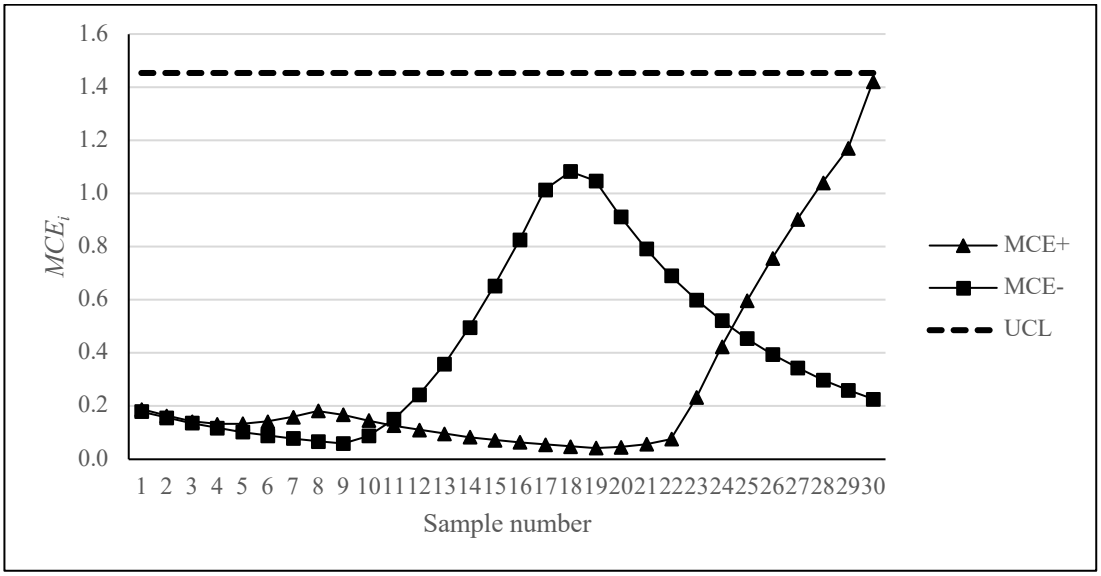

Figure 4.20 $MCE_{\tilde{X}}$ Chart for the DOC Data

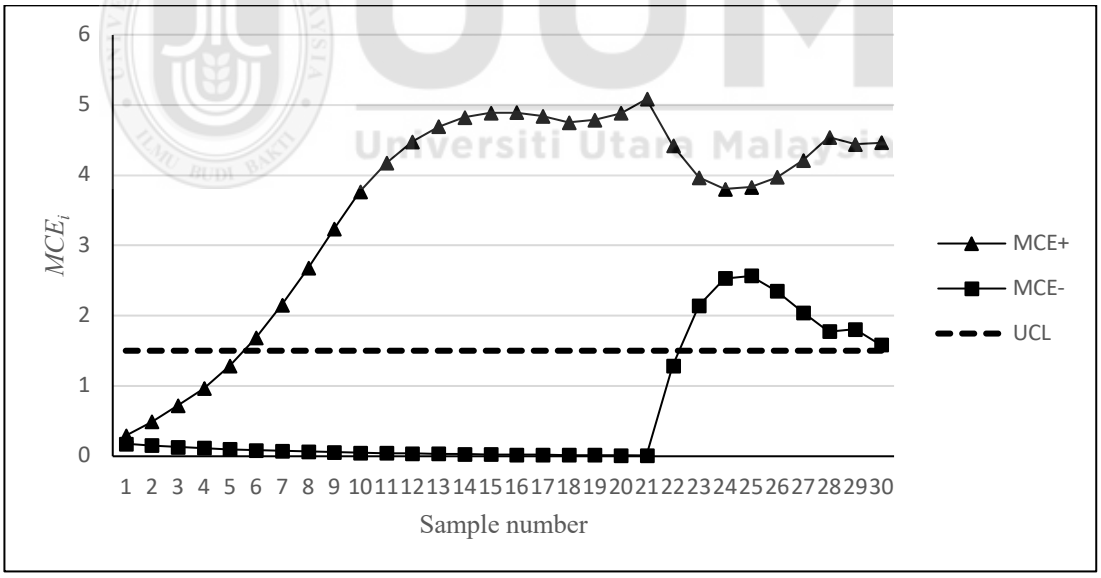

Figure 4.21 MCE_{MOM} for the DOC Data

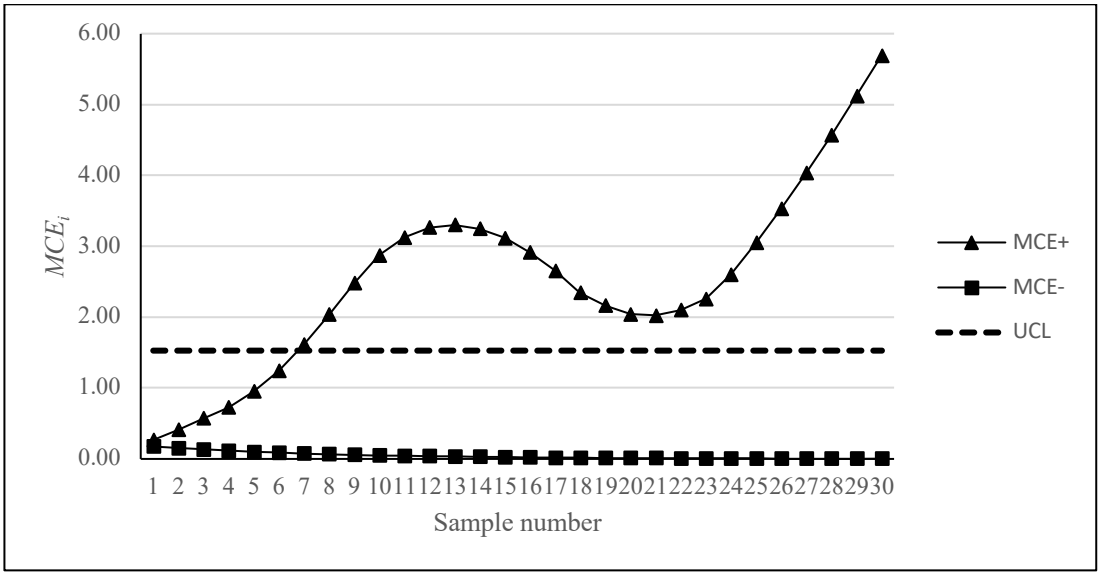

Figure 4.22 MCE_{WMOM} for the DOC Data

4.5.2 MEC and MCE Charts on Marker band Data

To further explore the robustness of the proposed charts, this study validates the findings using real manufacturing data. For this study, 375 data values from marker band data were selected and grouped into 75 samples (m = 75), each with a sample size of 5 (n = 5) as presented in Figure 4.23. The chart shows the increasing trend of the marker band data.

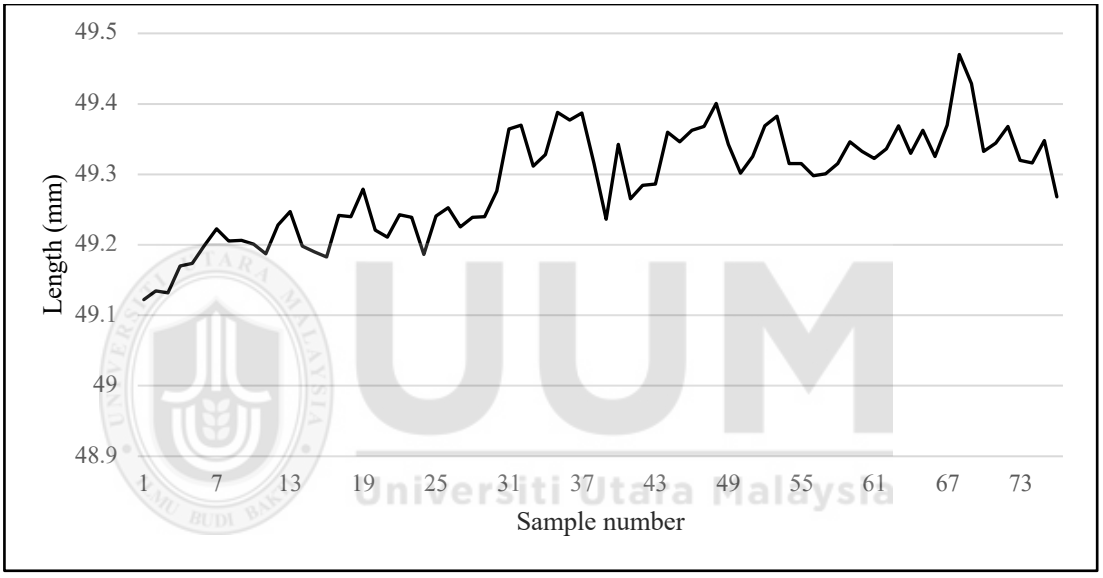

Figure 4.23 Line Chart of Marker Band Data

Table 4.22 shows the estimator values for marker band data. Based on the result, all estimator values including the mean, median, *MOM* and *WMOM* are approximately equal, indicating that the distribution shape is symmetric. Since the distribution is symmetric, the mean is the best estimator of central tendency for marker band data.

Table 4.22

Estimator Values of Marker Band Data

Estimator			
Mean	**Median**	***MOM***	***WMOM***
49.2895	49.2973	49.2890	49.2891

Figures 4.24 show the normality test using the Kolmogrov-Smirnov test on marker band for the 375 data values. With *p*-value = 0.08, the marker band data are concluded to be normally distributed at 5% significance level.

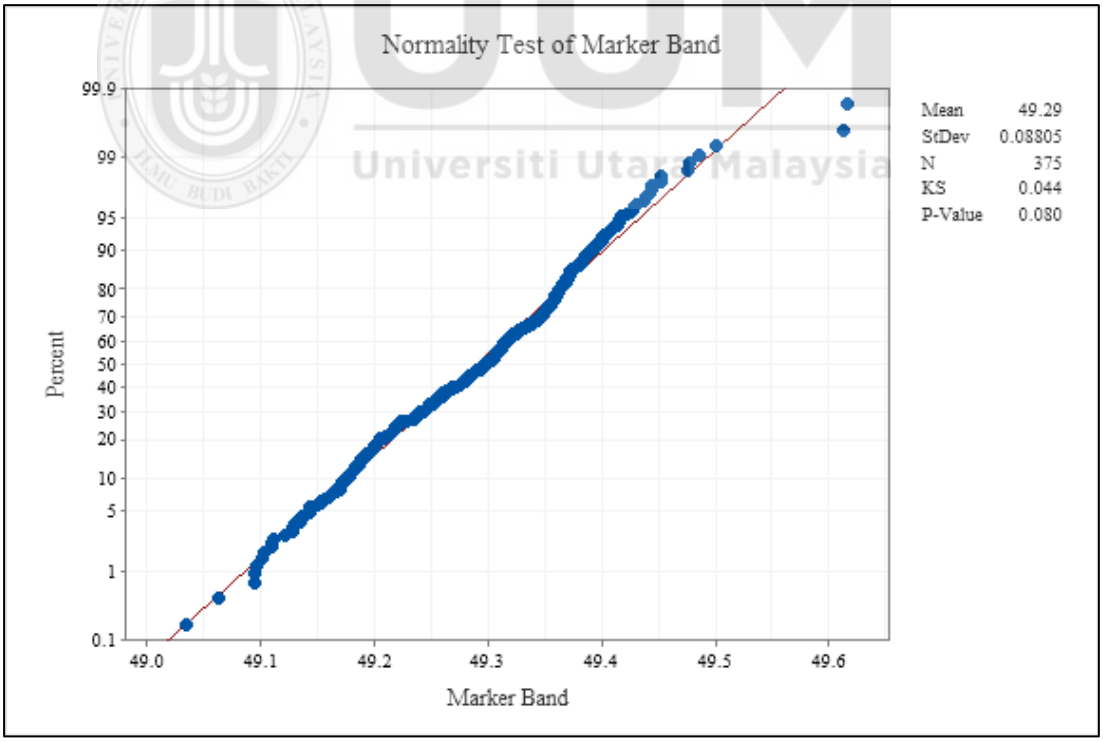

Figure 4.24 Normality Test of the Marker Band Data

Figures 4.25 to 4.28 illustrate the output of the MEC charts for the marker band data. The $MEC_{\bar{X}}$, as presented, in Figure 4.25 shows 7 out-of-control samples (samples 19 to 25) for the MEC_i^+. Meanwhile, the robust MEC charts ($MEC_{\tilde{X}}$ and MEC_{WMOM}) in Figures 4.26 and 4.28 indicate at least 4 out-of-control samples for the MEC_i^+. The robust MEC_{MOM} chart in Figure 4.27 shows 18 out-of-control samples (samples 8 to 25) for the MEC_i^+. This implies that the proposed robust MEC_{MOM} chart are more sensitive to changes in the marker band data when compared to the $MEC_{\bar{X}}$ and other robust charts. This finding aligns with the results obtained from the simulation study, which concluded that MEC_{MOM} chart demonstrate superior robustness and consistently high detection capability, particularly under non-normal data conditions.

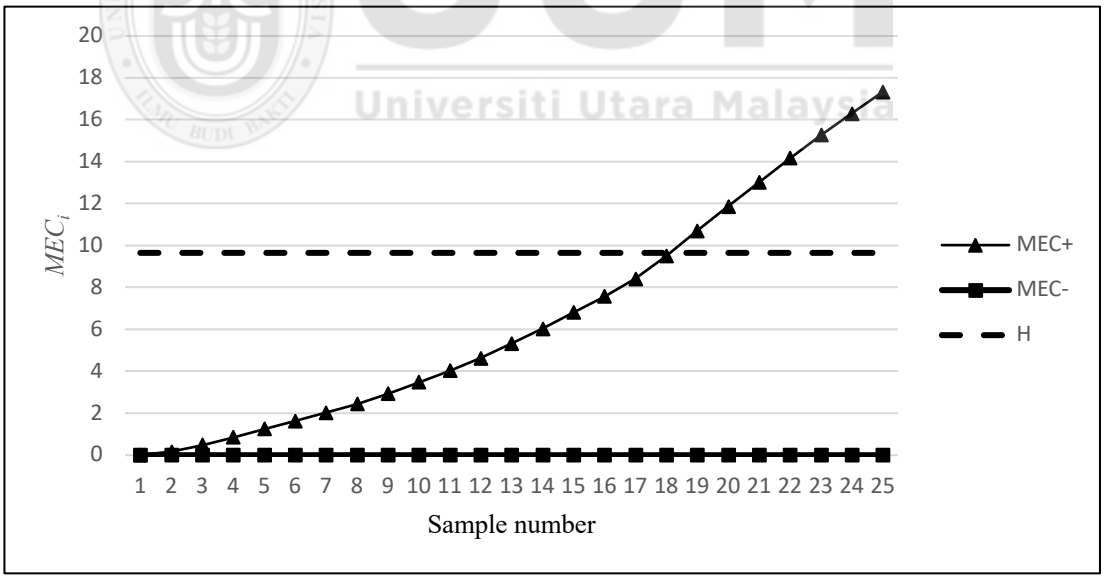

Figure 4.25 $MEC_{\bar{X}}$ Chart for the Marker Band Data

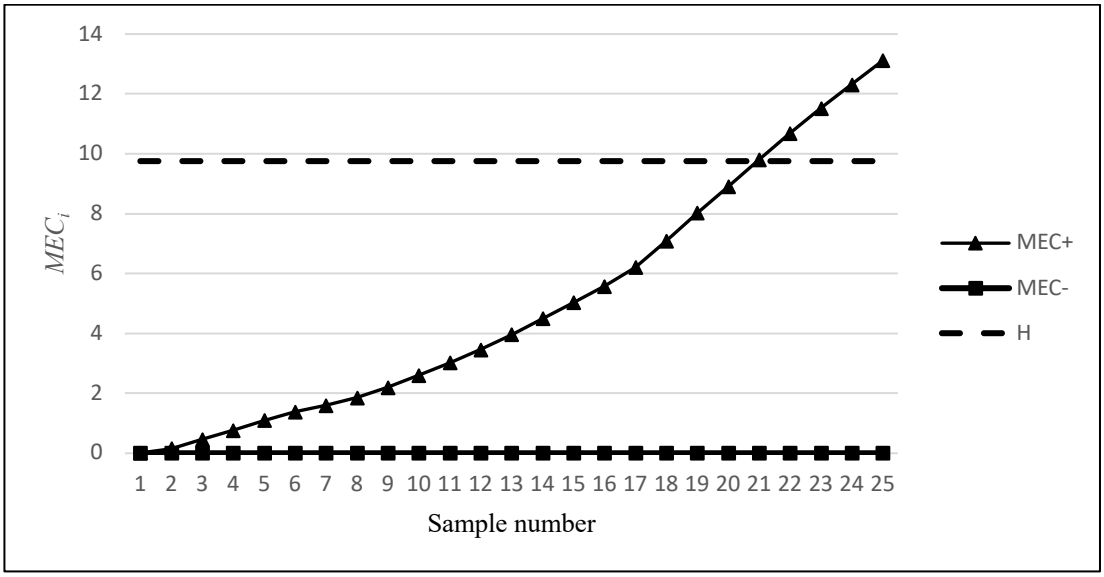

Figure 4.26 $MEC_{\tilde{X}}$ Chart for the Marker Band Data

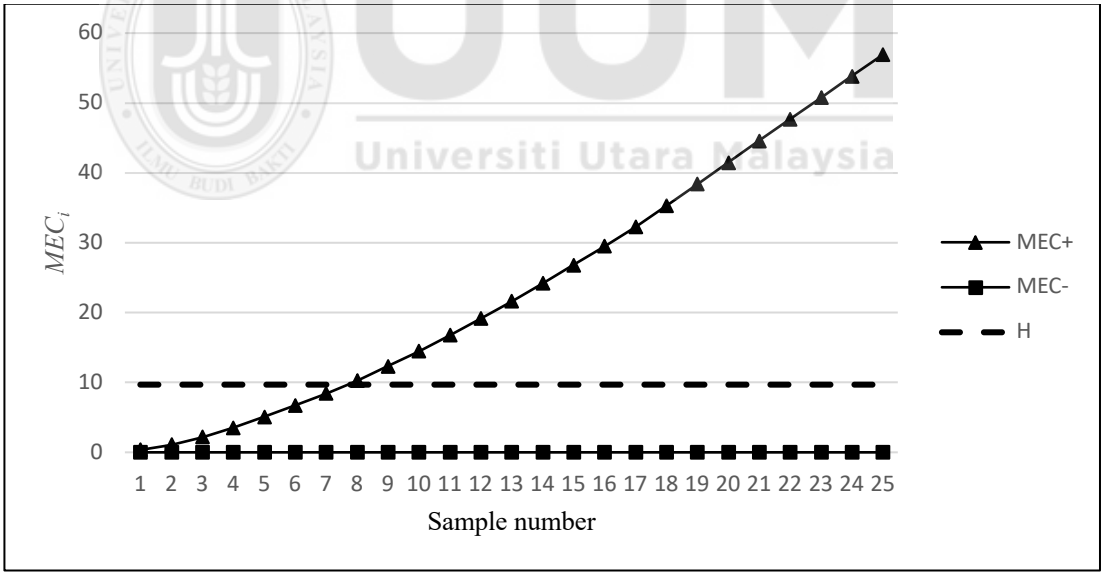

Figure 4.27 MEC_{MOM} Chart for the Marker Band Data

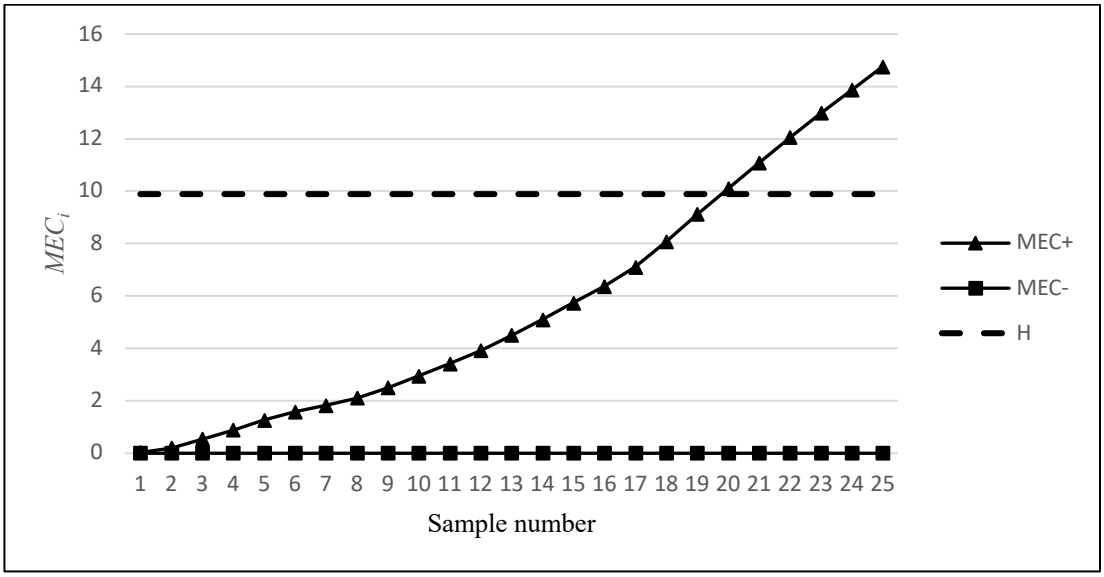

Figure 4.28 MEC_{WMOM} Chart for the Marker Band Data

Figures 4.29 to 4.32 illustrate the output of the MCE charts for the marker band data. All the control charts show the earliest 4 out-of-control samples (samples 1 to 4) at the very beginning for the MCE_i^+ and MCE_i^-.

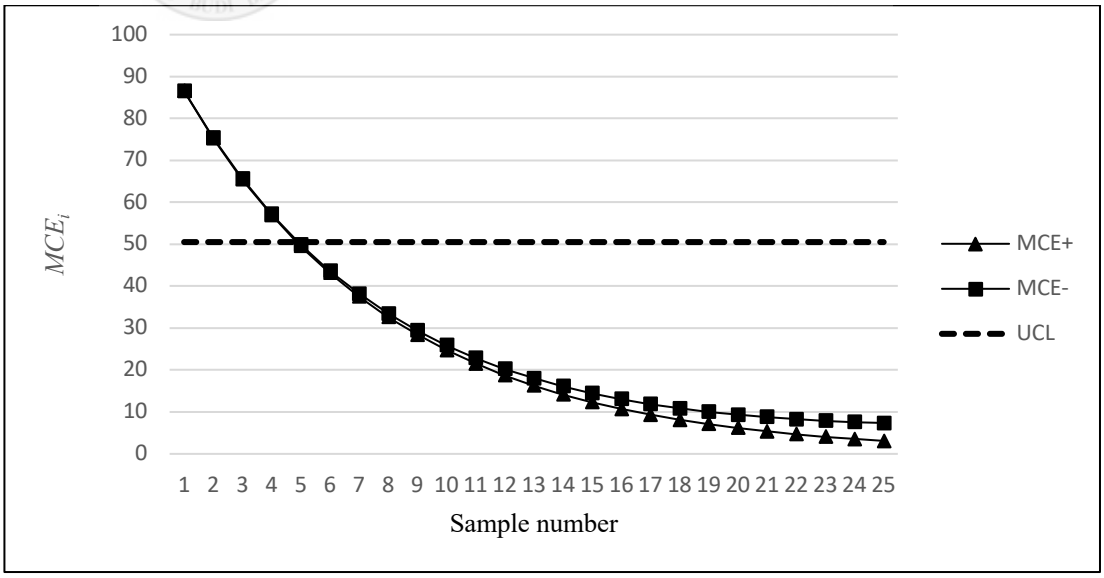

Figure 4.29 $MCE_{\bar{X}}$ Chart for the Marker Band Data

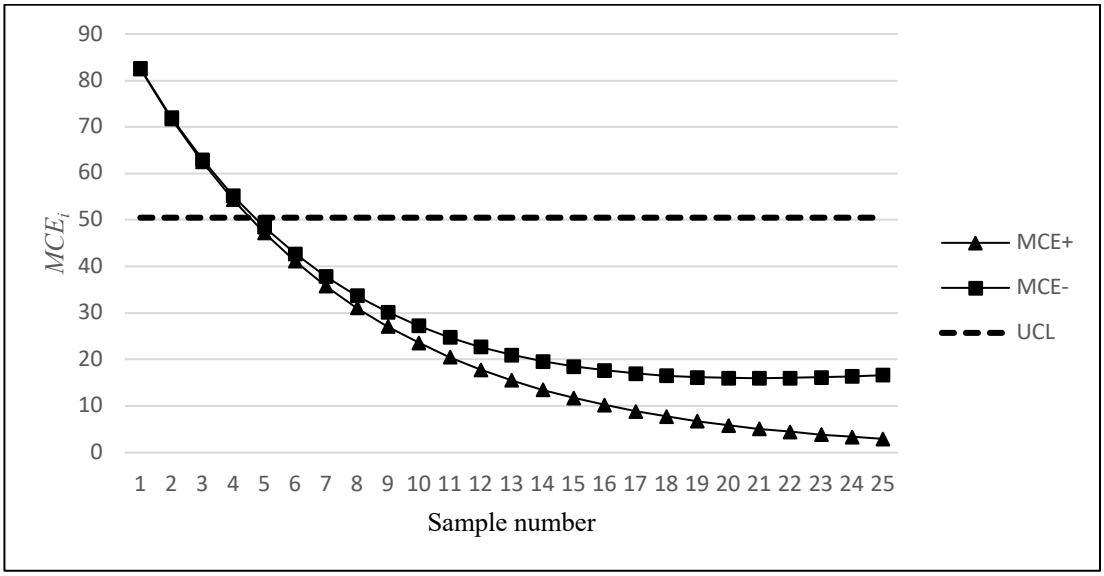

Figure 4.30 $MCE_{\bar{X}}$ Chart for the Marker Band Data

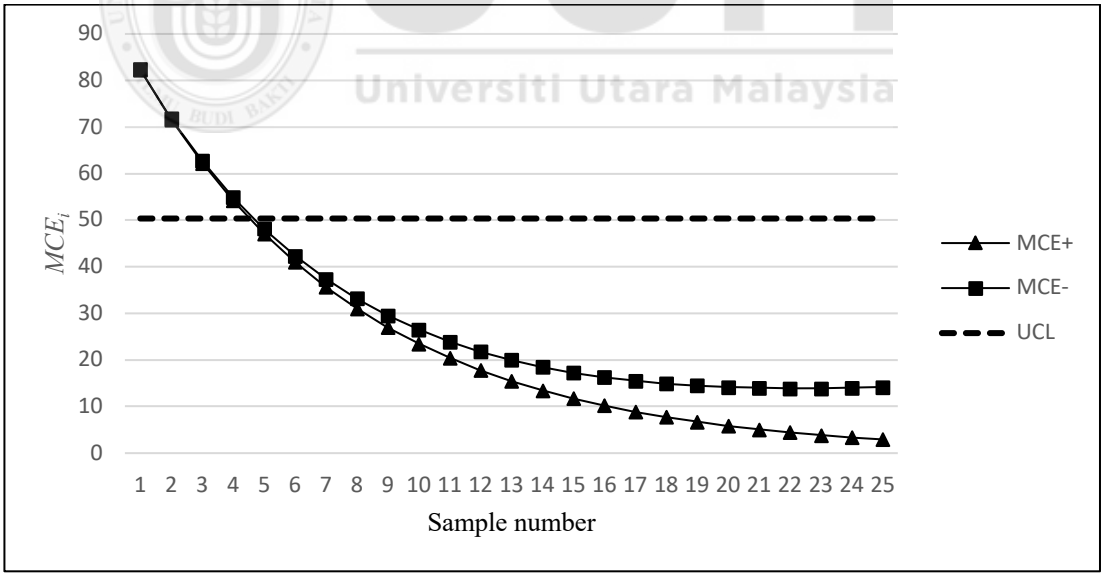

Figure 4.31 MCE_{MOM} Chart for the Marker Band Data

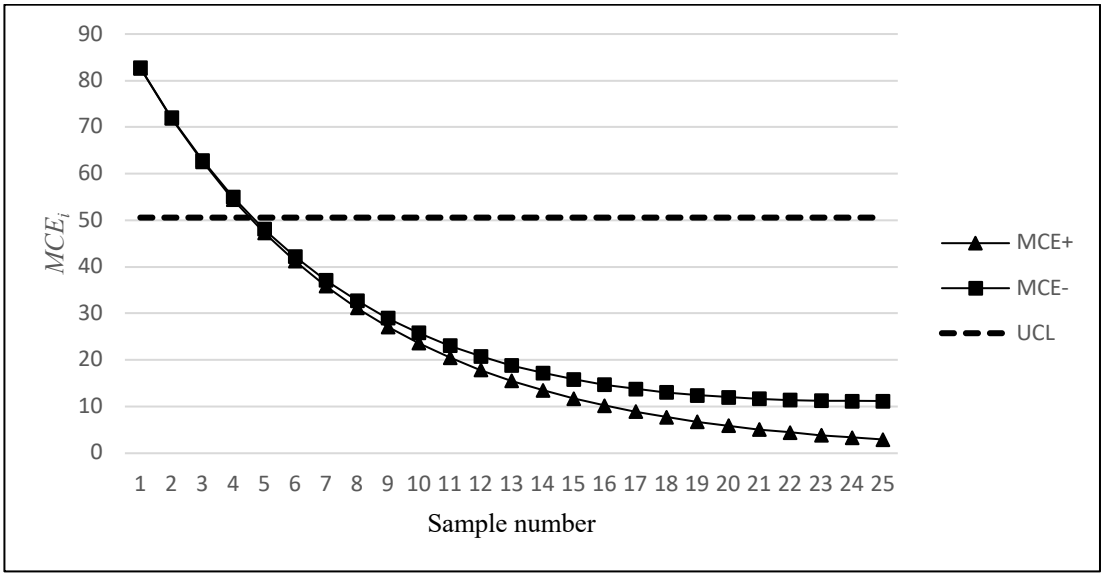

Figure 4.32 MCE_{WMOM} Chart for the Marker Band Data

In conclusion, the analysis of the real data from TSS, DOC and marker band data consistently supports the findings from the simulation study. The robust control charts, particularly MEC_{MOM} and MEC_{WMOM} charts, demonstrated superior performance in detecting shifts compared to $MEC_{\bar{X}}$ chart. The consistent results of real data and simulation study confirms the robustness and capability in detecting shifts of these control charts in handling non-normal data conditions.

CHAPTER FIVE
CONCLUSION

5.1 Introduction

This study aims to develop robust control charts which are able control the Type I error while improving the small shift detection capability. The focus is on the mixed EWMA-CUSUM (MEC) and mixed CUSUM-EWMA (MCE) charts as introduced by Abbas et al. (2013) and Zaman et al. (2015), respectively. In this study, three median based control charts were proposed under each category of the memory-type charts. Specifically, the median, modified one-step *M*-estimator (*MOM*), and winsorized *WMOM*; all possess 50% *BP*, were employed to construct the robust MEC and MCE charts. Six robust charts were produced which are denoted by $MEC_{\tilde{X}}$, MEC_{MOM}, MEC_{WMOM}, $MCE_{\tilde{X}}$, MCE_{MOM}, and MCE_{WMOM}. Their performances were evaluated based on the average run length (ARL) and compared against the standard MEC, MCE charts and Shewhart $\bar{X}$ chart.

In this study, the performance of the proposed MEC and MCE charts was evaluated based on ARL across 128 conditions. These conditions were generated via Monte Carlo simulation studies by manipulating types of distribution (i.e., *g*-and-*h*), design shifts (δ^*), sample sizes (n), and shift sizes (δ) to generate conditions that highlight the strengths and weaknesses of each chart. To fully utilize the salient features of the memory-type charts, the investigated charts in this study were designed for the optimal detection of small and moderate shifts only. The results can be found in section 4.4.

The Shewhart $\bar{X}$ chart was shown to be highly sensitive to non-normality and ineffective for small and moderate shifts. This attests to the loss of information in signaling out-of-control conditions as the chart only uses the most recent data and discards the rest of it. Conversely, the MEC and MCE charts use all samples in the process. With this wealth of information from the samples in the process, both charts are claimed to be effective in signaling out-of-control conditions even when only a small change occurs. Yet, the MEC and MCE charts are confined to the normality assumption as they use the sample mean to monitor a change in the process location, making the charts highly susceptible to the effect of outliers. This rigidity to the normality assumption and its impact on the charts' performance is further emphasized when the process parameters in Phase I are unknown. Parameter estimation in Phase I can be perturbed by the presence of outliers. With this, the control limits can either be overestimated or underestimated. Thus, fluctuating the Type I and Type II errors of the charts. In SPC, these measurement criteria are analogous to the ARL.

5.2 Comparison of the Robustness, ARL_0

The Bradley's stringent criterion was used to determine robust charts among the investigated control charts. Specifically, charts with an ARL_0 [337, 412] were identified to be robust when the pre-determined value was set at 370. The results in section 4.4 depicted that the proposed MEC and MCE charts are highly robust compared to the standard MEC and MCE charts across various conditions tested. Specifically, in the MEC charts' performance, all the proposed MEC charts ($MEC_{\tilde{X}}$, MEC_{MOM}, and MEC_{WMOM}) are comparable in robustness against the $MEC_{\bar{X}}$. Under G0H0.5, as n increases, the MEC_{WMOM} remains as the most robust chart, followed by the $MEC_{\tilde{X}}$ and MEC_{MOM} . The $MEC_{\tilde{X}}$ results in the best control of the ARL_0 when $\delta^* = 1$ and $n = 5$, while the MEC_{WMOM} is the most robust when $\delta^* = 1$ and $n = 9$ under G0.5H0. When G0.5H0.5, the MEC_{MOM} chart indicates as the most robust chart compared to the $MEC_{\tilde{X}}$ and the MEC_{WMOM} when $\delta^* = 0.5$ and $n = 9$.

Focusing on the MCE charts performance, only certain median based MCE charts are robust under G0H0.5. The MCE_{MOM} and MCE_{WMOM} are identified as the most robust charts when compared to the $MCE_{\tilde{X}}$ under this symmetric heavy-tailed distribution when $\delta^* = 1$ and $n = 5$. Meanwhile, the MCE charts under G0.5H0 and G0.5H0.5 fail to meet the robustness criteria because their ARL_0 values fall outside the Bradley's stringent criterion. It can be concluded that the MEC_{MOM} and MEC_{WMOM} exhibit the best control of the ARL_0 when compared to the rest of the charts under investigation across the specified scenarios.

5.3 Comparison of the Shift Detection Capability, ARL_1

The results of this comparison can be found in the section 4.3.2. The ARL_1 value evaluates the shift detection capability of the chart. The smallest ARL_1 indicates that the chart has the fastest detection capability. Under normality, the MCE charts exhibit better performance and can quickly detect small shifts in the process compared to the MEC charts. This is indicated by smaller ARL_1 for the MCE charts, especially when n increases. Specifically, the MCE_{WMOM} chart has a consistent detection capability, yielding small ARL_1 values across different process shifts and sample sizes. The MCE_{WMOM} chart exhibits a greater detection power than the MEC_{WMOM} chart, particularly when the actual shift is relatively small.

When the distribution is heavy-tailed, G0H0.5, the MCE_{MOM} detects the shifts faster compared to other charts when $\delta^* = 1$ and $n = 5$. For G0.5H0 and G0.5H0.5, the robust MEC charts emerges as the best choice with consistently high detection performance. The MEC_{WMOM} shows the best detection capability under G0.5H0. Again, the MEC_{WMOM} shows a good detection capability followed by MEC_{MOM} and $MEC_{\tilde{X}}$ under G0.5H0.5. It can be concluded that all median based MEC charts are comparable in term of the detection capability, and result in a better out-of-control performance than the standard charts.

5.4 Real Data Application

The real data application of the MEC and MCE charts results in all eight charts being applied to the water quality data and marker band data. All the robust MEC charts ($MEC_{\tilde{X}}$, MEC_{MOM}, MEC_{WMOM}) are shown with quick detection to small changes in the TSS and DOC data when compared to the MCE charts. From the TSS real data analysis, the robust $MEC_{\tilde{X}}$ chart outperforms the rest of the robust charts. In contrast, for the DOC real data study, all the robust MEC charts ($MEC_{\tilde{X}}$, MEC_{MOM}, MEC_{WMOM}) outperform the standard $MEC_{\bar{X}}$ and MCE charts. For marker band data analysis, the MEC_{MOM} shown a quick detection to small changes compared to other control charts. These findings align with the results obtained from the simulation study in terms of the detection capability. All robust charts perform comparably with the MEC_{MOM} and MEC_{WMOM} being considered as the best charts, followed by the $MEC_{\tilde{X}}$ in detecting many out-of-control samples.

5.5 Implications

In this chapter, the key findings from Chapter 4 were highlighted which offer advantages in utilizing the proposed robust MEC_{MOM} and MEC_{WMOM} which demonstrated both robustness and fast detection capability, while attesting to the disadvantages of using the standard charts under non-normality. The findings suggest that relying solely on standard control charts, with normality assumption, may lead to poor performance in shifts detection capability, especially in the presence of non-normal data. Under simulation and real data study, the standard charts display poor detection capability when the real data followed skewed distributions, unlike the median based charts. Thus, highlighting the importance of using robust approaches in process monitoring.

5.6 Recommendation for Future Study

In this study, the analysis focused on the univariate data under non-normal distribution. Based on the good performance of the proposed charts in terms of robustness and detection capability under non-normality, it is recommended to continue the work in the multivariate version of the charts.

However, to comprehensively explore the effects on ARL, future research should extend the investigation to include the estimation of the dispersion parameter. Thus, further research is needed to develop appropriate design procedures for the MEC and MCE control charts based on an estimated dispersion parameter with consideration of the robustness perspectives. By exploring this new challenge, valuable insights can be provided which are worth pursuing in future research.

REFERENCES

Abbas, N., Raji, I. A., Riaz, M., & Al-Ghamdi, K. (2018). On designing mixed EWMA dual-CUSUM chart with applications in petro-chemical industry. *IEEE Access*, *6*, 78931-78946.

Abbas, N., Riaz, M., & Does, R. J. (2011). Enhancing the performance of EWMA charts. *Quality and Reliability Engineering International*, *27*(6), 821-833.

Abbas, N., Riaz, M., & Does, R. J. (2013a). Mixed exponentially weighted moving average–cumulative sum charts for process monitoring. *Quality and Reliability Engineering International*, *29*(3), 345-356. 345–356. https://doi.org/10.1002/qre.1385.

Abbas, N., Riaz, M., & Does, R. J. (2013b). CS-EWMA chart for monitoring process dispersion. *Quality and Reliability Engineering International*, *29*(5), 653-663.

Abbas, Z., Nazir, H. Z., Abid, M., Akhtar, N., & Riaz, M. (2020). Enhanced nonparametric control charts under simple and ranked set sampling schemes. *Transactions of the Institute of Measurement and Control*, *42*(14), 2744-2759.

Abdiweli, A. J. (2023). *Simulation study on the performance of robust outlier labelling methods* [Doctoral dissertation, Kampala International University, College of Economics and management].

Abdul Rahman, A., Syed Yahaya, S. S., & Atta, A. M. A. (2018). The effect of median based estimators on CUSUM chart. *Journal of Telecommunication, Electronic and Computer Engineering*, *10*(1-10), 49-52.

Abdul-Rahman, A. (2020). *Robust control charts via winsorized and trimmed estimators.* [Doctoral dissertation, Universiti Utara Malaysia].

Abdul-Rahman, A., Syed-Yahaya, S. S., & Atta, A. M. A. (2021). Robust Synthetic Control Charting. *International Journal of Technology*, *12*(2).

Abdul-Rahman, A., Yahaya, S. S. S., & Atta, A. M. A. (2020). Robustification of CUSUM control structure for monitoring location shift of skewed distributions based on modified one-step *M*-estimator. *Communications in Statistics-Simulation and Computation*, *49(11), 3001-3018.*

Abu-Shawiesh, M. O. (2008). A simple robust control chart based on MAD. *Journal of Mathematics and Statistics*, *4*(2), 102.

Abu-Shawiesh, M. O. A. (2009). A control chart based on robust estimators for monitoring the process mean of a quality characteristic. *International Journal of Quality & Reliability Management*, *26*(5*), 480-496.*

Abu-Shawiesh, M. O., & Abdullah, M. B. (1999). New robust statistical process control chart for location. *Quality Engineering, 12(2), 149-159.*

Acharya, A., Hashemi, A., Jain, P., Sanghavi, S., Dhillon, I. S., & Topcu, U. (2022). Robust training in high dimensions via block coordinate geometric median descent. *International Conference on Artificial Intelligence and Statistics, 11145-11168.*

Adekeye, K. S. (2012). Modified simple robust control chart based on median absolute deviation. *International Journal of Statistics and Probability*, *1*(2), 91.

Adeoti, O. A. (2020). On control chart for monitoring exponentially distributed quality characteristic. *Transactions of the Institute of Measurement and Control, 42(2), 295-305.*

Aguinis, H., Gottfredson, R. K., & Joo, H. (2013). Best-practice recommendations for defining, identifying, and handling outliers. Organizational Research Methods, 16(2), 270-301.

Ahsan, M., Mashuri, M., Lee, M. H., Kuswanto, H., & Prastyo, D. D. (2020). Robust adaptive multivariate Hotelling's T2 control chart based on kernel density estimation for intrusion detection system. *Expert Systems with Applications, 145, 113105.*

Ajadi, J. O., & Riaz, M. (2017). Mixed multivariate EWMA-CUSUM control charts for an improved process monitoring. *Communications in Statistics-Theory and Methods*, *46*(14), 6980-6993.

Ajadi, J. O., Riaz, M., & Al-Ghamdi, K. (2016). On increasing the sensitivity of mixed EWMA–CUSUM control charts for location parameter. *Journal of Applied Statistics*, *43*(7), 1262-1278.

Akhtar, N., Abid, M., Amir, M. W., Abbas, Z., Nazir, H. Z., Raza, Z., & Riaz, M. (2022). Design and analysis of exponentially weighted moving average control charts for monitoring the variability of log-normal processes with estimated parameters. *Quality and Reliability Engineering International, 38(4), 1590-1611.*

Alduais, F. S., & Khan, Z. (2023). EWMA control chart for Rayleigh process with engineering applications. *IEEE Access, 11, 10196-10206.*

Ali, S. (2020). A predictive Bayesian approach to EWMA and CUSUM charts for time-between-events monitoring. *Journal of Statistical Computation and Simulation, 90(16), 3025-3050.*

Alshqaq, S. S., & Abuzaid, A. H. (2023). An Efficient Method for Variable Selection Based on Diagnostic-Lasso Regression. *Symmetry*, *15*(12), *2155.*

Alwan, W., Ngadiman, N. H. A., Hassan, A., Saufi, S. R., & Mahmood, S. (2023). Ensemble Classifier for Recognition of Small Variation in X-Bar Control Chart Patterns. *Machines*, *11*(*1), 115.*

Amin, R. W., Reynolds Jr, M. R., & Saad, B. (1995). Nonparametric quality control charts based on the sign statistic. *Communications in Statistics-Theory and Methods, 24(6), 1597-1623.*

Amiri, A., Abossedgh, S., & Saghaei, A. (2022). Enhancing the Performance of Monitoring the DCSBM Using Multivariate Control Charts with Estimated Parameters. *Advances in Industrial Engineering. 56 (1).*

André, Q. (2022). Outlier exclusion procedures must be blind to the researcher's hypothesis. *Journal of Experimental Psychology: General*, *151*(1*), 213.*

Arslan, M., Anwar, S., Gunaime, N. M., Shahab, S., Lone, S. A., & Rasheed, Z. (2023). An improved charting scheme to monitor the process mean using two supplementary variables. *Symmetry, 15(2), 482.*

Aslam, M., Shafqat, A., Albassam, M., Malela-Majika, J. C., & Shongwe, S. C. (2021). A new CUSUM control chart under uncertainty with applications in petroleum and meteorology. *PLoS One, 16(2), e0246185.*

Astivia, O. L. O., & Edward, K. (2022). Theoretical considerations when simulating data from the g-and-h family of distributions. *British Journal of Mathematical and Statistical Psychology, 75(3), 699-727.*

Atalay, M., Testik, M. C., Duran, S., & Weiß, C. H. (2020). Guidelines for automating Phase I of control charts by considering effects on Phase-II performance of individuals control chart. *Quality Engineering, 32(2), 223-243.*

Balcerowska-Czerniak, G., & Gorczyca, B. (2024). Rapid assessment of surface water quality using statistical multivariate analysis approach: Oder River system case study. *Science of The Total Environment, 912, 168754.*

Batool, Z., & Haq, A. (2024). An adaptive EWMA chart for Poisson process. *Quality Technology & Quantitative Management, 1-16.*

Bondarenko, Y., Nagel, M., & Blankevoort, T. (2024). Quantizable transformers: Removing outliers by helping attention heads do nothing. *Advances in Neural Information Processing Systems, 36.*

Bradley, J. V. (1978). Robustness?. *British Journal of Mathematical and Statistical Psychology, 31(2), 144-152.*

Capizzi, G., & Masarotto, G. (2003). An adaptive exponentially weighted moving average control chart. *Technometrics, 45(3), 199-207.*

Castagliola, P. (2005). A new S2-EWMA control chart for monitoring the process variance. *Quality and Reliability Engineering International, 21(8), 781-794.*

Castagliola, P., Celano, G., & Fichera, S. (2009). A new CUSUM-S 2 control chart for monitoring the process variance. *Journal of Quality in Maintenance Engineering, 15(4), 344-357.*

Ceriani, L., & Verme, P. (2012). The origins of the Gini index: extracts from Variabilità e Mutabilità (1912) by Corrado Gini. *The Journal of Economic Inequality, 10(3), 421-443.*

Chakraborti, S., & Van de Wiel, M. A. (2008). A nonparametric control chart based on the Mann-Whitney statistic. *Institute of Mathematical Statistics*, 1, 156-172. https://arxiv.org/abs/0805.2292v1

Chakraborti, S., Eryilmaz, S., & Human, S. W. (2009). A phase II nonparametric control chart based on precedence statistics with runs-type signaling rules. *Computational Statistics & Data Analysis*, *53*(4), *1054-1065*.

Chaudhary, A. M., Sanaullah, A., Hanif, M., Almazah, M. M., Albasheir, N. A., & Al-Duais, F. S. (2023). Efficient Monitoring of a Parameter of Non-Normal Process Using a Robust Efficient Control Chart: A Comparative Study. *Mathematics, 11(19), 4157.*

Cheng, C. S., Chen, P. W., & Wu, Y. T. (2023). Phase I Analysis of Nonlinear Profiles Using Anomaly Detection Techniques. *Applied Sciences, 13(4), 2147.*

Chong, Z. L., Tan, K. L., Khoo, M. B., Teoh, W. L., & Castagliola, P. (2022). Optimal designs of the exponentially weighted moving average (EWMA) median chart for known and estimated parameters based on median run length. *Communications in Statistics-Simulation and Computation, 51(7), 3660-3684.*

Crisp, A., & Burridge, J. (1993). A note on the uniqueness of M-estimators in robust regression. The Canadian *Journal of Statistics/La Revue Canadienne de Statistique, 205-208.*

Croux, C., & Rousseeuw, P. J. (1992). A class of high-breakdown scale estimators based on subranges. *Communications in statistics-theory and methods, 21(7), 1935-1951.*

Crowder, S. V. (1989). Design of exponentially weighted moving average schemes. *Journal of Quality technology, 21(3), 155-162.*

David, H. A. (1968). Miscellanea: Gini's mean difference rediscovered. *Biometrika, 55(3), 573-575.*

Dibal, N. P., & Dallah, H. (2021). Stratified sampling in highly polluted data as an effective and reliable alternative to high breakdown point estimators. *Model Assisted Statistics and Applications, 16(2), 109-115.*

Diko, M. D., Goedhart, R., & Does, R. J. (2020). A head-to-head comparison of the out-of-control performance of control charts adjusted for parameter estimation. *Quality Engineering, 32(4), 643-652.*

Dixon, W. J., & Tukey, J. W. (1968). Approximate behavior of the distribution of Winsorized t (Trimming/Winsorization 2). *Technometrics*, *10*(1), *83-98.*

Does, R. J., Goedhart, R., & Woodall, W. H. (2020). On the design of control charts with guaranteed conditional performance under estimated parameters. *Quality and Reliability Engineering International, 36(8), 2610-2620.*

Domański, P. D. (2020). Study on statistical outlier detection and labelling. International Journal of Automation and Computing, 17(6), 788-811.

Donoho, D. L. (1982). *Breakdown properties of multivariate location estimators*. Technical report, Harvard University, Boston. http://www-stat. stanford. edu/~ donoho/Reports/Oldies/BPMLE. pdf.

Donoho, D. L., & Huber, P. J. (1983). *The notion of breakdown point*. A festschrift for Erich L. Lehmann, 157184.

Duong-Tran, D., Dastoorian, R., & Wells, L. (2022). Revisiting the one-sided EWMA control chart. *Journal of applied research on industrial engineering, 9(2), 151-164.*

Emad, A., Naimi, S., Altaie, M. R., & Hameed, M. R. A. (2023). Artificial intelligence based statistical process control for monitoring and quality control of water resources: A complete digital solution. *International Journal of Intelligent Systems and Applications in Engineering, 11(5s), 314-324.*

Faisal, M., Zafar, R. F., Abbas, N., Riaz, M., & Mahmood, T. (2018). A modified CUSUM control chart for monitoring industrial processes. *Quality and Reliability Engineering International*, *34(6), 1045-1058.*

Fan, W., Jiang, F., Li, Y., & Peng, Z. (2024). A Hankel Matrix-Based Multivariate Control Chart With Shrinkage Estimator for Condition Monitoring of Rolling Bearings. IEEE Transactions on Automation Science and Engineering.

Fan, Z., Ng, S. H., & Hu, Q. (2023). A Novel Framework for Improving the Breakdown Point of Robust Regression Algorithms. *arXiv preprint arXiv:2305.12220*. https://doi.org/10.48550/arXiv.2305.12220

Fishbone, J., & Mili, L. (2023). New highly efficient high-breakdown estimator of multivariate scatter and location for elliptical distributions. *The Canadian Journal of Statistics.*

Galetto, F. (2020). Six Sigma: Hoax against Quality Ignorant Professionals fond of money and not of Quality MINITAB wrong T Charts. https://hal.science/hal-02492499

Geyer, C. J. (2006). *Breakdown point theory notes. Class Notes on Nonparametric Statistics*. https://www.stat.umn.edu/geyer/s06/5601/theo/break.pdf

Gini, C. (1912). *Variabilità e Mutuabilità. Contributo allo Studio delle Distribuzioni e delle Relazioni Statistiche*. C. Cuppini, Bologna.

Haanchumpol, T., & Sermpongpan, C. (2023). Remodeling multivariate control chart by using spatial signed rank for detecting mean shift in normal and non-normal processes. *Thailand Statistician, 21(3), 691-724.*

Haddad, F. S., Syed-Yahaya, S. S., & Alfaro, J. L. (2013). Alternative Hotelling's T^2 charts using winsorized modified one-step *M*-estimator. *Quality and Reliability Engineering International*, *29*(4), 583-593. https://doi.org/10.1002/qre.1407

Hamasha, M. M., Obeidat, M. S., Alzoubi, K., Shawaheen, G., Mayyas, A., Almomani, H. A., Al-Sukkar, A., & Mukkatash, A. (2023). Symmetry of gamma distribution data about the mean after processing with EWMA function. *Scientific Reports, 13(1), 15096.*

Hampel, F. R. (1968). *Contributions to the theory of robust estimation*. University of California, Berkeley.

Hampel, F. R. (1971). A general qualitative definition of robustness. *The annals of mathematical statistics, 42(6), 1887-1896.*

Hampel, F. R. (1974). The influence curve and its role in robust estimation. *Journal of the american statistical association, 69(346), 383-393.*

Haq, A., Khoo, M. B., Ha Lee, M., & Abbasi, S. A. (2021). Enhanced adaptive multivariate EWMA and CUSUM charts for process mean. *Journal of Statistical Computation and Simulation, 91(12), 2361-2382.*

Haridy, S., & Benneyan, J. C. (2024). Shewhart-EWMA chart for monitoring binomial data subject to shifts of random amounts. *Computers & Industrial Engineering*, *193*, 110252.

Hawkins, D. M. (1993). Cumulative sum control charting: an underutilized SPC tool. *Quality Engineering*, *5*(3), *463-477.*

Hawkins, D. M., & Deng, Q. (2010). A nonparametric change-point control chart. *Journal of Quality Technology*, *42*(2), *165-173.*

Hernandez, H. (2021). Testing for normality: What is the best method. *ForsChem Research Reports, 6, 2021-05.*

Huber, P. J. (1981). *Robust Statistics*. John Wiley & Sons, New York.

Human, S. W., Kritzinger, P., & Chakraborti, S. (2011). Robustness of the EWMA control chart for individual observations. *Journal of Applied Statistics*, *38*(10), *2071-2087.*

Jardim, F. S., Chakraborti, S., & Epprecht, E. K. (2020). Two perspectives for designing a phase II control chart with estimated parameters: *The case of the Shewhart X Chart. Journal of Quality Technology, 52(2), 198-217.*

Jensen, W.A, Montgomery, D. C., Tsung, F., & Vining, G. G. (2018). 50 years of the Journal of Quality Technology. *Journal of Quality Technology, 50:1, 2-16*. https://doi.org/10.1080/00224065.2018.1404881

Jiang, W., Shu, L., & Apley, D. W. (2008). Adaptive CUSUM procedures with EWMA-based shift estimators. *IIE Transactions, 40(10), 992-1003.*

John, B., & Subhani, S. M. (2020). A modified control chart for monitoring non-normal characteristics. *International Journal of Productivity and Quality Management, 29(3), 309-328.*

Jones-Farmer, L. A., Jordan, V., & Champ, C. W. (2009). Distribution-free phase I control charts for subgroup location. *Journal of Quality Technology*, *41*(3), *304-316.*

Jorge, M., & Boris, I. (1984). Some properties of the Tukey *g*-and-*h* family of distributions. *Communications in Statistics-Theory and Methods, 13(3), 353-369.*

Karch, J. D. (2023). Outliers may not be automatically removed. *Journal of Experimental Psychology: General, 152(6), 1735.*

Kelter, R. (2021). Bayesian and frequentist testing for differences between two groups with parametric and nonparametric two-sample tests. *Wiley Interdisciplinary Reviews: Computational Statistics, 13(6), e1523.*

Knoth, S., Saleh, N. A., Mahmoud, M. A., Woodall, W. H., & Tercero-Gómez, V. G. (2023). A critique of a variety of "memory-based" process monitoring methods. *Journal of Quality Technology, 55(1), 18-42.*

Knoth, S., Tercero-Gómez, V. G., Khakifirooz, M., & Woodall, W. H. (2021). The impracticality of homogeneously weighted moving average and progressive mean control chart approaches. *Quality and Reliability Engineering International, 37(8), 3779-3794.*

Knott, J. A., Liknes, G. C., Giebink, C. L., Oh, S., Domke, G. M., McRoberts, R. E., Quirino, V. F., and Walters, B. F. (2023). Effects of outliers on remote sensing-assisted forest biomass estimation: A case study from the United States national forest inventory. *Methods in Ecology and Evolution 14, no. 7 (2023): 1587-1602.*

Kostyszyn, K. N. (2021). *Statistical testing for sufficient control chart performances based on short runs and small mixed batches*. [Doctoral Dissertation, RWTH Aachen University].

Koutras, M. V., Bersimis, S., & Maravelakis, P. (2007). Statistical process control using Shewhart control charts with supplementary runs rules. *Methodology and Computing in Applied Probability, 9, 207-224.*

Kruskal, W. H. (1960). Some remarks on wild observations. *Technometrics, 2(1), 1-3.*

Kuiper, A., & Goedhart, R. (2023). Optimized control charts using indifference regions. *Quality Engineering, 1-19.*

Kumar, N., & Singh, R. K. (2020). A comparative study of ANI-and ARL-unbiased geometric and CCC G control charts. *Sequential Analysis, 39(3), 399-416.*

Langenberg, P., & Iglewicz, B. (1986). Trimmed mean X and R charts. *Journal of Quality Technology*, *18*(3*), 152-161.*

Lepore, A., Palumbo, B., & Sposito, G. (2022). Neural network based control charting for multiple stream processes with an application to HVAC systems in passenger railway vehicles. *Applied Stochastic Models in Business and Industry, 38(5), 862-883.*

Letshedi, T. I., Malela-Majika, J. C., Castagliola, P., & Shongwe, S. C. (2021). Distribution-free triple EWMA control chart for monitoring the process location using the Wilcoxon rank-sum statistic with fast initial response feature. *Quality and Reliability Engineering International, 37(5), 1996-2013.*

Ley, C. (2015). Flexible modelling in statistics: past, present and future. *Journal de la Société Française de Statistique, 156(1), 76-96.*

Li, C., Wang, J., & Wang, X. L. (2024). Monitoring aggregate warranty claims with dynamically designed CUSUM and EWMA charts. *International Journal of Production Research, 62(7), 2370-2397.*

Li, H., Deng, J., Yuan, S., Feng, P., & Arachchige, D. D. (2021). Monitoring and identifying wind turbine generator bearing faults using deep belief network and EWMA control charts. *Frontiers in Energy Research, 9, 799039.*

Li, J., Yu, D., Song, Z., Mukherjee, A., Chen, R., & Zhang, J. (2022). Comparisons of some memory-type control chart for monitoring Weibull-distributed time between events and some new results. *Quality and Reliability Engineering International, 38(7), 3598-3615.*

Li, S. Y., Tang, L. C., & Ng, S. H. (2010). Nonparametric CUSUM and EWMA control charts for detecting mean shifts. *Journal of Quality Technology*, *42*(2), *209-226.*

Liu, Z., Li, Z., He, H., Fu, Y., & Ran, J. (2023). Robust solution of coordinate transformation parameters with a high breakdown point. *Measurement Science and Technology, 34(9), 095021.*

Lopuhaä, H. P. (2023). Highly efficient estimators with high breakdown point for linear models with structured covariance matrices. *Econometrics and Statistics, 15 (21).* https://doi.org/10.1016/j.ecosta.2023.03.003

Lu, Y., Mathur, A. K., Blunt, B. A., Glüer, C. C., Will, A. S., Fuerst, T. P., Jergas, M. D., Andriano, K. N., Cummings, S. R., & Genant, H. K. (2020). Dual X-ray absorptiometry quality control: Comparison of visual examination and process-control charts. *Journal of Bone and Mineral Research, 11(5), 626-637.*

Lucas, J. M. (1982). Combined Shewhart-CUSUM quality control schemes. *Journal of Quality Technology*, *14*(2), 51-59.

Lucas, J. M., & Crosier, R. B. (1982). Fast initial response for CUSUM quality-control schemes: give your CUSUM a head start. *Technometrics*, *24*(3), *199-205.*

Lucas, J. M., & Saccucci, M. S. (1990). Exponentially weighted moving average control schemes: properties and enhancements. *Technometrics*, *32*(1), *1-12.*

Malela-Majika, J. C. (2021). New distribution-free memory-type control charts based on the Wilcoxon rank-sum statistic. *Quality Technology & Quantitative Management, 18(2), 135-155.*

Malela-Majika, J. C., Human, S. W., & Chatterjee, K. (2024). Homogeneously weighted moving average control charts: overview, controversies, and new directions. *Mathematics*, *12(5), 637.*

Malela-Majika, J. C., Shongwe, S. C., Castagliola, P., & Mutambayi, R. M. (2022). A novel single composite Shewhart-EWMA control chart for monitoring the process mean. *Quality and Reliability Engineering International, 38(4), 1760-1789.*

Mao, J., Wang, H., & Spencer Jr, B. F. (2021). Toward data anomaly detection for automated structural health monitoring: Exploiting generative adversarial nets and autoencoders. *Structural Health Monitoring, 20(4), 1609-1626.*

Maravelakis, P. E., Rakitzis, A. C., & Castagliola, P. (2022). Exponentially weighed moving average charts for monitoring zero-inflated proportions with applications in health care. *Statistical Methods in Medical Research*, *31*(5), *959-977.*

Masnar, H. M., & Namoco Jr, C. S. (2024). utilizing student performance data in monitoring new curriculum in construction technology using statistical process control (spc). sci. int.(lahore), 36(1), 59-63.

Mim, F. N., Khoo, M. B., Saha, S., & Khaw, K. W. (2023). A side-sensitive group runs median control chart with measurement errors. *Communications in Statistics-Simulation and Computation*, *52*(4), 1660-1678.

Mohamadkhani, A., & Amiri, A. (2022). Developing mixed EWMA-CUSUM and CUSUM-EWMA control charts based on MRSS and DRSS procedures. *Scientia Iranica, 29(5), 2756-2771.*

Mohammed, M. A. (2024). *Statistical process control*. Elements of Improving Quality and Safety in Healthcare.

Mondal, S., Abdulah, S., Ltaief, H., Sun, Y., Genton, M. G., & Keyes, D. E. (2022). Parallel approximations of the Tukey *g*-and-*h* likelihoods and predictions for non-Gaussian geostatistics. *In 2022 IEEE International Parallel and Distributed Processing Symposium (IPDPS), 79-389.*

Montgomery, D. (2009). *Introduction to statistical quality control (6th Edition)*. John Wiley & Sons Inc., New York.

Montgomery, D. C. (2024). The 100th anniversary of the control chart. *Journal of Quality Technology, 56:1, 2-4.* https://doi.org/10.1080/00224065.2023.2282926.

Morales, V. H., & Panza, C. A. (2022). Control Charts for Monitoring the Mean of Skew-Normal Samples. *Symmetry, 14(11), 2302.*

Muhammad, I., Sun, J., Zaidi, F. S., Abbas, Z., & Nazir, H. Z. Effect of measurement error on the multivariate cusum control chart for compositional data. *CMES-Computer Modeling in Engineering & Sciences 136, no. 2 (2023).*

Mukherjee, A., Chong, Z. L., & Khoo, M. B. (2019). Comparisons of some distribution-free CUSUM and EWMA schemes and their applications in monitoring impurity in mining process flotation. *Computers & Industrial Engineering, 137, 106059.*

Murat, U., Testik, M. C., & Pinar, A. (2024). Patient-based real-time quality control in medical laboratories: On the design and robustness of the moving average control chart with truncation limits. *Quality and Reliability Engineering International, 1-25.*

Nariswari, T. N., & Nugraha, N. M. (2020). Profit growth: impact of net profit margin, gross profit margin and total assests turnover. *International Journal of Finance & Banking Studies (2147-4486), 9(4), 87-96.*

Naveed, M., Azam, M., Khan, N., & Aslam, M. (2018). Design of a control chart Using Extended EWMA Statistic. *Technologies*, *6(4), 108.*

Naveed, M., Azam, M., Khan, N., Aslam, M., Saleem, M., & Saeed, M. (2024). Control charts using half-normal and half-exponential power distributions using repetitive sampling. *Scientific Reports, 14(1), 226.*

Nawaz, M., Maulud, A. S., Zabiri, H., Taqvi, S. A. A., & Idris, A. (2021). Improved process monitoring using the CUSUM and EWMA-based multiscale PCA fault detection framework. *Chinese Journal of Chemical Engineering, 29, 253-265*.

Nawaz, T., & Han, D. (2020). Neoteric ranked set sampling based combined Shewhart-CUSUM and Shewhart-EWMA control charts for monitoring the process location. *European Journal of Industrial Engineering, 14(5), 649-683.*

Nazir, H. Z., Abbas, N., Riaz, M. and Does, R.J.M.M. (2016). A comparative study of memory-type control charts under normal and contaminated normal environments. *Quality and Reliability Engineering. 32 (4), 1347-1356.*

Nazir, H. Z., Abid, M., Akhtar, N., Riaz, M., & Qamar, S. (2021). An efficient mixed-memory-type control chart for normal and non-normal processes. *Scientia Iranica, 28(3), 1736-1749.*

Nazir, H. Z., Riaz, M., & Does, R. J. (2015). Robust CUSUM control charting for process dispersion. *Quality and Reliability Engineering International, 31(3), 369-379.*

Nidsunkid, S., & Chomtee, B. (2022). The Average Run Length Performance of Shewhart Control Chart when the Process Data are Sampled from Finite Population. *International Journal of Mathematics and Computer Science, 17, 509-524.*

Noor, N. F. M., Abdul-Rahman, A. & Atta, A. M. A. (2023). The effectiveness of robust mixed EWMA-CUSUM control chart on *g*-and-*h* distribution. *Journal of Theoretical and Applied Information Technology, 101(13).*

Noor, N.F.M, Abdul-Rahman, A., & Atta, A.M. A. (2024). The performances of mixed EWMA-CUSUM control charts based on median-based estimators under non-normality. *Jurnal Teknologi*. *86(1):135-143.*

Orr, J. M., Sackett, P. R., & Dubois, C. L. (1991). Outlier detection and treatment in I/O psychology: A survey of researcher beliefs and an empirical illustration. *Personnel Psychology*, *44*(3), *473-486.*

Osborne, J. W., & Waters, E. (2019). Four assumptions of multiple regression that researchers should always test. *Practical assessment, research, and evaluation, 8(1), 2.*

Osei-Aning, R., Abbasi, S. A., & Riaz, M. (2017). Mixed EWMA-CUSUM and mixed CUSUM-EWMA modified control charts for monitoring first order autoregressive processes. *Quality Technology & Quantitative Management, 14(4), 429-453.*

Ottenstreuer, S., Weiß, C. H., & Testik, M. C. (2023). A review and comparison of control charts for ordinal samples. *Journal of Quality Technology, 55(4), 422-441.*

Page, E. S. (1954). Continuous Inspection Schemes. *Biometrika, 41(1/2), 100–115.*

Park, H. I. (2009). median control charts based on bootstrap method. *Communications in Statistics—Simulation and Computation®*, *38*(3), 558-570.

Parkash, V., Kumar, D., & Rajoria, R. (2013). Statistical process control. *International Journal of Research in Engineering and Technology, 2(8), 70–72.*

Peerajit, W. (2023). Accurate Average Run Length Analysis for Detecting Changes in a Long-Memory Fractionally Integrated MAX Process Running on EWMA Control Chart. *WSEAS Transactions on Mathematics, 22, 514-530.*

Prabawani, N. A., & Mashuri, M. (2020). Performance of robust EWMA control chart for variability process using non-normal data. *In Journal of Physics: Conference Series 1511 (1), 012054.*

Qiu, P., & Li, Z. (2011). On nonparametric statistical process control of univariate processes. *Technometrics*, *53*(4), *390-405.*

Quinino, R. C., Cruz, F. R., & Quinino, V. B. (2021). Control chart for process mean monitoring combining variable and attribute inspections. *Computers & Industrial Engineering, 152, 106996.*

Rakotosaona, M. J., La Barbera, V., Guerrero, P., Mitra, N. J., & Ovsjanikov, M. (2020). Pointcleannet: Learning to denoise and remove outliers from dense point clouds. *In Computer graphics forum, 39 (1), 185-203.*

Ratcliff, R. (1993). Methods for dealing with reaction time outliers. *Psychological bulletin, 114(3), 510.*

Raymaekers, J., & Rousseeuw, P. J. (2023). The cellwise minimum covariance determinant estimator. *Journal of the American Statistical Association, 1-12.*

Relles. D. A. & Rogers W. H. (1977). Statisticians are Fairly Robust Estimators of Location. *Journal of the American Statistical Association, 72 (357), 107-111.*

Riaz, M., & Saghirr, A. (2007). Monitoring process variability using Gini's mean difference. *Quality Technology & Quantitative Management*, *4*(4), *439-454.*

Riaz, M., Abbas, N., & Does, R. J. (2011). Improving the performance of CUSUM charts. *Quality and Reliability Engineering International*, *27*(4), *415-424.*

Riaz, M., Abid, M., Shabbir, A., Nazir, H. Z., Abbas, Z., & Abbasi, S. A. (2021). A non-parametric double homogeneously weighted moving average control chart under sign statistic. *Quality and Reliability Engineering International*, *37*(4), *1544-1560.*

Rivest, L. P. (1994). Statistical properties of Winsorized means for skewed distributions. *Biometrika*, *81*(2), *373-383.*

Roberts, S. W. (1959). control chart Tests Based on Geometric Moving Averages. *Technometrics*, 1(3), *239–250.*

Rocke, D. M. (1989). Robust control charts. *Technometrics*, *31*(2), *173-184.*

Rocke, D. M. (1992). $\bar{X}_Q$ and R_Q charts: robust control charts. *Journal of the Royal Statistical Society: Series D (The Statistician)*, *41*(1), *97-104.*

Rosa Lakus, D., Pizzolato, M., de Medeiros Albano, F., & Langer Menin, P. (2022). Shewhart, CUSUM and EWMA control charts: A comparative study on intermediate check of balances. *MAPAN, 37(2), 453-464.*

Rousseeuw, P. J. (1991). Tutorial to robust statistics. *Journal of chemometrics, 5(1), 1-20.*

Rousseeuw, P. J., & Croux, C. (1993). Alternatives to the median absolute deviation. *Journal of the American Statistical association*, *88(424), 1273-1283.*

Rousseeuw, P. J., & Hubert, M. (2018). Anomaly detection by robust statistics. *Wiley Interdisciplinary Reviews: Data Mining and Knowledge Discovery, 8(2), e1236.*

Rousseeuw, P. J., & Verboven, S. (2002). Robust estimation in very small samples. *Computational Statistics & Data Analysis*, *40*(4), *741-758.*

Sabahno, H., & Amiri, A. (2023). Simultaneous monitoring of the mean vector and covariance matrix of multivariate multiple linear profiles with a new adaptive Shewhart-type control chart. *Quality Engineering, 35(4), 600-618.*

Saeed, N., & Kamal, S. (2016). The EWMA control chart based on robust scale estimators. *Pakistan Journal of Statistics and Operation Research, 659-672.*

Samanta, B., & Bhattacherjee, A. (2004). Problem of "non-normality" in statistical quality control: a case study in a surface mine. *Journal of the Southern African Institute of Mining and Metallurgy*, *104(5), 257-264.*

Santhanasamy, D. K., & Abdul-Rahman, A. (2022). Robustification of shewhart control chart by median based estimators: A study on Malaysia stock data. *Journal of Quality Measurement and Analysis JQMA, 18(1), 13-26.*

Sanusi, R. A., Riaz, M., & Abbas, N. (2017). Combined Shewhart CUSUM charts using auxiliary variable. Computers & Industrial Engineering, 105, 329-337.

Schoonhoven, M., Nazir, H. Z., Riaz, M., & Does, R. J. (2011). Robust Location Estimators for the $\bar{U}$ Control Chart. *Journal of Quality technology, 43(4), 363-379.*

Shafqat, A., Shahzad, F., Aslam, M., & Abreu, R. P. (2023). An enhanced design of nonparametric modified EWMA sign control chart using repetitive sampling. *Brazilian Journal of Probability and Statistics, 37(3), 552-565.*

Shamsuzzaman, M., Haridy, S., Bashir, H., & Maged, A. (2023). An economic combined Shewhart-EWMA scheme for monitoring process mean. *AIP Conference Proceedings. 2643 (1).*

Shamsuzzaman, M., Haridy, S., Maged, A., Bashir, H., Shamsuzzoha, A., & Ali, A. (2022). An effective statistical process control scheme for industrial environmental monitoring. *Chemometrics and Intelligent Laboratory Systems, 229, 104651.*

Shan, T., & Huang, W. (2021). Treating Measurement Errors in the Run Rule Schemes Integrated with Shewhart X Chart. *Mathematical Problems in Engineering, 2021, 1-13.*

Shongwe, S. C., & Malela-Majika, J. C. (2022). Shewhart-type monitoring schemes with supplementary w-of-w runs-rules to monitor the mean of autocorrelated samples. *Communications in Statistics-Simulation and Computation, 51(1), 293-322.*

Shper, V., Khunuzidi, E., Sheremetyeva, S., & Smelov, V. (2023). Shewhart Control Chart: Long-Term Data Analysis Tool with High Development Capacity. *IntechOpen*. doi: 10.5772/intechopen.113991

Shu, L., Jiang, W., & Tsui, K. L. (2011). A comparison of weighted CUSUM procedures that account for monotone changes in population size. *Statistics in medicine*, *30*(*7), 725-741.*

Sindhumol, M. R., Srinivasan, M. R., & Gallo, M. (2016). Robust control charts based on modified trimmed standard deviation and Gini's mean difference. *Journal of Applied Quantitative Methods, 11(3), 18-30.*

Sinha, A. K., & Vatsa, R. (2022). control charts and Capability Analysis for Statistical Process Control. *In Promoting Statistical Practice and Collaboration in Developing Countries. 301-320.*

Smajdorova, T., & Noskievicova, D. (2016). Parametric and nonparametric methods of statistical process control. *MM Science Journal*.

Smajdorová, T., & Noskievičová, D. (2022). Analysis and application of selected control charts suitable for smart manufacturing processes. *Applied Sciences*, *12*(*11), 5410.*

Steiner, S. H. (1999). EWMA control charts with time-varying control limits and fast initial response. *Journal of Quality Technology*, *31*(1), *75-86.*

Sunaryo, D. (2021). Analysis of current ratio, debt to assets ratio and gross profit margin on financial distress with moderated share prices in retail companies listed in securities exchange. *International Journal of Educational Research and Social Sciences (IJERSC), 2(1), 23-33.*

Sunthornwat, R., & Areepong, Y. (2020). Average run length on CUSUM control chart for seasonal and non-seasonal moving average processes with exogenous variables. Symmetry, 12(1), 173.

Sunthornwat, R., Areepong, Y., & Sukparungsee, S. (2024). Performance evaluation of HWMA control chart based on AR (p) with trend model to detect shift process mean. *WSEAS Transactions on Business and Economics*, *21*, 603-616.

Swamidass, P. M. (Ed.). (2000). *Encyclopedia of production and manufacturing management*. Springer Science & Business Media.

Taboran, R., & Sukparungsee, S. (2023). On designing of a new EWMA-DMA control chart for detecting mean shifts and its application. *Thailand Statistician, 21(1), 148-164.*

Taboran, R., Sukparungsee, S., & Areepong, Y. (2021). Design of a new Tukey MA-DEWMA control chart to monitor process and its applications. *IEEE Access, 9, 102746-102757.*

Tegegne, D. A., Kitaw, D., & Berhan, E. (2022). Advances in statistical quality control chart techniques and their limitations to cement industry. *Cogent Engineering, 9(1), 2088463.*

Teoh, W. L., Khoo, M. B., & Teh, S. Y. (2013). Optimal designs of the median run length based double sampling X chart for minimizing the average sample size. *PLoS One*, *8*(7), e68580.

Testik, M. C., Kara, O., & Knoth, S. (2020). An algorithmic approach to outlier detection and parameter estimation in Phase I for designing Phase II EWMA control chart. *Computers & Industrial Engineering, 144, 106440.*

Thanwane, M., Malela-Majika, J. C., Castagliola, P., & Shongwe, S. C. (2021). The effect of measurement errors on the performance of the homogenously weighted moving average $\bar{X}$ monitoring scheme. *Transactions of the Institute of Measurement and Control, 43(3), 728-745.*

Tu, X., & Zi, X. (2020). On-line Change Detection with Practical Importance. *In Proceedings of the 4th International Conference on Computer Science and Application Engineering, 1-5.*

Tukey, J. W. (1948). Some elementary problems of importance to small sample practice. *Human Biology*, *20*(4), *205.*

Tukey, J. W. (1977). Exploratory Data Analysis. *Reading, MA: Addison-Wesley*

Tukey, J. W., & McLaughlin, D. H. (1963). Less vulnerable confidence and significance procedures for location based on a single sample: Trimming/Winsorization 1. *Sankhyā: The Indian Journal of Statistics, Series A*, 25 (3), *331-352.*

Wada, K. (2020). Outliers in official statistics. *Japanese Journal of Statistics and Data Science, 3(2), 669-691.*

Wang, T., Li, Y., & Cui, H. (2007). On weighted randomly trimmed means. *Journal of Systems Science and Complexity*, *20(1), 47-65.*

Wei, Y., Wu, D., & Terpenny, J. (2020). Robust incipient fault detection of complex systems using data fusion. IEEE *Transactions on Instrumentation and Measurement, 69(12), 9526-9534.*

Wilcox, R. (2003). Multiple comparisons based on a modified one-step M-estimator. *Journal of Applied Statistics, 30(10), 1231-1241.*

Wilcox, R. (2022). One-way and two-way ANOVA: Inferences about a robust, heteroscedastic measure of effect size. *Methodology, 18(1), 58-73.*

Wilcox, R. R., & Keselman, H. J. (2003a). Modern robust data analysis methods: measures of central tendency. *Psychological methods*, *8(3), 254.*

Wilcox, R. R., & Keselman, H. J. (2003b). Repeated measures one-way ANOVA based on a modified one-step M-estimator. *British Journal of Mathematical and Statistical Psychology, 56(1), 15-25.*

Wu, C., Zhao, Y., & Wang, Z. (2002). The median absolute deviations and their applications to Shewhart control charts. *Communications in Statistics-Simulation and Computation, 31(3), 425-442.*

Wu, M., & Zuo, Y. (2009). Trimmed and winsorized means based on a scaled deviation. *Journal of Statistical Planning and Inference*, *139(2), 350-365.*

Wu, T. L. (2018). Distribution-free runs-based control charts. *Preprint submitted to Computational Statistics & Data Analysis. arXiv preprint arXiv:1801.06532*.

Yan, Y., & Genton, M. G. (2019a). Non-Gaussian autoregressive processes with Tukey-and-h transformations. *Environmetrics, 30(2), e2503.*

Yan, Y., & Genton, M. G. (2019b). The Tukey *g*-and-*h* distribution. *Significance, 16(3), 12–13*. https://doi.org/10.1111/j.1740-9713.2019.01273.x

Yang, L., Pai, S., & Wang, Y. R. (2010). A novel CUSUM median control chart. *In Proceedings of International Multiconference of Engineers and Computer Scientists, 3, 1707-1710.*

Yao, Y., Chakraborti, S., Yang, X., Parton, J., Lewis Jr, D., & Hudnall, M. (2023). Phase I control chart for individual autocorrelated data: application to prescription opioid monitoring. *Journal of Quality Technology, 55(3), 302-317.*

Yashchin, E. (1989). Weighted cumulative sum technique. *Technometrics, 31(3), 321-338.*

Yeganeh, A., & Shadman, A. (2021). Monitoring linear profiles using Artificial Neural Networks with run rules. *Expert Systems with Applications, 168, 114237.*

Yeganeh, A., & Shongwe, S. C. (2023). A novel application of statistical process control charts in financial market surveillance with the idea of profile monitoring. *PloS one, 18(7), e0288627.*

Yitzhaki, S., & Lambert, P. J. (2012). The Relationship between Gini's Mean Difference and the Absolute Deviation from a Quantile. *Available at SSRN 2048397*. https://dx.doi.org/10.2139/ssrn.2048397

Yourstone, S. A., & Zimmer, W. J. (1992). Non-normality and the design of control charts for averages. *Decision sciences, 23(5), 1099-1113.*

Yue, J., & Liu, L. (2022). A New Nonparametric Multivariate Control Scheme for Simultaneous Monitoring Changes in Location and Scale. *Computational and Mathematical Methods in Medicine*, *2022, 1-11.*

Zaman, B., Abbas, N., Riaz, M., & Lee, M. H. (2016). Mixed CUSUM-EWMA chart for monitoring process dispersion. *The International Journal of Advanced Manufacturing Technology*, *86(9-12), 3025-3039.*

Zaman, B., Riaz, M., Abbas, N., & Does, R. J. (2015). Mixed cumulative sum–exponentially weighted moving average control charts: an efficient way of monitoring process location. *Quality and Reliability Engineering International*, *31(8), 1407-1421.*

Zamzmi, G., Venkatesh, K., Nelson, B., Prathapan, S., Yi, P. H., Sahiner, B., & Delfino, J. G. (2024). Out-of-distribution detection and data drift monitoring using statistical process control. *arXiv preprint arXiv:2402.08088.*

Zhao, Y., Tsung, F., & Wang, Z. (2005). Dual CUSUM control schemes for detecting a range of mean shifts. *IIE Transactions, 37(11), 1047-1057.*

Zhuang, J., Wang, Y., Mao, G., Chen, X., Wang, Y., & Wei, Z. (2023). Anomaly Detection of Non-Normal Distribution Wafer Acceptance Test Data Via GMM-Based Method. *In 2023 China Semiconductor Technology International Conference (CSTIC), 1-4.*

Zou, C., Wang, Z., & Tsung, F. (2012). A spatial rank-based multivariate EWMA control chart. *Naval Research Logistics (NRL), 59(2), 91-110.*

Zwetsloot, I. M., Jones-Farmer, L. A., & Woodall, W. H. (2023). Monitoring univariate processes using control charts: *Some practical issues and advice. Quality Engineering, 1-13.*

Appendix

Real Dataset

Appendix 1

TSS Data for Sungai Udang Station (MB1004)

Station	Date	Time	TSS (mg/L)
MBI004	06/27/2023	5:00	141.50
MBI004	06/27/2023	6:00	130.75
MBI004	06/27/2023	7:00	131.00
MBI004	.	.	.
MBI004	.	.	.
MBI004	.	.	.
MBI004	07/22/2023	3:00	279.75
MBI004	07/22/2023	4:00	296.00
MBI004	07/22/2023	5:00	296.00
MBI004	07/22/2023	6:00	296.00
MBI004	07/22/2023	7:00	296.00
MBI004	07/22/2023	8:00	296.00
MBI004	07/22/2023	9:00	233.00
MBI004	07/22/2023	10:00	102.50
MBI004	07/22/2023	11:00	106.00
MBI004	07/22/2023	12:00	105.75
MBI004	07/22/2023	13:00	113.75
MBI004	07/22/2023	14:00	105.25
MBI004	07/22/2023	15:00	113.25
MBI004	07/22/2023	16:00	114.00
MBI004	07/22/2023	17:00	120.00
MBI004	07/22/2023	18:00	120.00
MBI004	07/22/2023	19:00	120.00
MBI004	07/22/2023	20:00	120.00
MBI004	07/22/2023	21:00	120.00
MBI004	07/22/2023	22:00	120.00
MBI004	07/22/2023	23:00	120.00

Appendix 2

DOC Data for Sungai Udang Station (MB1004)

Station ID	Date	Time	DOC (mg/L)
MBI004	07/08/2023	5:00	0.20
MBI004	07/08/2023	5:00	0.20
MBI004	07/08/2023	7:00	0.20
MBI004	.	.	.
MBI004	.	.	.
MBI004	.	.	.
MBI004	07/22/2023	0:00	0.21
MBI004	07/22/2023	1:00	0.21
MBI004	07/22/2023	2:00	0.21
MBI004	07/22/2023	3:00	0.21
MBI004	07/22/2023	4:00	0.21
MBI004	07/22/2023	5:00	0.21
MBI004	07/22/2023	6:00	0.21
MBI004	07/22/2023	7:00	0.21
MBI004	07/22/2023	8:00	0.21
MBI004	07/22/2023	9:00	0.21
MBI004	07/22/2023	10:00	0.21
MBI004	07/22/2023	11:00	0.21
MBI004	07/22/2023	12:00	0.21
MBI004	07/22/2023	13:00	0.21
MBI004	07/22/2023	14:00	0.21
MBI004	07/22/2023	15:00	0.21
MBI004	07/22/2023	16:00	0.21
MBI004	07/22/2023	17:00	0.21
MBI004	07/22/2023	18:00	0.21
MBI004	07/22/2023	19:00	0.21
MBI004	07/22/2023	20:00	0.21
MBI004	07/22/2023	21:00	0.21
MBI004	07/22/2023	22:00	0.21
MBI004	07/22/2023	23:00	0.21

Appendix 3

Marker Band Data

Marker Band Length (mm)	Begin Run Time	End Run Time
49.13	15:16.1	15:31.1
49.10	17:39.7	17:49.7
49.20	42:10.3	42:28.3
.	.	.
.	.	.
.	.	.
49.31	09:44.3	10:02.3
49.39	10:13.4	10:31.4
49.37	10:39.5	10:53.5
49.36	10:59.1	11:14.1
49.34	11:21.9	11:31.9
49.34	11:37.0	11:55.0
49.37	12:00.3	12:18.3
49.44	12:24.1	12:35.1
49.35	12:47.9	13:04.9
49.43	13:11.4	13:21.4
49.31	22:53.7	23:10.7
49.37	24:00.9	24:17.9
49.24	30:08.4	30:22.4
49.25	30:46.6	31:00.6
49.32	31:10.3	31:28.3
49.34	31:34.0	31:52.0
49.31	31:57.8	32:16.8
49.33	43:14.9	43:33.9
49.29	43:41.3	43:58.3
49.29	45:11.6	45:28.6
49.35	46:08.8	46:25.8
49.44	46:39.3	46:50.3
49.34	47:04.0	47:22.0
49.31	47:31.5	47:48.5